

Aus dem Molekularen Krebsforschungszentrum
der Medizinischen Fakultät Charité – Universitätsmedizin Berlin

DISSERTATION

Functional genomic investigation of the human aggressive
lymphoma derived genetic lesions MYD88L265P, NFKBIZ,
CARD11L244P, CD79BY196H and PD-L1 in a murine
E μ -myc lymphoma model

zur Erlangung des akademischen Grades
Doctor medicinae (Dr. med.)

vorgelegt der Medizinischen Fakultät
Charité – Universitätsmedizin Berlin

von

Jens Florian Schrezenmeier

aus Ulm

Datum der Promotion: 1.3.2019

Contents

1. List of figures and tables	p. iii-vi
2. Abstract	p. 1-3
3. Introduction	p. 4-9
4. Materials and Methods	p. 10-40
a) Materials and Equipment	p. 10-23
b) Techniques and Procedures	p. 24-40
5. Results	p. 41-92
a) Fetal Liver Cell Approach	p. 41-65
b) Manifest E μ -myc Lymphoma Approach	p. 66-92
6. Discussion	p. 93-100
7. Bibliography	p. 101-122
8. RNA Sequencing Data: Annotation Cluster and Gene List	p. 123-138
Appendix	
a) Appendix 1: The E μ -myc Fetal Liver Cell approach	p. 123-131
b) Appendix 2: The manifest transduced E μ -myc lymphoma approach	p. 131-137
c) Appendix 3: T-cell activation and evasion signatures	p. 138
9. Eidesstattliche Versicherung	p. I
10. Curriculum Vitae	p. II
11. Publications not associated with this dissertation	p. III
12. Acknowledgements	p. IV-V

List of figures and tables

Figure 1	Retroviral vector map	p18
Figure 2	Power calculation and raw reads	p36
Figure 3	Sorting strategy and RNA quality	p37
Figure 4	Experimental approach FLC	p41
Figure 5	Efficiency of stem cell transduction	p42
Table 1	Overexpression of transduced mutants in RNA Seq data from manifest lesion transduced E μ -myc lymphomas	p44
Table 2	Penetrance of mutants in MSCV- GFP transduced E μ -myc transgenic FLCs and MSCV-GFP transduced wildtype FLCs	p44
Figure 6	Number of GFP+B220+ cells in MSCV-lesion-GFP transduced E μ -myc tg FLC lymphomas	p45
Figure 7	Survival curve for mice presenting with lymphadenopathy transplanted with MSCV-GFP transduced E μ -myc transgenic FLCs	p45
Figure 8	Survival curve for mice presenting with GFP positive lymphoma transplanted with MSCV-GFP transduced E μ -myc transgenic FLCs	p46
Figure 9	Whole lymphoma Ki67 stains from empty, MYD88L265P, NFKBIZ and CD79BY196H MSCV-GFP transduced E μ -myc transgenic FLC lymphomas	p47
Figure 10	100x magnification of HE and Ki67 stains from empty, MYD88L265P, NFKBIZ and CD79BY196H MSCV-GFP transduced E μ -myc transgenic FLC lymphomas	p48
Figure 11	Immune cell subpopulations within lymphomas	p49
Figure 12a	Transcript levels of B220 in the different sequenced MSCV- lesion-GFP transduced E μ -myc transgenic FLC lymphomas	p51
Figure 12b	Sample distance clustering	p52
Figure 13	Histogram for counts of unadjusted p-values	p53
Figure 14	Principal component analysis of transcriptome data	p54

Figure 15	Overlap of significantly differentially regulated genes between groups	p56
Figure 16	PD-L1 and PD-L2 expression on MSCV-lesion-GFP driven $E\mu$ -myc transgenic FLC lymphomas and MSCV-empty-GFP transduced $E\mu$ -myc transgenic FLC lymphomas	p58
Table 3	Penetrance of PD-L1 driven MSCV-PD-L1-GFP transduced $E\mu$ -myc transgenic FLC lymphomas and PD-L1 surface expression on empty and PD-L1 MSCV-GFP transduced $E\mu$ -myc transgenic FLC lymphomas	p58
Figure 17	E and Ki67 stains of three independent PD-L1 driven lymphomas	p59
Figure 18	Survival impact of PD-L1 knockdown on MYD88L265P driven lymphomagenesis	p60
Figure 19	Knockdown efficiency of MYD88L265PshPD-L1 vs. MYD88L265Pshscrambled	p61
	Histopathological analysis of MSCV-	
Figure 20	MYD88L265Pshscrambled-GFP and MSCV-MYD88shPD-L1 $E\mu$ -myc transgenic FLC lymphomas	p61
Figure 21	Exemplary genotyping of used FLC of SUV39H1 $-/-$ or SUV39H1 $-/+$ $E\mu$ -myc transgenic fetal liver cells	p63
	Senescence associated beta galactosidase staining in GFP positive vs. GFP negative cells from MSCV-CARD11L244P-	
Figure 22	GFP transduced $E\mu$ -myc transgenic FLC and MSCV-empty-GFP transduced $E\mu$ -myc transgenic FLC transplanted C57BL6/N mice	p63
	Survival curve for C57BL6/N mice presenting with GFP positive lymphoma in MSCV-CARD11L244P-GFP or MSCV-empty-GFP transduced SUV39H1 $-/-$ $E\mu$ -myc FLC transplanted mice	
Figure 23		p64

	GFP enrichment in total viable cells from spleens of MSCV-	
Figure 24	CARD11L244P -GFP transduced E μ -myc transgenic	
	SUV39H1 -/- FLC transplanted C57BL6/N mice	p64
Figure 25	Experimental approach matched pair lymphomas	p66
	Overall survival from transplantation to lymphoma	
Figure 26	manifestation in empty-GFP and MYD88L265P transduced	
	and retransplanted E μ -myc transgenic manifest lymphomas	p67
Figure 27	Histopathological Analysis of MYD88L265P and empty	
	transduced manifest E μ -myc transgenic lymphomas I	p68
Figure 28	Histopathologic Analysis of MYD88L265P and empty	
	transduced manifest E μ -myc transgenic lymphomas II	p69
Figure 29	Ki67 and H3K9me3 staining of investigated lesions	p70
Figure 30	Histogram for count of unadjusted p-values	p72
Figure 31	Sample distance clustering	p73
Figure 32	Principal component analysis of transcriptome data	p74
Figure 33	Overlap of significantly differentially regulated genes between	
	groups	p76
Figure 34	T-cell infiltration in empty GFP and MYD88L265P transduced	
	lymphomas	p77
Figure 35	Volcano plot of differentially regulated genes in PD-L1	
	transduced manifest E μ -myc lymphomas	p78
Table 4	Differentially regulated NF κ B players from RNA Seq data in	
	MYD88L265P vs. empty lymphomas	p79
Figure 36	NFKBIZ mRNA is upregulated by LPS and MYD88L265P in	
	manifest E μ -myc lymphomas	p80
Figure 37	Trans AM NF κ B consensus site binding assay	p81
Figure 38	Analysis interface for Image Stream Flow Microscopy	p82
Figure 39	p65 nuclear localization histograms	p82
Table 5	p65 nuclear localization statistics for MSCV-lesion	
	transduced manifest E μ -myc transgenic lymphomas	p83

	Heatmap of NFkB Fingerprint in MSCV-lesion-GFP transduced E μ -myc transgenic FLC lymphomas compared to MSCV-empty-GFP transduced E μ -myc transgenic FLC lymphomas	p84
Figure 40		
	BTK Tyrosine 223 phosphorylation in NFKBIZ and MYD88L265P transduced manifest E μ -myc relative to empty E μ -myc lymphomas	p85
Figure 41		
	Number of biological and technical replicates in lesion	
Table 6	transduced E μ -myc transgenic manifest lymphomas used for metabolomics	p87
Figure 42	Experimental setup metabolomics	p88
Figure 43	Overall principal component analysis of all analysed groups	p89
Figure 44	P-value histograms of overall data for samples measured depicted in table 6	p89
Figure 45	Restricted principal component analysis and p-value histograms for transduced manifest E μ -myc lymphomas	p90
	Restricted principal component analysis for MSCV-empty-GFP transduced and MSCV-NFKBIZ-GFP transduced manifest E μ -myc transgenic lymphomas and Box-Whisker plots for one exemplary metabolite	
Figure 46		p91
	Metabolites showing significantly different levels between NFKBIZ and empty transduced manifest E μ -myc lymphomas	p91
Table 7	Box-Whisker Plots for relative levels of cytosine metabolites measured in empty and NFKBIZ transduced manifest E μ -myc lymphomas	
Figure 47		p92

Abstract

Introduction: MYC hyperactivation and genetic lesions affecting B-cell receptor and NFkB signaling have been described in recent years to be central features of aggressive non-Hodgkin-lymphoma. Yet little is currently known about the capacity of NFkB and B-cell receptor-associated lesions to drive lymphoma in co-operation with MYC and how they affect cell signaling and phenotype of manifest disease. Additionally, it is still not understood how MYD88L265P, NFKBIZ, CD79BY196H, CARD11L244P and PD-L1 affect the interaction between lymphoma cells and the immune system.

Methods: We approached those enigmas of lymphoma biology using two transplantation models in which the transplanted cells were retrovirally transduced with genetic lesions MYD88L265P, NFKBIZ, CD79BY196H, CARD11L244P and PD-L1: (i) stem cell transplantation of retrovirally transduced E μ -myc transgenic fetal liver cells as a source of hematopoietic stem cells to study lymphomagenesis and (ii) a retransplantation approach of retrovirally transduced manifest E μ -myc lymphomas as model systems to study the lymphoma biology in vivo. For functional analysis of these models, we used histopathological, biochemical and classical molecular biology approaches, FACS, microscopy-coupled FACS, transcriptome and metabolomics analyses.

Results: Of these in vivo approaches, NFKBIZ and MYD88L265P were found to be highly E μ -myc co-operative genetic lesions in contrast to CARD11L244P in the fetal liver cell approach. NFKBIZ and MYD88L265P-driven lymphomas were found to form transcriptionally clustering and distinguishable entities compared to empty control E μ -myc lymphomas. PD-L1 was found to be able to drive lymphoma in co-operation with E μ -myc in the fetal liver cell model and was identified as an important mechanism contributing to lymphoma aggressiveness in MYD88L265P-driven E μ -myc lymphomas. Overexpression of PD-L1 in the transplantation model of E μ -myc transgenic fetal liver cell-induced lymphomas. Regarding the inability of CARD11L244P to drive lymphoma in our model,

we found CARD11L244P-induced senescence to be a critical principle preventing lymphomagenesis.

Conclusion: Our systematic *in vivo* analysis of different lesions indicated that MYD88L265P and NFKBIZ cooperate with Myc while CARD11L244P requires upfront senescence-ablating lesions to license Myc-driven lymphomagenesis. Immune evasive mechanisms were found to be central aspects of MYD88L265P driven lymphomas with an increase of PD-L1 expression as an important mechanism. Altogether these investigations provide mouse models of MYD88L265P, PD-L1 and NFKBIZ driven lymphomas, a mechanistic analysis of the MYD88L265P-NFKBIZ-PD-L1 triangle in aggressive lymphoma biology and senescence as a central barrier in CARD11L244P-driven lymphomagenesis.

Abstract in deutscher Fassung

Einleitung: In den letzten Jahren wurde im aggressiven non-Hodgkin Lymphom gezeigt, dass die Hyperaktivierung von MYC und genetische Läsionen innerhalb immunologischer Signalkaskaden wesentliche Merkmale dieser Krankheitsentität darstellen. Im Moment ist wenig über das Zusammenspiel dieser Signalkaskaden mit MYC in der Lymphomgenese bekannt. Zudem ist es immer noch unklar, wie MYD88L265P, NFKBIZ, CD79BY196H, CARD11L244P und PD-L1 die Interaktion aggressiver Lymphome mit dem Immunsystem beeinflussen.

Methoden: Um die aufgeworfenen Fragen beantworten zu können, nutzten wir zwei Transplantationsmodelle, bei denen die transplantierten Zellen jeweils retroviral mit genetischen Läsionen transduziert wurden, welche in humanen aggressiven Lymphomen beschrieben wurden: (i) die Transplantation von retroviral transduzierten Eμ-myc transgenen murinen fetalen Leberzellen als Quelle hämatopoietischer Stammzellen, um die Lymphomgenese *in vivo* zu untersuchen und (ii) die Transplantation retroviral transduzierter, manifester murine Eμ-myc Lymphome, um die Lymphobiologie *in vivo* zu untersuchen. Dabei wurden histopathologische Untersuchungen, klassisch

molekularbiologische Methoden, Fluoreszenzmikroskopie gekoppelte FACS Analysen sowie RNA Sequenzierung und Metabolom Analysen genutzt

Ergebnisse: Aus diesen *in vivo* Untersuchungen ergab sich, dass MYD88L265P und NFKBIZ im Gegensatz zu CARD11L244P wesentlich mit E μ -myc in der Lymphomgenese zusammenwirken. Auf transkriptionaler Ebene zeigte sich, dass NFKBIZ und MYD88L265P getriebene und Leervektor E μ -myc Lymphome transkriptional klar voneinander unterscheidbare Entitäten darstellten. Bei der Modellierung und Untersuchung des Einflusses von PD-L1 auf die Biologie aggressiver Lymphome zeigte sich, dass PD-L1 sowohl ein zentraler Regulator der Interaktion zwischen Lymphom und Immunsystem ist als auch wesentlich auf intrazelluläre Signalkaskaden der Lymphomzellen wirkt. Die Überexpression von PD-L1 generierte im Zusammenspiel mit E μ -myc ebenfalls Lymphome im fetalen Leberzellmodell. Bezuglich der nicht onkogenen Eigenschaften von CARD11L244P im Zusammenspiel mit E μ -myc zeigte sich, dass onkogen-induzierte Seneszenz dies in unserem System verhindert.

Schlussfolgerung: Unsere systematische *in vivo* Analyse verschiedener genetischer Läsionen zeigte, dass MYD88L265P und NFKBIZ mit Myc kooperieren, wohingegen CARD11L244P initiale Seneszenzdefekte benötigt, um mit Myc in der Lymphomgenese zusammenzuarbeiten. Wir konnten feststellen, dass immunevasive Mechanismen zur MYD88L265P-getriebenen Lymphomgenese im fetalen Leberzellmodell beitragen. PD-L1 ist hierfür eine wichtige Schaltstelle.

Insgesamt werden in dieser Arbeit die ersten Mausmodelle für PD-L1- und NFKBIZ-getriebene Lymphome und eine mechanistische Analyse der MYD88L265P–NFKBIZ–PD-L1 Interaktionen in der Biologie aggressiver Lymphome dargelegt. Zudem wird Seneszenz als zentrale Barriere, welche die Lymphomgenese durch CARD11L244P im E μ -myc Modell verhindert, dargestellt.

Introduction

What are aggressive lymphomas?

Aggressive non-Hodgkin lymphomas (NHL) (1) are a disease entity arising from unphysiologic and atypical hyperproliferation of B-cells (2) and rarely T-cells (3) and present with abnormal cell morphology, distinguishing themselves histopathologically in their overall architecture and appearance from other neoplasms. They are characterized by fast disease progression and rapid lethality in untreated individuals and frequently show organ tropism (4). Aggressive NHL comprise about 3% of all malignant neoplasms (5). The most common form is diffuse large B-cell lymphoma (DLBCL) comprising around 30-40 percent of all diagnosed non-Hodgkin lymphomas. Burkitt's lymphoma, a lymphoma subgroup biologically closely related to DLBCL (6), also belongs to the group of aggressive lymphomas (7, 8). Burkitt's lymphoma frequently carries the t(8;14) MYC-IgH translocation and shows extremely high Ki67 indices (>90%) but occurs far less frequently than DLBCL (9).

Aggressive NHL was among the first diseases to be subjected to effective cyclophosphamide treatment in the late 1950s (10, 11). It is among few cancers that can be cured even in advanced stages and was among the first ones to be treated with a monoclonal antibody, Rituximab, in first-line therapy (12, 13). Yet those relapsing or not responding to current standard therapy R-CHOP regimes still have a poor prognosis (14). The disease is currently still defined based on histopathological assessment of a tissue biopsy (15). It is a prominent feature of aggressive lymphomas, as in most other hematological malignancies, to present frequently with an incoherent immunophenotypic profile compared to their normal tissue progenitor cells (16). Thus, definitions and classifications are often blurred. Many copy number alterations and somatic mutations have been described in DLBCL, whereas Burkitt's lymphoma seems to be a genomically more consistent disease (17).

The Microarray era

From a research perspective, aggressive NHL was one of the first diseases that underwent extensive gene expression studies (8, 18, 19). These led to a molecular definition of Burkitt's lymphoma, distinguishing it on a genomic level from diffuse large B-cell lymphoma (7, 8). The microarray studies claimed to identify molecular subgroups of diffuse large B-cell lymphoma (18) and tried to link those molecular alterations to clinical response to chemotherapy (20).

These and ensuing studies, predominantly by the groups of Louis Staudt and Margaret Shipp, indicated a strong role for B-cell specific programs, discovered principally by the Klaus Rajewsky group (21-23), to be hijacked, leading to lymphomagenesis (23-25). Within the studies published by the Staudt group, DLBCL is classified into an activated B-cell (ABC) and a germinal center B-cell (GCB) subgroup resembling transcriptionally their claimed cell of origin (18). Contrasting this classification system, the Shipp group used a clustering approach that subdivided DLBCL into a first group dependent on B-cell receptor signaling (26). A second group showed severe metabolic derangements with the dominant feature of upregulation of many genes from the domain of oxidative phosphorylation and oxidative stress response, named "Ox/Phos" by the Shipp group (27-29). Finally, a third functional subgroup defined by stromal signatures and immune interactions was identified (29). This stromal impact on patient survival was also identified by the Staudt group in a prognostic study (30). Independent of the transcriptomic DLBCL subgroup, treatment is currently still the same for all (31). Although the Staudt group argued that ABC DLBCL would have much poorer survival than GCB DLBCL when treated with both CHOP and R-CHOP regimes in a retrospective study (20) the German high-grade non-Hodgkin-lymphoma study group failed to show the prognostic impact of ABC and GCB DLBCL subgroups towards R-CHOP treatment in two independent prospective trials published in 2017 (32).

Identifying crucial signaling relays – sequencing studies

CD79B (24), CARD11 (33), MYD88 (34), and TNFAIP3 (35) and many players in the context of NFkB signaling, e.g. NFKBIZ (36, 37) are frequently mutated or amplified in DLBCL. Additionally, inactivation of crucial B-cell transcription factors like BLIMP1 (38),

BCL6 (39) and KLF2 (40) are among the most frequent dysregulated players within diffuse large B-cell lymphoma. Finally, epigenetic modifiers like MLL2, KDM2B, SMARCA1 (41) and cell cycle regulators like P53 and PIM1 are in many cases genetically lesioned (42-46). On the one hand, these findings revealed that a relevant mutational correlate of dysregulated immune signaling is observed in subclasses of DLBCL. However, they were also a reminder of some neglected aspects of DLBCL biology (47).

Aspects apart from B-cell receptor and NF κ B signalling

MYC amplifications and overexpression (48, 49) and BCL2 amplifications (47) were neglected players in recent years, since there was a very strong focus on B-cell receptor, NF κ B and Toll-like-receptor (TLR) signaling. However, a study by the Gascoyne group published in 2012 revealed that 30-50% of DLBCL cases show high MYC protein levels (50-52) with profound clinical implications. Additionally, work from the lab of M. Shipp demonstrated the pronounced impact of the E2F1-MYC tandem on DLBCL aggressiveness (53). This shifted some focus back to other equally important components in lymphoma signaling (54) that are crucial regulators of cell cycle, apoptosis and senescence (55-57).

Mouse models in lymphoma

For modelling the impact of multiple players on an immune cell-derived disease and analyzing the causality of specific genetic lesions, murine models are an invaluable tool (58).

The model of Burkitt's lymphoma showing the critical biological impact of the MYC gene behind the enhancer of the immunoglobulin μ chain (named E μ) that was among the first breakthroughs made in this area already published in the 1980s (59). Recently, the co-operativity of MYD88L265P with BCL2 in driving lymphoma (60) was presented. A model from the K. Rajewsky group showing the co-operativity of BCL6, alternative NF κ B signaling and the importance of BLIMP1 in lymphomagenesis (61, 62) began to reveal interdependent pathways in lymphoma development. These studies made the crucial step from descriptive to functional lymphoma genomics.

Scope of the dissertation, research questions and choice of model systems

Against the background of an E μ -myc lymphoma model (59), we wanted to use MYC as a constant variable to combine it with other genetic lesions to address the following central questions:

- a) Which genetic lesions affecting NFkB and B-cell receptor signalling are able to drive lymphomagenesis in co-operation with E μ -myc?

For those that would give rise to lymphomas:

- 1) Would this alter their histopathology, histopathological features like Ki67 and cellular failsafe programs like senescence?
 - 2) Would they differ in their transcriptome?
 - 3) Would the genetic lesions affect the lymphoma/immune system interactions?
 - 4) Are the genetic lesions redundant and which cell signaling impacts are specific for each lesion?
 - 5) Can we find genetic vulnerabilities that can be therapeutically exploited?
-
- b) How would these genetic lesions affecting NFkB and B-cell receptor signaling influence the biology of manifest E μ -myc driven lymphomas?
-
- 1) Would this alter their histopathology, histopathological features like Ki67 and cellular failsafe programs like senescence?
 - 2) Would they differ in their transcriptome?
 - 3) Would the genetic lesions affect the lymphoma/immune system interactions?
 - 4) Are the genetic lesions redundant and which cell signaling impacts are specific for each lesion?
 - 5) Can we find genetic vulnerabilities that can be therapeutically exploited?
 - 6) Would they change their metabolic phenotype?

To address the questions discussed in a), we chose a fetal liver cell (FLC) based approach for hematopoietic stem cell transplantation. In this approach, fetal liver cells with

a desired genetic background (e.g. wildtype, E μ -myc transgenic) are retrovirally transduced with a gene or knockdown construct of interest based on the MMLV-derived MSCV retroviral vector (63). This allows the relatively fast screening of a clonal-hematopoiesis-like impact of genetic lesions (43). The E μ -myc transgenic fetal liver cells specifically overexpress MYC in the B-cell lineage, since MYC is under the IgM enhancer control in this system (59).

To be able to see the enrichment of a mutant, however, only 5-10% of an FLC population was transduced with a GFP-tagged retroviral construct. Thus, the enrichment of cells carrying the genetic lesion can be easily checked by monitoring the GFP positive cell fraction (64). After transduction, FLCs were transplanted into total body-irradiated, syngeneic C57BL6/N mice.

To address the questions discussed in section b), we randomly picked eight primary E μ -myc tg lymphomas from our animal matings. To determine the biological impact of a chosen set of genetic lesions, we also decided for a retroviral transduction approach. However, requiring pure populations in this system, we flow-sorted the cells after transduction to purities of >95% GFP positivity (i.e. carrying the genetic lesion of interest). The E μ -myc system has the advantage that cells can be short-term-transduced in cell culture and afterwards retransplanted into non-immunocompromised syngeneic animals without losing or changing their properties and characteristics (65). After very short transduction periods, flow sorting and keeping the cells a maximum of 72 hours in cell culture, we were able to study the biology of the genetic lesions in a *primary cell in vivo* setting. Additionally, only the retransplantation approach allowed us to study 1) organ tropism, (not presented within this dissertation) 2) immune lymphoma interactions and 3) tumor architecture and histopathological features *in situ*. The named aspects were severe restrictions of previous mainly cell-line-based functional approaches (24, 33, 34). After looking for the appropriate system, the second most important issue was to select the genetic lesions to study. We decided to use CARD11 and MYD88 as two TLR/MALT signaling components, CD79B as a highly important surface molecule in B-cell receptor signaling and NFKBIZ as a recently discovered and frequent directly NFkB dysregulating feature of DLBCL upregulated upon LPS stimulation (7). They are all mutated (CD79B, CARD11, MYD88) or amplified (NFKBIZ) in at least 15% of DLBCLs used in the

respective studies and are therefore all “hot spot” loci in DLBCL biology. As we chose our mutants with a focus on immune signaling, we looked for a possibility to oppose this principle by transducing the lymphomas with another construct. We therefore decided to use the $\text{IkB}\alpha\Delta N$ “superrepressor” (66, 67) that has a C-terminal 70 amino acid truncation to prevent its ubiquitination and proteasomal degradation and is supposed to inhibit NFkB activation (58, 68)

After having chosen the system and the intervention variables we also needed to agree on the desired read-outs for appropriate pre-analytic sample preparation from a relatively early time-point.

Concerning histopathological analysis, we decided to have an evaluation done by a professional pathologist. As central parameters, we were first looking for Ki67 staining as a proliferation mark (69), H3K9me3 staining as a senescence mark (70, 71) and overall architecture via a hematoxylin-eosin stain.

Coming to the transcriptome analysis, we had the opportunity to perform large-scale RNA sequencing within the DKFZ high-throughput sequencing facility and a bioinformatics collaboration with Dr. Liam Childs (Deutsches Krebsforschungszentrum) and Dr. Dorothee Childs (European Molecular Biology Laboratory). This method is superior to microarrays with regard to technical reproducibility, dynamic range of transcript detection and exploratory analysis (72, 73).

Regarding the study of lymphoma/immune interactions, the most important aspect was to be able to study the system in genetically unmodified C57BL6/N mice with undisturbed architecture of lymphoid organs.

The metabolically disturbed subgroups of DLBCL have so far only been described on basis of transcriptome or proteome data (27, 74). We wanted to approach the question concerning the extent to which genetic interventions can alter the metabolic phenotype of manifest lymphomas immediately on a metabolite level (75). We approached this through a LC/GC MS screening in collaboration with Dr. Jan Lisec (76-78) (Max Planck Institute for Plant Physiology and the Metabolomics Core Facility of the German Cancer Research Center). Metabolomics has been proven to be a successful tool in plant functional genomics (79).

Materials and Methods

All mouse experiments described in this thesis were approved by the Landesamt für Gesundheit und Soziales Berlin under legal permissions G0229/15 and G0133/16 and conform with the appropriate regulatory standards for improved animal care at the research center for experimental medicine (FEM) and the three R principle (80).

Chemicals

5-Bromo-4-chloro-3-indolyl β-D-galactopyranoside (X-Gal)	Sigma-Aldrich, St. Louis, MO, USA
Acetonitril	Sigma-Aldrich, St. Louis, MO, USA
Agarose	Carl Roth GmbH + Co. KG, Karlsruhe
Ampicillin	Carl Roth GmbH + Co. KG, Karlsruhe
Bovine-Albumine	Carl Roth GmbH + Co. KG, Karlsruhe
Bradford Reagent	Carl Roth GmbH + Co. KG, Karlsruhe
Bromphenolblue Powder	Carl Roth GmbH + Co. KG, Karlsruhe
Calciumchloriddihydrate	Carl Roth GmbH + Co. KG, Karlsruhe
Chloroform	J.T. Baker, St. Philipsburg, NJ, USA
Chloroquine	Carl Roth GmbH + Co. KG, Karlsruhe
DAPI	Thermo Fisher Scientific, Waltham, MA, USA
Dextrose	Carl Roth GmbH + Co. KG, Karlsruhe
DMSO	Sigma-Aldrich, St. Louis, MO, USA
dNTPs	Analytik Jena, Jena
EDTA	Carl Roth GmbH + Co. KG, Karlsruhe
Ethanol	Carl Roth GmbH + Co. KG, Karlsruhe
Ethidiumbromide Powder	Carl Roth GmbH + Co. KG, Karlsruhe
Formaldehyde	Merck Millipore, Billerica, MA, USA
Formic acid	Sigma-Aldrich, St. Louis, MO, USA
GhostRed	Tonbo Biosciences, San Diego, CA, USA
Glycerol	Carl Roth GmbH + Co. KG, Karlsruhe
Isoflurane	Abbvie, Chicago, IL, USA
Isoproanol	Carl Roth GmbH + Co. KG, Karlsruhe

KCl	Carl Roth GmbH + Co. KG, Karlsruhe
KH ₂ PO ₄	Carl Roth GmbH + Co. KG, Karlsruhe
LPS (E.Coli 0111:B4, phenol purified)	Sigma-Aldrich, St. Louis, MO, USA
Methanol	J.T. Baker, St. Philipsburg, NJ, USA
MgCl ₂	Carl Roth GmbH + Co. KG, Karlsruhe
MgSO ₄	Carl Roth GmbH + Co. KG, Karlsruhe
MTBE	J.T. Baker, St. Philipsburg, NJ, USA
NaHCO ₃	Carl Roth GmbH + Co. KG, Karlsruhe
NH ₄ Cl	Carl Roth GmbH + Co. KG, Karlsruhe
NP40	Sigma-Aldrich, St. Louis, MO, USA
Paraformaldehyde	Carl Roth GmbH + Co. KG, Karlsruhe
Phenylmethylsulfonyl flouride	Sigma-Aldrich, St. Louis, MO, USA
Phosphatase inhibitors	F. Hoffmann-La Roche, Base, CH
Polybrene	Carl Roth GmbH + Co. KG, Karlsruhe
Potassium hexacyanoferrate	Sigma-Aldrich, St. Louis, MO, USA
Potassium hexacyanoferrate trihydrate	Sigma-Aldrich, St. Louis, MO, USA
Protease Inhibitors	F. Hoffmann-La Roche, Basel, CH
Sodium Dodecylsulfate	Sigma-Aldrich, St. Louis, MO, USA
Sodiumazide	Carl Roth GmbH + Co. KG, Karlsruhe
Sodiumdeoxycholate	Carl Roth GmbH + Co. KG, Karlsruhe
Triton X-100	J.T. Baker, St. Philipsburg, NJ, USA
Tryptone/Pepton from casein	Carl Roth GmbH + Co. KG, Karlsruhe
Xylene Cyanol	Sigma-Aldrich, St. Louis, MO, USA
β-mercaptoethanol	Carl Roth GmbH + Co. KG, Karlsruhe

Antibodies

AF555 Goat anti Rabbit IgG	Thermo Scientific, Waltham, MA, USA
Anti Goat IgG polyclonal Donkey IgG	R&D, Minneapolis, MN, USA
HRP conjugated	
Anti Mouse IgG2a F4/80 PE BM8	BioLegend, San Diego, CA, USA
Anti-Biotin APC Bio3-18E7	Miltenyi Biotech, Bergisch-Gladbach

BioPlex Pro Phospho-Btk (Tyr 223)	Cell Signalling, Danvers, MA, USA
BioPlex pro total Btk	Cell Signalling, Danvers, MA, USA
CD3e Rabbit monoclonal IgG D4V8L	Cell Signalling, Danvers, MA, USA
Detection cocktail lineage mouse biotin conjugated: CD5, CD11b, CD45R, Anti-7-4, Anti-Gr-1 (Ly6G/C), and Anti-Terr-119.	Miltenyi Biotech, Bergisch-Gladbach
F(ab')-goat anti Mouse IgM	eBioscience, Waltham, MA, USA
H3K9me3 rabbit polyclonal ab 8898	Abcam, Bristol, UK
Isotype ctrl. rat IgG2a kappa PE/Cy7	BioLegend, San Diego, CA, USA
RTK2758	
Isotype ctrl. rat IgG2a kappa RTK2758	BioLegend, San Diego, CA, USA
APC	
Isotype ctrl. rat IgG2a kappa RTK2758	BioLegend, San Diego, CA, USA
FITC	
Isotype ctrl. rat IgG2a kappa RTK2758	BioLegend, San Diego, CA, USA
PE	
Mouse alpha Tubulin IgG1B-5-1-2	Sigma-Aldrich, St. Louis, MO, USA
MyD88 polyclonal goat IgG	R&D, Minneapolis, MN, USA
PE Rat Anti Mouse CD274 Clone	BD Biosciences, Heidelberg
MIH5, IgG2a	
Polyclonal rabbit anti mouse NFkB p65 Sc 8008	Santa Cruz, Dallas, TX, USA
Polyclonal Rabbit Syk IgG 2712	Cell Signalling, Danvers, MA, USA
Polyclonal Rabbit Zap70/pSyk (Tyr 352) 2701	Cell Signalling, Danvers, MA, USA
Rat anti B220 IgG2a, micro beads RA3-62B	Miltenyi Biotech, Bergisch-Gladbach
Rat anti mouse Ki67 IgG2a Tec3	Dako, Santa Clara, CA, USA
Rat IgG2a anti mouse CD8 53-6.7 PE	BioLegend, San Diego, CA, USA
Rat IgG2a anti mouse Sca1 PE D7	Miltenyi Biotech, Bergisch-Gladbach

Rat IgG2b anti mouse CD117 PerCP 3C11	Miltenyi Biotech, Bergisch-Gladbach
Rat IgG2b anti mouse CD3 17A2 PE/Cy7	BioLegend, San Diego, CA, USA
Rat IgG2b anti mouse CD4 Gk 1.5 FITC	BioLegend, San Diego, CA, USA
Rat IgG2b anti-Mouse CD11b M1/70 APC	BioLegend, San Diego, CA, USA

Buffers

Luria-Bertani medium

Tryptone	10g
Yeast extract	5g
NaCl	10g
add H ₂ O to 1L and autoclave	

HBS

NaCl	280mM
KCl	10mM
Na ₂ HPO ₄	1.5mM
dextrose	12mM
HEPES	50mM

adjust pH to 7.05 with 0.5 N NaOH;

RIPA Cell lysis buffer

sodium chloride	150mM
NP-40	1%
sodium deoxycholate	0.5%
SDS (sodium dodecyl sulfate)	0.1%
Tris, pH 8.0	50mM
Protstop	1 Tablet/10ml
Phosstop	1Tablet/10ml

Triton X lysis buffer

Triton X-100	1%
NaCl	150mM
Tris-Cl, pH 8.0	50mM
Protstop	1 Tablet/10ml
Phosstop	1Tablet/10ml

TAE

Tris	40mM
EDTA	2mM
Acetic acid	20mM
pH adjusted to 8.5	

DNA Loading Buffer 6x

Glycerol	30%
Bromphenol blue	0.25%
Xylene cyanol	0.25%

PBS

NaCl	137mM
KCl	27mM
Na ₂ HPO ₄	10mM
KH ₂ PO ₄	1.8mM

Proteinase K Lysis Buffer

Tris, pH 8	1M
EDTA, pH 8	0.5M
SDS	10%
NaCl	5M

FACS Buffer

PBS

Bovine albumin 0.5%

Sodium azide 0.09%

Senescence associated β -galactosidase fixation solution

PBS containing 1mM MgCl₂ to pH 6

Paraformaledhyde 2%

Glutaraldehyde 0.25%

Senescence associated β -galactosidase staining solution

K₃Fe(CN)₆ 41mg

K₄Fe(CN)₆ trihydrate 52.5mg

40 mg/ml DMSO X-Gal 0.25ml

PBS containing 1mM MgCl₂ add to 10ml

Cell Culture Media

3T3 Medium

89% DMEM high Glucose Thermo Scientific, Waltham, MA, USA

10% FCS Sigma-Aldrich, St. Louis, MO, USA

1% Penicillin/Streptomycin Merck Millipore, Billerica, MA, USA

FluxMedium

DMEM no D-Glucose, no Sodium Thermo Scientific, Waltham, MA, USA

pyruvate

20% FCS Sigma-Aldrich, St. Louis, MO, USA

BCM

44% IMDM	Thermo Scientific, Waltham, MA, USA
44% DMEM Glucose High	Thermo Scientific, Waltham, MA, USA
20% FCS	Sigma-Aldrich, St. Louis, MO, USA
1% Pen/Strep	Merck Millipore, Billerica, MA, USA
1% Glutamine	Merck Millipore, Billerica, MA, USA
0.89µl β-mercaptoethanol	

FLC Medium

BCM	80%
FLC Cocktail (81) consisting of:	20%
	information for 1ml 5x stock
IL3	5ng
IL6	50ng
SCF	500ng
	all cytokines bought from Peprotech, Hamburg
WEHI supernatant	10%
FCS	90%

Plasmids

MSCV 2.2 Empty IRES-GFP	AG Schmitt
pRS H1-shscrambled-PGK GFP (a random scrambled sequence of shA20)	AG Schmitt/Maurice Reimann and Sven Masswig
MSCV MYD88L265P IRES GFP	AG Schmitt/Maurice Reimann and Sven Masswig
MSCV CARD11L244P IRES GFP	AG Schmitt/Soyoung Lee
MSCV PD-L1 wildtype IRES GFP	AG Schmitt/Maurice Reimann and Sven Masswig

MSCV CD79BY196H IRES GFP	AG Schmitt/Maurice Reimann and Sven Masswig
MSCV IkB α ΔN IRES GFP	Claus Scheidereidt (67)
MSCV NFKBIZ IRES GFP	Cloning procedure see methods section
LTR MYD88L265P H1 scrambled PGK GFP	AG Schmitt/ Maurice Reimann and Sven Masswig
LTR MYD88L265P H1 shPD-L1 PGK GFP	AG Schmitt/ Maurice Reimann and Sven Masswig

Human aggressive lymphoma-derived mutations are depicted. For cloning the ortholog murine sequence was used. Thus, for human CARD11L244P, murine CARD11L251P was cloned, for human MYD88L265P, murine MYD88L252P was cloned, and for human CD79B196H murine CD79Y195H was cloned and used in subsequent experiments. The nomenclature in this dissertation always refers to the human mutation.

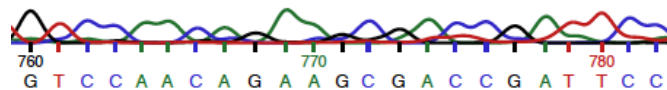
Confirmation of mutations in vectors encoding mutant proteins

Below the blasted (82) sequencing results for the regions, where we expected the respective mutations, are shown (highlighted in red, bold letters). The aligned nucleotide to amino acid sequence, and the trace of the base calls in the mutation-bearing region are shown. Note that the mismatch between the NCBI Reference Sequence: NP_780571.2 and the sequence in our CARD11L244P vector (highlighted in green) is a naturally occurring polymorphism that can be accessed via GenBank: AY135367.1 and was not reported to have functional consequences.

MYD88L252P (murine ortholog of MYD88L265P)

→blastx

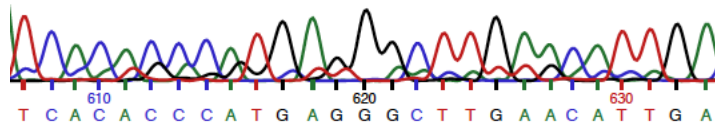
Query	730	LSLSPGVQQKR P IPIKYKAMKKDFPSILRFITICDYTNPCTKSWFWTRLAKALSLP	897
		LSLSPGVQQKR IPIKYKAMKKDFPSILRFITICDYTNPCTKSWFWTRLAKALSLP	
Sbjct	241	LSLSPGVQQKR L IPIKYKAMKKDFPSILRFITICDYTNPCTKSWFWTRLAKALSLP	296



CD79BY195H (murine ortholog of CD79BY196H)

→blastx

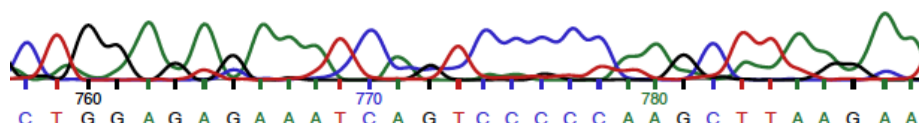
Query	560	DKDDGKAGMEEDH T HEGLNIQDTATYEDIVTLRTGEVKWSVGEHPGQE	703
		DKDDGKAGMEEDH T EGLNIQDTATYEDIVTLRTGEVKWSVGEHPGQE	
Sbjct	181	DKDDGKAGMEEDH T YEGLNIDQDTATYEDIVTLRTGEVKWSVGEHPGQE	228



CARD11L251P (murine ortholog of CARD11L244P)

→blastx

Query	733	EECKLERNQS P KLKNDIENRPRKE H VLELERENEMLTKIHELQSIIQAGKRSLPDSDK	909
		EECKLERNQS KLKNDIENRPRKE VLELERENEMLTKIHELQSIIQAGKRSLPDSDK	
Sbjct	241	EECKLERNQS L KLKNDIENRPRKE Q VLELERENEMLTKIHELQSIIQAGKRSLPDSDK	299



Retroviral vector

The vector used throughout this study was the MSCV 2.2 vector. A detailed plasmid map retrieved from Addgene 11/15/17 (83) depicting the vector without an insert is shown below. The full sequence can be obtained via <https://www.addgene.org/60206/>.

Vector map

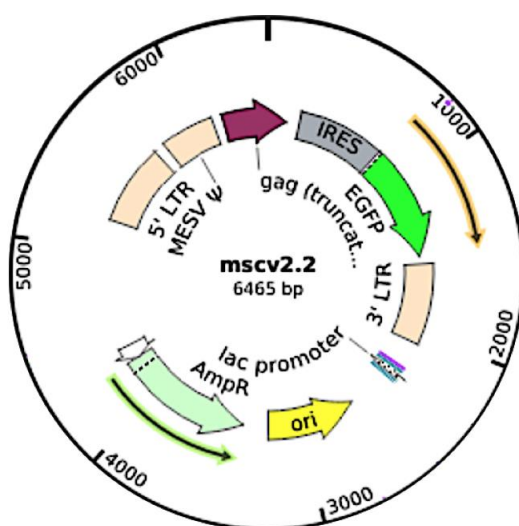


Figure 1: Vector map of MSCV 2.2 empty-IRES GFP

Enzymes

DnaseI	Quiagen, Hilden
Dream Taq	Thermo Scientific, Waltham, MA, USA
EcoRI	New England BioLabs, Ipswich, MA, USA
Proteinase K	Merck Millipore, Billerica, MA, USA
Rnasin	Promega, Madison, WI, USA
Superscript II	Thermo Scientific, Waltham, MA, USA
T4 ligase	Promega, Madison, WI, USA
Trypsin/EDTA	Merck Millipore, Billerica, MA, USA
XbaI	New England BioLabs, Ipswich, MA, USA
Xhol	New England BioLabs, Ipswich, MA, USA

Disposables

0.22µM & 0.45µM female Luer Lock	VWR, Radnor, PN, USA
Filters	
0.9 ml rolled micro flasks glass	Bischoff Chromatografie, Leonberg
1,5 ml sterile PCR grade tubes	Eppendorf, Wesseling-Berzdorf
10cm cell cultures dishes, 6 well & 96 well cell culture test plates	TPP techno Plastic Products, Trasadingen, CH
50 ml & 15 ml Falcons	BD Bioscience, Heidelberg
45µM cell strainers	BD Bioscience, Heidelberg
5, 10, 20, 50 ml serological pipets	BD Bioscience, Heidelberg
50ml Bacterial tubes	BD Bioscience, Heidelberg
FACS tubes	BD Bioscience, Heidelberg
GentleMACS C tubes	Miltenyi Biotech, Bergisch-Gladbach
MP fast prep lysing beads & matrix tubes matrix D	MP Biomedicals, Eschwege

OptiPlate RQ PCR tubes	Thermo Scientific, Waltham, MA, USA
Pasteur glass pipets	VWR, Radnor, PN, USA
PCR strips	VWR, Radnor, PN, USA
Scalpel	B. Braun, Melsungen
Sterile pipet tips	Biozym Scientific, Hessisch Oldendorf
1, 10, 30 ml male luer lock syringe	BD Bioscience, Heidelberg
19G, 25G, 27G, 30G canullas	B. Braun, Melsungen
10 mm disposable cuvettes	VWR, Radnor, PN, USA

Lab Instruments

-80° freezer	NuAire laboratory Equipment, Fernbrook, MD, USA
4°C and -20°C fridge	Liebherr, Biberach
Bacteria Incubator & Shaker Innova	Eppendorf, Wesseling-Berzdorf
Balance	Sartorius, Göttingen
Bioanalyzer 2100	Agilent Technologies, Santa Clara, CA, USA
BioPhotometer	Eppendorf, Wesseling-Berzdorf
Cell Culture Centrifuge	Thermo Scientifc, Waltham, MA, USA
Christ alpha 2-4 LD plus	Martin Christ Gefriertrocknungsanlagen, Osterode
Christ RVC 2-33	Martin Christ Gefriertrocknungsanlagen, Osterode
Eppendorff pipets 1-10µl, 2-20µl, 10-100µl, 100-1000µl	Eppendorf, Wesseling-Berzdorf
Electrophoresis Power Supply	Consort, Turnhout, BEL
Ferm Press	Synopac, Aesch, CH
Gene Flash UV imager	Syngene, Cambridge, UK
Gentle MACS dissociator	Miltenyi Biotech, Bergisch-Gladbach
horizontal Gel chambers	Thermo Scientific, Waltham, MA, USA
IKA chip vortex	IKA, Staufen
Incubator CB160	Binder, Tuttlingen

Microscope Standard 25	Zeiss, Oberkochen
Mouse Cages and air removal system	Tecniplast, Buguggiate, IT
Mouse Strainer	
MP FastPrep 24	MP Biomedicals, Eschwege
Nanodrop	Thermo Fisher, Waltham, MA, USA
Octo MACS cell separator	Miletnyi Biotech, Bergisch-Gladbach
Olympus Flourescence Microscope	Olympus, Hamburg
Phase Contrast Microscope PrimoVert	Zeiss, Oberkochen
Pipet boy	Integra Bioscience, Biebertal
Sterile Cell Culture Bench	NuAire laboratory Equipment, Fernbrook, MD, USA
Sterile Mouse Bench	Heraeus, Hanau
Table centrifuge	Eppendorf, Wesseling-Berzdorf
Thermo Cycler T100	BioRad, Hercules, CA, USA
Thermomixer	Eppendorf, Wesseling-Berzdorf
Vortex Shaker	IKA, Staufen
BioPlex Pro wash Station	BioRad, Hercules, CA, USA
pH meter five easy plus	Mettler Toledo, Columbus, OH, USA

Analysis Instruments

Amnis Image Stream Mark II Imaging	Amnis, Seattle, WA, USA
Flow Cytometer	
Biorad S3e FlowSorter	BioRad, Hercules, CA, USA
Bruker Impact II MS	Bruker Corporation, Billerica, MA, USA
GSR D1 γ irradiator	Gamma Service Medical, Leipzig
Guava 12 HT Flow Cytometer	Merck Millipore, Billerica, MA, USA
HiSeq2000 Sequencing System	Illumina, San Diego, CA, USA
Luminex MAGPIX	BioRad, Hercules, CA, USA
Perkin Elmer Viktor Plate Reader	Perkin Elmer, Waaltham, MA, USA
Applied Biosystems Step One Plus	Thermo Scientific, Waltham , MA, USA

Simon Western Blot System	ProteinSimple, San Jose, CA, USA
Kits	
Agilent Nano 6000 eukaryote Total RNA	Agilent Technologies, Santa Clara, CA, USA
BD Fix/Perm	BD Bioscience, Heidelberg
Cell Signalling reagent Kit	BioRad, Hercules, CA, USA
CSH-C18 column	Waters, Eschborn
HSS-T3 column	Waters, Eschborn
Luminex instrument validation Kit	Luminex, Austin, TX, USA
Luminex instrument calibration Kit	Luminex, Austin, TX, USA
MACS MS cell separation columns	Milentyi Biotech, Bergisch-Gladbach
NEBNext ChIP Seq	New England BioLabs, Ipswich, MA, USA
Proline Universal Calibration Beads	BioRad, Hercules, CA, USA
PureLink Maxi Prep	Thermo Fisher Scientific, Waltham, MA, USA
PureLink MiniPrep	Thermo Fisher Scientific, Waltham, MA, USA
QuiaQuick Gel extraction Kit	Qiagen, Hilden
RneasyPlus Mini Kit	Qiagen, Hilden
Simon Master Kit Mouse & Rabbit	ProteinSimple, San Jose, CA, USA
SmarTer Ultra low Input RNA Kit	Takara, Tokyo, JPN
TaqManMasterMix	Thermo Scientific, Waltham, MA, USA
TransAM NFkB Flex Kit	Active Motif, Carlsbad, CA, USA
TruSeq RNA library prep Kit v2	Illumina, San Diego, CA, USA
Cell Signalling reagent Kit	BioRad, Hercules, CA, USA

Software for data analysis

Amnis Ideas	Amnis, Seattle, WA, USA
GraphPadPrism8	GraphPadInc, San Diego, CA, USA
R version 3.3.2 x86_64-apple-darwin13.4.0	The R Foundation for Statistical Computing, Vienna, AU

Genotyping

a) DNA prep of mouse tail biopsies

25 μ l Proteinase K was added to 475 μ l lysis buffer and the tail biopsy was digested overnight in the solution at 55°C. The digested tail biopsy was spun down at maximum speed for 10 min. The supernatant was mixed with 500 μ l 4°C isopropanol and vigorously shaken. The tube was spun down again for 10 min at maximum speed. Afterwards, the supernatant was discarded. 500 μ l EtOH was added to the mixture and incubated for 10 min at RT. Afterwards, the tube was again spun for 5 min at maximum speed and the supernatant was discarded with the remaining pellet, which is the purified DNA, and can be dissolved in H₂O and placed overnight at 4°C for complete solution.

b) E μ -myc PCR (59)

PUC1	17mer	5'-CAG CTG GCG TAA TAG CGA AGA G-3'
PUC2	20mer	5'-CTG TGA CTG GTG AGT ACT CAA CC-3'
Mouse Tubulin Hin	19mer	5'-CGC GAG TGC ATT TCA GTC C-3'
Mouse Tubulin Rück	20mer	5'-TCC CAG TGA TAA GCT GCT CT-3
19,3 μ l		dH ₂ O
2,5 μ l		10x DreamTaq Puffer
0,4 μ l		dNTP
0,3 μ l		Tubulin Hin
0,3 μ l		Tubulin Rück
0,5 μ l		PUC1
0,5 μ l		PUC2
0,2 μ l		DreamTaq Polymerase
1 μ l		DNA at 100ng/ μ l

94°C 3 min

94°C	60 sec	
65°C	60 sec	32 cycles
72°C	90 sec	

72°C 5 min

c) Suva PCR (89)

MB3131	23mer	5'-GTT GAT GCT TCC TGG TGT GTA GG-3'
MB3132	24mer	5'-TTT GAG GGG ACG ACG ACA GTA TCG-3'
MB3133	22mer	5'-AAC AGA TGT GGG GTT GGT GGA G-3'
14,90µL		dH ₂ O
2,50µL		10xPuffer (I)
1,00µL		dNTP
2,50µL		DMSO
0,80µL		MB3131
1,00µL		MB3132
0,30µL		MB3133
1,00µL		TaqPolymerase
1,00µL		DNA

92°C 5 min

92°C	1 min	
55,9°C	1 min	34 cycles
72°C	70 sec	
72°C	10 min	

d) p53 PCR (87)

X7	18mer	5'-TAT ACT CAG AGC CGG CCT-3'
X6.5	20mer	5'-ACA GCG TGG TGG TAC CTT AT-3'
16,30µl	dH ₂ O	
2,00µL	10x Buffer	
0,40µl	dNTP	

0,40µl	X7
0,20µl	X6.5
0,20µl	TaqPolymerase
0,50µl	DNA

92°C 5 min

92°C	30 sec
62°C	1 min 34 cycles
72°C	1 min
72°C	5 min

Cell preparation

a) Fetal liver cells (FLC)

Fetal liver cells were generated by mating E μ -myc transgenic SUV39H1 y/- male mice and SUV39H1 -/- female mice or by mating E μ -myc transgenic male mice with wildtype female mice. After vaginal plaques were detectable, pregnant mice were sacrificed and fetuses (12-14 d) were extracted. Livers from fetuses were explanted and fetal cells were isolated. Heads of fetuses were used for genotyping and processed as mouse tail biopsies. Fetal livers were smoothly crushed between two glass slides and filtered through a 45µm nylon mesh and afterwards used for experiments (88)

b) Lymphomas:

After palpability of cervical lymph nodes could be repeatedly felt within an interval of at least 2 days in fetal liver cell transplanted total body irradiated mice, animals were euthanized using isoflurane anesthesia (94) and final suffocation was performed using CO₂ at a flow rate of 8l/min. The time of the second, confirmatory tumor palpation is shown in the fetal liver cell generated lymphoma Kaplan-Meier plot as lymphoma onset.

For retransplanted, retrovirally transduced and sorted manifest E μ -myc transgenic lymphomas, initial tumor palpability, which was almost always accompanied by moribund appearance, served as the “survival” time point which is depicted in the Kaplan-Meier curves.

Mice were flushed with 70% ethanol and fixated on aluminium coated styrofoam. At first, skin was prepared from underlying serosa, and superficial inguinal and cervical lymph nodes were isolated. Afterwards, a median sterno-laparotomy was performed for the evaluation of position of internal organs, size and gross anatomic abnormalities. Afterwards a mostly enlarged lymph node along the superior mesenteric artery was also excised.

Blood smears were made by puncturing the abdominal aorta and aspirating remaining blood. One inguinal lymph node was immediately fixed in 4% formaldehyde for subsequent histopathological analysis and the other one snap frozen for subsequent metabolomics analyses. The residual lymph nodes were crushed using the gentle MACS isolation system and filtered through a 45 μ m nylon mesh to generate a single cell suspension (75).

Cells were spun down for 5min at 300g and the supernatant was discarded. The remaining pellet was checked for color to exclude excessive erythrocyte contamination. For long term storage, cells were resuspended in 10% DMSO and 90% BCM, aliquoted in 1.5ml freeze tubes and cooled down slowly in 4°C pre-cooled isopropanol filled Mr Frosty freezing containers and frozen to -80°C. After 24 hours -80°C tubes were transferred to liquid nitrogen tanks.

Cell culture

Cells stored in liquid nitrogen were put into the incubator until a slight film of fluid inside the freezing tube became visible. Immediately afterwards cells were spun down in 10ml of BCM for 5 min at 300g and the supernatant was discarded afterwards.

Lymphoma cells were grown in 2ml of BCM within tissue culture six-well test plates. Medium was conditioned using 3T3 fibroblast feeders exploiting their senescence associated phenotype by irradiating them with 30Gy. Irradiated 3T3 feeders were exchanged and prepared freshly every week. Cells were grown at an optimal density of approximately 10⁶ cells per ml (57).

Medium composed of one third 2 days 3T3 pre-conditioned medium and two thirds fresh BCM was replaced every 2 days by spinning down the lymphoma cells for 5 min at 300g and resuspending them in fresh medium.

FLCs were also grown in tissue culture six-well plates using 1ml of FLC medium per well. Cells were grown at an optimal density of approximately 5×10^5 cells per ml. Medium was exchanged every day. For medium exchange, cells were spun down for 5 min at 300g and resuspended in 1ml of FLC medium.

NIH 3T3 cells and phoenix cells were grown in DMEM supplemented with 10% FCS and one percent penicillin/streptomycin in 10-cm dishes. Cells were grown to confluence and then split by washing twice with PBS and then incubated for 5 min at 37°C. Cells were washed off their dishes by gently pipetting up and down with 3T3 medium and replated on new dishes. Finally, 10ml of medium was added.

Incubator conditions for all cells were 37°C temperature, 5% CO₂ and 95% humidity.

Plasmid amplification

To obtain sufficient amounts of plasmid DNA for transfections and ensuing retroviral transductions, competent bacteria (95) were transformed using the 42°C heat shock method and afterwards selected for 24 hours on ampicillin agar plates. Afterwards a single clone was picked and an overnight broth using 500ml of LB-medium supplemented with 100mg/l ampicillin was prepared and put into a 37°C pre-warmed shaker at 200 rpm and ambient air. After 14-16 hours bacteria were harvested and plasmid DNA was isolated using Invitrogen DNA plasmid maxi prep kit yielding approximately 500µg plasmid DNA per prep. Plasmid inserts were partially sequenced after every amplification to ensure that the correct material was used with Verify_hin primer 5' CTTTATCCAGCCCTCACTCCTT 3'.

Cloning of NFKBIZ

The murine NFKBIZ (NM_001159395.1) cDNA was obtained from OriGene. The gene was amplified out of the OriGene plasmid using following primers:

NFKBIZ-hin: 5' **AGTTCTCGAGGCCACC**ATGATCGTGGACAAGCTGCTG 3'

NFKBIZ-rück: 5' **AGTTGAATTCTAGTATGGTGGTGCTCGCT** 3'

purple: 4 bp overhang **green**: restriction sites for Xhol (NFKBIZ-hin) and EcoRI (NFKBIZ-rück) **red**: Kozak sequence (96) black: complementary sequence to NFKBIZ

The primers contain both an Xhol and the EcoRI restriction sites, a Kozak overexpression sequence and a 4-base pair overhang in addition to the complementary sequences to NFKBIZ. Primers were designed with the help of Primer3 Plus (97).

92°C	5 min
92°C	30 sec
62°C	1 min 35 cycles
72°C	3 min
72°C	6 min

The amplified PCR product was run on a 1% agarose gel supplemented with 0.5 µg/ml ethidium bromide at 80 V for 1 hour. The gel band was visualized using a UV imaging system and purified with the QuiaQick gel extraction Kit. Xhol and EcoRI cut MSCV empty backbone was ligated with the amplicon using T4 ligase by coincubation for 1 hour at 16 °C. The same reaction was also set up without NFKBIZ insert as a ligation control.

T4 ligase	1µl
T4 DNA ligase Buffer	2µl
Xhol and EcoRI cut MSCV empty backbone	100ng
NFKBIZ insert/ H2O control	50ng
H ₂ O	To 20µl

Competent bacteria were transformed with the ligation products and plated overnight on ampicillin plates. Mini Preps of individual clones were made from various clones and digested with Xhol and EcoRI. Clones that showed an appropriate insert size after digestion were sequenced using Sven_hin primer having the following sequence 5' TCCCTTTATCCAGCCCTC 3'.

Retroviral transduction and transplantation

a) Transfection and Virus Production

For retroviral transduction, Phoenix cells (91, 98) at a passage number <18 were grown to a confluence of approximately 80% on 10-cm cell culture plates. 1 hour prior to transfection 3T3 medium was exchanged.

For CaCl₂ transfection 62.5µl of 2M CaCl₂ were mixed with 10µg of helper plasmid (99) and plasmid of interest for infection. H₂O was added to 500µl in a FACS tube. Using a glass Pasteur pipette, 2xHBS buffer was added in droplets under gentle bubbling. 2µl of chloroquine and the precipitate was added to the medium of prepared phoenix plates (100).

14 hours after the addition of the precipitate, 3T3 medium was replaced by 5ml of BCM.

Efficient transfection was visually checked by fluorescence microscopy.

After 24 hours, virus containing medium was harvested and filtered using a 0.45µm luer lock syringe. 5ml of BCM was added, harvested and filtered for another three 12 hours cycles (57).

b) Lymphoma transduction

Retroviral supernatant was supplemented with polybrene and added to 1 day pre-cultured lymphoma cells plated on 3T3 feeders. Medium was exchanged every 12 hours. After 48 hours virus containing medium was removed and replaced with normal B-cell medium. Cells were grown for another 12 hours to achieve maximal GFP expression for quantification. Cells were gated for FL1log vs. FL2log fluorescence intensity. Sorting was performed with 5x10³ events per second in purity mode. Cells were checked to contain >95% GFP+ cells of the viable population. Immediately after sorting, cells were transplanted into 8 to 12 week-old C57BL6/N mice via tail vein injection (65).

c) Fetal liver cell (FLC) transduction (101-103)

FLCs were pre-cultured for two days before transduction. For transduction cells were resuspended in 1.6ml retroviral supernatant and 0.4ml of 5xFLC cocktail was added. Retroviral supernatant and FLC cocktail were exchanged after 24 hours. After 48 hours,

cells were replated in FLC medium and left for 12 hours to allow for maximal GFP expression of transduced cells.

Immediately prior to transplantation, GFP positivity was assessed and documented via FACS. In case of GFP positivity >10% of total FLCs cells were diluted with untransduced FLCs to a maximum of 10% GFP+ total viable cells.

8 to 12 week-old C57BL6/N mice with weights between 20g and 22g were total-body-irradiated with 9Gy for bone marrow ablation and 8 hours post irradiation transplanted with at least 10^6 total FLCs. E μ -myc fetal liver cell transductions in experiments shown in this dissertation were performed in equal shares by Dr. Maurice Reimann and Jens Schrezenmeier with technical assistance from Sven Masswig. From day 7-14 post transplantation mice were controlled daily for weight development and scored for well-being. In case of weight reductions >20% from d0 weight of transplantation mice were euthanized using isoflurane anaesthesia and CO₂ suffocation.

d) Disease Onset Monitoring

Mice were monitored for the onset of the disease every day by palpation of the peripheral, prescapular and cervical lymph nodes (LN). "well palpable" lymphoma reflects LN enlargements of 5mm or more.

Florescence-activated cell sorting (FACS) analyses

For FACS analysis, antibodies were diluted 1:500 in FACS buffer and 5×10^5 cells were incubated for 30 min at RT in 1ml staining solution protected from light. The respective isotype controls and unstained controls were always equally treated and measured before and after the experimental samples. Assessment of true positivity was made by clear distinction of log vs. log plots of adjacent channels to distinguish staining from autofluorescence (104). PD-L1/2 staining and data acquisition on E μ -myc transgenic MYD88L265P, NFKBIZ and empty FLC lymphomas, FLC immune cell infiltration and stem cell stainings were performed by Dr. Maurice Reimann with the respective antibodies being tested and verified in wildtype C57BL6/N spleen and bone marrow cells by myself.

Immunohistochemistry

Lymph nodes were fixed in 4% formaldehyde and transferred to PBS 24 hours later.

At the Institute of Pathology formalin sections were paraffin embedded, tissue sections were prepared and stained for HE, H3K9me3 (105), Ki67 (69) and initially evaluated by Dr. P. Lohneis.

RT quantitative PCR

Reverse transcription was performed using the following reaction setup

Oligo dT primer	500ng
Total RNA	1µg
dNTP mix	1µl
H ₂ O	to 12µl

The reaction was heated for 5 min to 65°C and afterwards quickly chilled on ice.

Thereafter following reagents were added

5x First strand buffer	5µl
0.1M DTT	1µl
RNAsin	1µl

The reaction was thereafter heated for 2 min at 42°C.

Finally, 1µl of superscript II reverse transcriptase was added and incubated using following protocol

42°C	50min
70°C	15min

For RQ analysis of selected transcripts TaqMan probes were obtained from ThermoScientific, Waltham, MA, USA.

The following probes were used

GAPDH	Mm99999915_g1
NFKBIZ	Mm00600522_m1
MYD88	Mm00440339_g1
CARD11	Mm01201965_m1

All reactions were carried out in triplicates including H₂O and no RT controls

H ₂ O	16
cDNA at a pre-diluted concentration of 100ng/ μ l	1 μ l
MasterMix	2 μ l
Assay probe	1 μ l

The following protocol was run for RQ PCR

50°C	2min	
95°C	10min	
95°	15s	40 cycles
60°C	1min	

Trans AM NFkB DNA binding ELISA (106)

For Trans AM NFkB Binding assays, 5x10⁶ freshly thawed cells were lysed for 20 min on ice using 200 μ l RIPA lysis buffer and afterwards spun down for 10 min at 15 000g in a pre-cooled microfuge.

Protein concentration was determined by using Roti Quant reagent. A standard row was prepared using a concentration range of 1-10 μ g/ml bovine albumin. 1ml of Bradford solution was therefore placed in a cuvette and read using a spectrophotometer. For sample protein concentration determination, 1 μ l of sample was added to 1ml Bradford solution and the concentration was determined after inverting the cuvette. The assay was performed according to the manufacturer's protocol. Ten μ g of total cell protein lysate was used per well. The final reaction was read on a Perkin Elmer Viktor Plate reader at 450nm absorbance for 0.1 s per well.

p65 nuclear translocation assay (107, 108)

For p65 nuclear translocation assay, freshly thawed cells were immediately fixed for 20 min on ice in BD Fix buffer. Afterwards, cells were washed with 1xBD Perm buffer and incubated for 12 hours in 1:1000 polyclonal rabbit anti-mouse p65 AB diluted in 1xBD Perm buffer at 4°C protected from light. The isotype control aliquot was equally treated with IgG2a isotype control antibody. Cells were washed twice with BD perm buffer and incubated for 2 hours in 1:100 goat anti rabbit IgG conjugated with AF555 diluted in 1xBD

Perm buffer. Then, the cells were washed once with BD Perm buffer and again with PBS. Finally, cells were resuspended in PBS and immediately prior to run DAPI was added at a final concentration of 300nM.

20 000 ungated events were acquired for each sample on an Amnis Image Stream Mark II Flow Cytometer. Laser settings for the Image Stream X were as follows: 405nm 5mW, 561nm 100mW, 642nm 0.78mW. The 488nm laser was shuttered to avoid spill over between neighboring channels. Analysis was performed using the Amnis Image Stream Ideas Software. The method implemented in IDEAS software for assessing nuclear translocation is made by a linearized form of Pearson's correlation coefficient (109, 110) of median pixel intensity for each pixel of the DAPI image and p65 image, respectively. This is performed using following formula summed over all 4256 pixels into which every picture is decomposed:

$$\rho = \frac{\sum_i (x_i - \bar{X})(y_i - \bar{Y})}{\sqrt{\sum_i (x_i - \bar{X})^2} \sqrt{\sum_j (y_j - \bar{Y})^2}}$$

Pearson's formula is transformed using the following operator as described by George et al.:

$$\text{Similarity} = \ln \left(\frac{1 + \rho}{1 - \rho} \right) \quad (107)$$

Senescence-associated β -galactosidase staining (111)

For detection of senescence-associated beta galactosidase staining, 10^5 cells were centrifuged on a glass slide using a cytopsin insert. Cells were afterwards fixated using freshly prepared fixative solution. After fixation, cells were washed twice with PBS containing 1mM MgCl₂. The staining solution was added and cells were incubated overnight at 37°C protected from light. Intervention and control samples were always stained in parallel. The reaction was stopped by washing the sample three times with PBS. Senescence-associated β -galactosidase stainings shown within this dissertation were performed by Sven Masswig.

Luminex assays (112)

a) Bruton's Tyrosine Kinase Assay

For Luminex-based BTK and BTK Tyrosine 223 phosphorylation assays, cells were immediately lysed after thawing using BioPlex cell lysis Kit according to the protocol and protein concentration was determined as described in the TransAm section. For positive controls, thawed cells were incubated with 25 μ g/ml F(ab') got anti mouse IgM for 30 min and 120 min to estimate activation dynamics or 75 μ g/ml E. coli LPS for 120 min (113). Lysates from growing NIH3T3 cells served as negative controls. The assay was performed according to the manufacturer's instructions using the BioRad Cell Signalling reagent Kit and BioPlex Pro Phospho-Btk (Tyr 223) and BioPlex pro total BTK antibodies. 10 μ g protein per well were used for total and phosphoprotein assays from the same lysis batch. Wash steps were automatically performed using the BioPlex Pro wash station with a magnetic plate holder after accurate programming. The final reaction was read on a Luminex MAGPIX system counting 10³ events per well. Results were analyzed with BioRad Xponent software.

RNA Sequencing for transcriptome profiling (73, 114)

Before we began our study, we calculated the power in terms of biological replicates and sequencing depths using the "scotty" web tool (115). The final number of aligned reads shows, whether we achieved the desired power (Figure 2).

For RNA isolation generated FLC samples were B220+ (MSCV-empty-GFP transduced E μ -myc transgenic FLC lymphomas) or GFP+ purified (MSCV-lesion-GFP transduced E μ -myc transgenic FLC lymphomas) via cell sorting. All lymphomas were incubated with B220+ antibody during sorting. Cells were afterwards checked via FACS to be >90% B220 or GFP positive (Figure 3) (116). RNA was prepped using Quiagen Rneasy+ kit which involves genomic DNA extraction columns and an on-column DNA digest according to the protocol. Manifest MSCV-lesion-GFP-transduced E μ -myc lymphoma samples were immediately subjected to RNA extraction after thawing of liquid-nitrogen-stored single-cell whole lymph node samples containing B-cells and tumor stroma.

Purified RNA was analyzed on an Agilent 2100 Bioanalyzer with the 6000 Agilent Nano Eukaryote total RNA kit for assessment of concentration, RNA quality and DNA contamination (Figure 3) (117).

Power calculation for RNA sequencings studies

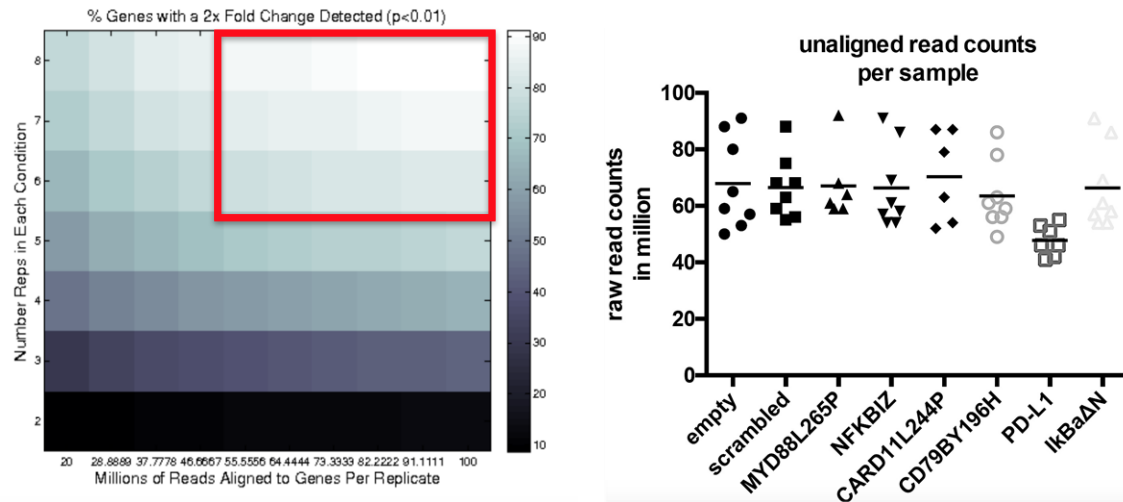


Figure 2: Power calculation using “scotty” (115). The red quadrangle represents power of $>80\%$ to detect genes with a two-fold change for $p<0.01$ for a model of human lymphocyte cell line sequencing data provided by Kasowski et al. (97). The graph on the right depicts the number of unaligned reads per sample after sequencing of manifest lesion-transduced lymphomas. Each dot represents one biological replicate. Approximately 70%-80% of reads could be ensuingly aligned and used for statistical modelling.

Sorting strategy and RNA quality

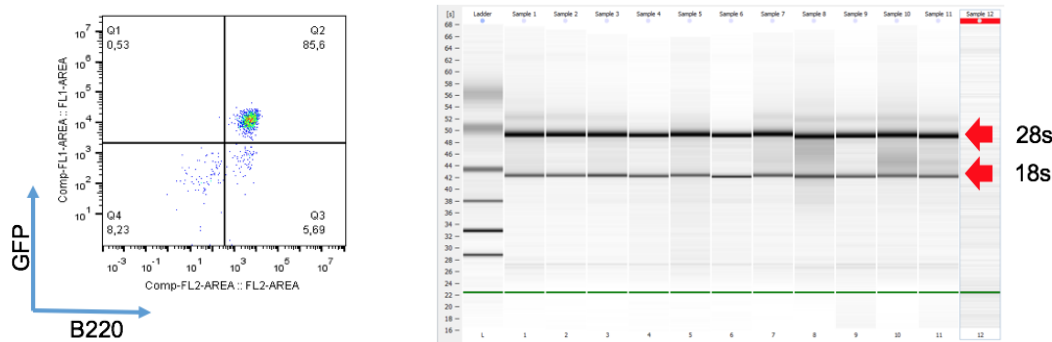


Figure 3: Exemplary FACS plots for MYD88L265P GFP+ purified cells. Cells were stained with B220 PE (FL2). FL1 shows GFP positivity of cells. Plots are representative for input RNA quality. Samples on lanes 8 and 10 show high residual DNA contamination between the 28s and 18s rRNA peaks and were re-DNA digested before proceeding to library prep.

Libraries were prepared with the TruSeq Low Input Kit (Illumina) with an input of 1 μ g of total RNA in matched-pair lymphoma samples. Libraries from FLC samples were prepared using SmarTer Ultra low Input RNA Kit and NEBNext ChIP Seq from 10ng (118) total RNA due to low material availability.

The samples were sequenced with a depth of ca. 7×10^7 50 base pair single-end reads on a HiSeq 2000 Illumina Sequencer (Figure 2) (119, 120). Library preparation and sequencing were performed by the DKFZ High Throughput Sequencing Facility.

Fastq output files were aligned using STAR aligner (121). BAM/SAM Files were analyzed using DSeq2 (122) implemented in the current R 3.2 version. All software mentioned is publicly available via Bioconductor (84). Graphs were created using ggplot2 (123). Alignment and analysis were performed in collaboration with Dr. Liam Childs (German Cancer Research Center, Heidelberg) and Dr. Dorothee Childs (European Molecular Biology Laboratories, Heidelberg).

Metabolic profiling (77-79)

a) Metabolite Snapshot Profiling

For total metabolite GC and LC MS metabolomics experiments (78), whole lymph nodes from euthanized animals were snap frozen in liquid nitrogen.

For LC/GC runs representative pieces of approximately 15mg were cut with a scalpel from snap-frozen lymph nodes and weighed afterwards. Tissue pieces were disrupted using a tissue homogenizer.

Sample aliquots were extracted in 750 μ l MMC (1:1:1 Methanol:MTBE:Chloroform mixture, -20°C). In a SpeedDry centrifuge, 100 μ l and 200 μ l of the upper, polar phase and 300 μ l of the lower non-polar phase of each sample were dried down separately. Polar aliquots were further subjected to either GC-APCI-MS (gas chromatography-atmospheric pressure chemical ionization-mass spectrometry, using automated derivatization with Pyridin/MSTFA (76), or LC-ESI-MS (liquid chromatography-electrospray ionization-mass spectrometry) using a HSS-T3 column and 0.1% formic acid and acetonitrile/0.1% formic acid as mobile phases, A and B, respectively. The non-polar aliquot was subjected to LC-ESI-MS using a CSH-C18 column and 60% acetonitrile/0.1% formic acid/10mM ammonium formate and 90% isopropanol/10% acetonitrile/0.1% formic acid/10mM ammonium formate as mobile phase A and B respectively.

Raw data files were processed using an in-house tool chain based on xcms (124) to chromatographically align samples, subtract chemical noise, detect peaks and deconvolute spectra. Spectra were further annotated in targeted (through library comparison) and non-targeted (de novo interpretation) fashion, which ultimately allows relative quantification of compounds between samples. Metabolite levels were finally normalized for weight of cut lymph nodes pieces.

Statistical Evaluation

RNA sequencing data

For the analysis of RNA Seq data, a generalized linear model (125) , assuming that gene x in sample L follows negative binomial distribution, was used (114). This initial matrix was multiplied by a normalization factor matrix s to account e.g. for differences in

sequencing depth, gene length etc. Within group variability was additionally modelled with the empirical Bayes shrinkage method (126) in Dseq2 making within-group variance dependent on dispersion to a pre-formed fit model and degrees of freedom (127) of the examined system. In the case of our still rather low numbers of biological replicates per group, we tested against the null hypothesis of zero log fold change. The principal steps described for deriving a linear model from count matrix data and testing against the H_0 hypothesis are all implemented with modifiable default parameters in the Dseq function within the Dseq2 R package (122). Adjustment of p-values is implemented in DSeq2 by the padjust command and correcting with the method proposed by Benjamini and Hochberg (128).

Kaplan-Meier curves and Log-Rank test

For the analysis of survival, the Kaplan-Meier estimator (129) was used to model behavior of data relating to mouse survival. The Log-Rank test (130) was used to test the H_0 hypothesis that there is no difference in survival between two groups.

Analysis of Variance (ANOVA)

A one-way analysis of variance was used to test in histopathological analyses and Luminex assays the H_0 hypothesis that all samples were drawn from the same group using the Bonferroni method for multiple testing correction (131).

Principal component analysis

We used this tool of multivariate analysis to reduce our multi-dimensional analyses from metabolomics and transcriptomics to two-dimensional vector spaces for depicting separating variables encompassed by those eigenvectors.

Essentially, PCA means to solve an eigenvalue equation for an n-dimensional matrix of observables potentially correlated with each other, with the components of the new vector system being the eigenvectors maximizing the variance between observables.

For excellent accounts on matrices and vector transformations see matrix section in Atkin's Physical Chemistry and Vectors and Tensors by Dan Fleisch (132, 133)

Sample distances

Sample distances were calculated using the Poisson distance command within PoiCICluster package (134). Sample distance is estimated using a hierarchical clustering approach on the dissimilarity of count matrices from each sample whose observables are presumed to be Poisson-distributed. For mathematical background see “Classification and clustering of sequencing data using a Poisson model” (134).

Annotation clustering

Functional annotation clustering was performed using the DAVID web tool (135). In the first step, a pre-curated database of gene-sets representing functional biological motives and a list of differentially regulated genes from an experiment are provided. Afterwards, all overlapping matching genes of the deposited gene lists are evaluated, a correlation matrix is built and the overlap of gene-sets with matching hits from the input gene list is calculated using kappa statistics (136). This initial correlation matrix is enriched by a seed-agglomeration algorithm described in “The DAVID Gene Functional Classification Tool: a novel biological module-centric algorithm to functionally analyze large gene lists” (137). Finally, an enrichment statistics is generated by the geometric mean of the individual clusters’ EASE scores (138).

Results

Capacity of genetic lesions to co-operate with E μ -myc in hematopoietic stem cells to induce lymphomagenesis

Experimental setup

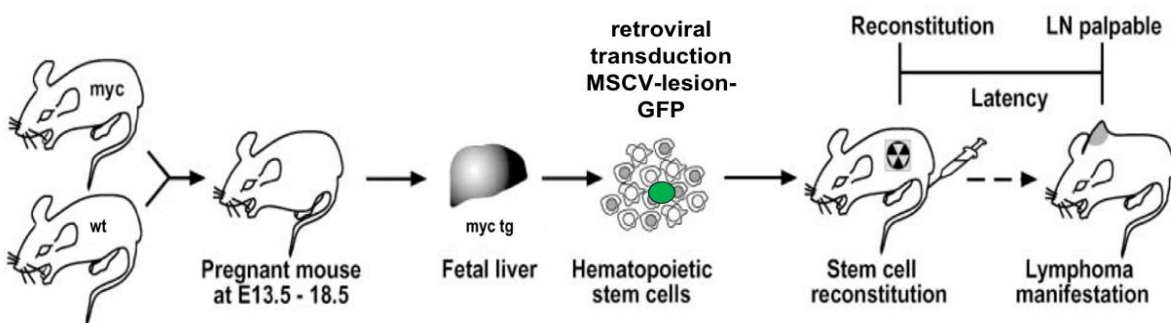


Figure 4: Illustration adapted from Schmitt et al. (88) presenting our experimental setup

Initially, we wanted to know which of our chosen lesions would be able to cooperate with MYC in lymphomagenesis. We transplanted MSCV-GFP transduced E μ -myc transgenic fetal liver cells (FLCs). These E μ -myc transgenic FLCs were transduced with either empty-GFP, MYD88L265P-GFP, NFKBIZ-GFP, CD79BY196H or CARD11L244P-GFP. Our aim was that 5-10% of transplanted total MSCV-GFP transduced E μ -myc transgenic FLCs were GFP positive i.e. carried the desired genetic lesion (illustration of procedure shown in Figure 4). Initial testing of 12 different MSCV-GFP transduced E μ -myc transgenic FLCs from different matings and infecting them with either MSCV-empty-GFP, MSCV-MYD88L265P-GFP, MSCV-NFKBIZ-GFP or MSCV-CARD11L244P-GFP showed that the proportion of infected cells in the hematopoietic stem cell population (i.e. Sca1+cKit+Lin-1) was always exactly twice as high as the proportion in the total FLC population. This means that a proportion of 10% GFP+ Sca1+cKit+Lin- (transduced "true" hematopoietic stem cells) cells were found when 5% of the total FLCs were measured to be GFP+. We usually achieved infection rates above 10% of total FLCs. Therefore, we always ran experiments with a population of untransduced cells in a neighboring well to

dilute transduced cells to an amount of <10% GFP+ FLCs before transplantation in case of the infection is too effective.

A representative example of the FACS analysis of the proportion of Sca1+Lin-cKit+GFP+ FLC is shown in Figure 5. The overexpression of the transduced mutations was confirmed by RNA sequencing (Table 1 and Appendix 1).

Effectiveness of stem cell transduction

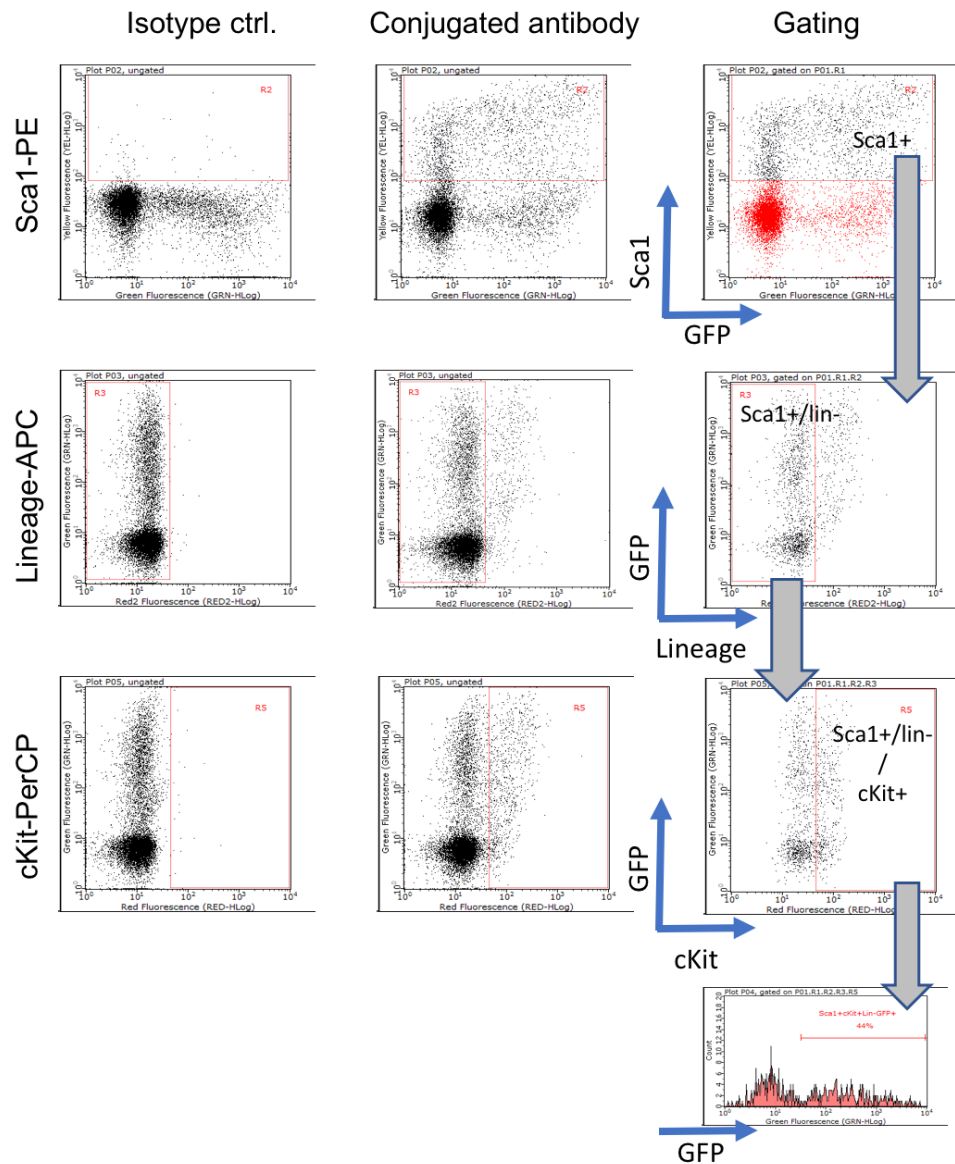


Figure 5: Twelve transduced total MSCV-GFP transduced μ -myc transgenic FLCs populations using either empty-GFP, CARD11L244P-GFP or MYD88L265P-GFP were

analyzed for the proportion of containing Sca1+cKit+lin- cells and the transduction effectiveness via GFP expression. The figure above depicts an exemplary image illustrating the gating strategy and amount of GFP+ cells and Sca1+cKit+lin- cells after transduction.

We examined which mutations were capable to be oncogenic drivers. We considered those lymphomas to be GFP positive (i.e. driven by our transduced genetic lesion) if lymph nodes from mice presenting with lymphadenopathy showed >70% of viable B220+ cells were GFP positive as determined by FACS. This scenario never occurred when we transduced either MYD88L265P or CARD11L244P into wildtype FLCs generated from C57BL/6 mice without additional genetic lesions (Table 2). In a E μ -myc transgenic background, three groups unveiled during the experiment. In transplantation experiments using MSCV-GFP transduced E μ -myc transgenic FLCs almost all mice carrying 5-10% of cells transduced with MSCV-NFKBIZ-GFP or MSCV-MYD88L265P-GFP developed lymphadenopathy in almost all transplanted mice. The extracted lymph nodes proved to be of B-cell origin and displayed >70% GFP+ for B220+ cells in subsequent FACS analysis (Figure 6 and 8). MYD88L265P lymphomas manifested as palpable lymphadenopathy between days 30 and 70 in almost all transplanted animals. In the case of NFKBIZ-transduced animals, palpable lymphadenopathy occurred between days 60 and 110 (Figures 7 and 8).

No mouse transplanted with MSCV-empty-GFP-transduced E μ -myc transgenic FLCs developed a GFP+ lymphoma (Table 2). A total of 20 empty lymphomas from 50 MSCV-empty-GFP-transduced E μ -myc FLC transplanted mice were generated.

MSCV-CD79BY196H-GFP transduced E μ -myc transgenic FLCs showed a much weaker phenotype, with approximately 20% of transplanted mice developing GFP+ lymphoma (Table 2). Another observation was that half of GFP+ MSCV-CD79BY196H-GFP-transduced E μ -myc transgenic FLC lymphomas developed after 240 days which did not occur in the other examined mutant settings (Figure 8). The third group is represented by CARD11L244P. CARD11L244P did not result in a single green lymphoma in 30 MSCV-CARD11L244P-GFP-transduced E μ -myc transgenic FLC transplanted mice over the observation period of 300 days (Table 2 and Figure 8).

Overexpression of transduced mutants in RNA Seq data from manifest lesion transduced E μ -myc lymphomas

Contrast	baseMean	log2FoldChange	pvalue	Padj	mgi_symbol
empty vs. CARD11L244P	12160.03005	-0.657108495	5.89328E-10	3.67476E-06	Card11
empty vs. CD79BY196H	41928.88429	-0.387291579	0.000546371	0.035677283	Cd79b
empty vs. <i>IkBαΔN</i>	13016.56199	-2.091471234	5.39401E-33	6.97715E-29	Nfkbia
empty vs. MYD88L265P	3733.00971	-1.060430423	8.12262E-09	6.22071E-06	Myd88
empty vs. NFKBIZ	2898.505739	-1.439644749	1.25623E-09	2.09778E-05	Nfkbiz
empty vs. PD-L1	7779.58205	-3.13035133	5.16102E-28	8.16989E-24	Cd274

Table 1: The statistics of overexpressed lesion-vector-transduced manifest E μ -myc lymphomas compared to the empty vector control transduced E μ -myc lymphomas as determined by RNA Seq is shown above. n=6 for MYD88L265P and n=7 for CARD11L244P and PD-L1 and n=8 for the other lesions and n=8 for empty vector control.

Penetrance of mutants in MSCV- GF-transduced E μ -myc transgenic FLCs and MSCV-GFP-transduced wildtype FLCs

E μ -myc +	Transplanted mice	Lymphomas	GFP+ Lymphomas
empty	50→	20→	0
MYD88L265P	19→	18→	17
NFKBIZ	14→	13→	13
CD79BY196H	31→	12→	6
CARD11L244P	30→	12→	0

Wildtype +	Transplanted mice	Lymphomas	GFP+ Lymphomas
empty	15→	2→	0
MYD88L265P	11→	3→	0
CARD11L244P	9→	2→	0

Table 2: The number of mice transplanted that did not meet the criterion of >20% of initial weight reduction until day 21 post irradiation, the numbers of these mice developing lymphadenopathy (blue column) and the number of animals whose lymphoma met the criterion of >70% of B220+ cells being GFP+ (green columns) are shown. The numbers

are shown for the transplant settings of transplantation of retrovirally transduced fetal livers cells without additional lesions and E μ -myc transgenic fetal liver cells.

Number of GFP+B220+ cells in MSCV-lesion-GFP-transduced E μ -myc tg FLC lymphomas

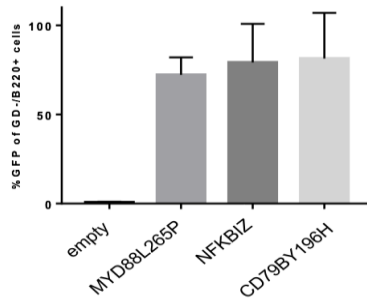


Figure 6: The number of GFP+B220+ cells in percent within the empty vector transduced cohort, MYD88L265P, NFKBIZ and CD79BY196H-driven lymphomas. n=6 for empty, n=11 for MYD88L265P, n=5 nor NFKBIZ and n=3 for CD79BY196H.

Survival curve for mice presenting with lymphadenopathy transplanted with MSCV-GFP-transduced-E μ -myc transgenic FLCs

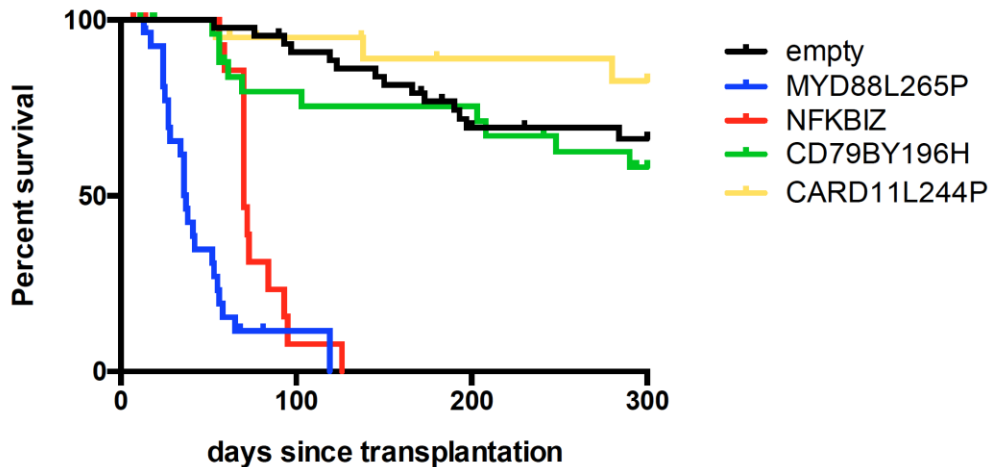


Figure 7: The Kaplan-Meier plot above depicts mice presenting with lymphadenopathy. The corresponding numbers of transplanted mice, resulting lymphomas and resulting GFP+ lymphomas can be found in table 2 with the absolute number of lymphomas shown in the blue column. Mice dying from other causes were censored and are marked as ticks in the curve. P<0.0001 for empty vs. MYD88L265P, P<0.0001 for empty vs. NFKBIZ,

$P=0.45$ for empty vs. CD79BY196H and $P=0.104$ for empty vs. CARD11L244P using the Log-rank test.

Survival curve for mice presenting with GFP positive lymphoma transplanted with MSCV-GFP transduced-E μ -myc transgenic FLCs

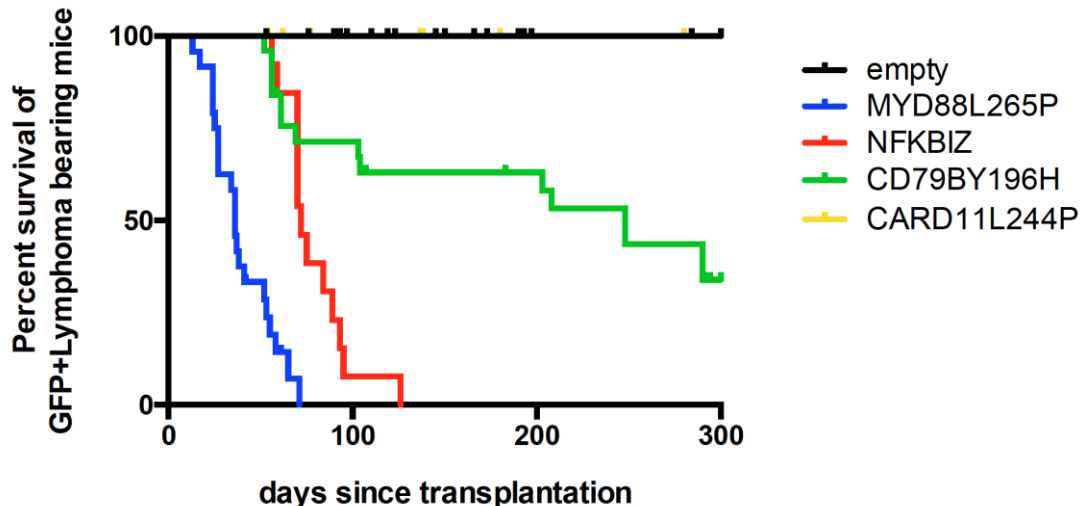


Figure 8: The Kaplan-Meier Plot above depicts the survival of mice presenting with lymphadenopathy fulfilling the criterion of >70% GFP+ for B220+ in subsequent FACS analysis. Since this event was never reached in either MSCV-empty-GFP or MSCV-CARD11L244P-GFP transduced E μ -myc FLC transplanted animals, curves without steps are shown for both groups. Animals presenting with GFP negative lymphomas or other causes are depicted as ticks in the curve. The number of mice corresponding to the respective curves can be found in the green column of table 2. $P<0.0001$ empty vs. MYD88L265P, $P<0.0001$ empty vs. NFKBIZ, $P=0.123$ for empty vs. CD79BY196H, calculated using Log-Rank test.

We continued by a histopathological analysis of the lymphomas. We were particularly interested in histopathologic observations within MYD88L265P and NFKBIZ driven lymphomas compared to empty E μ -myc transgenic lymphomas.

Whole lymphoma Ki67 stains from empty, MYD88L265P, NFKBIZ and CD79BY196H MSCV-GFP-transduced $E\mu$ -myc transgenic FLC lymphomas

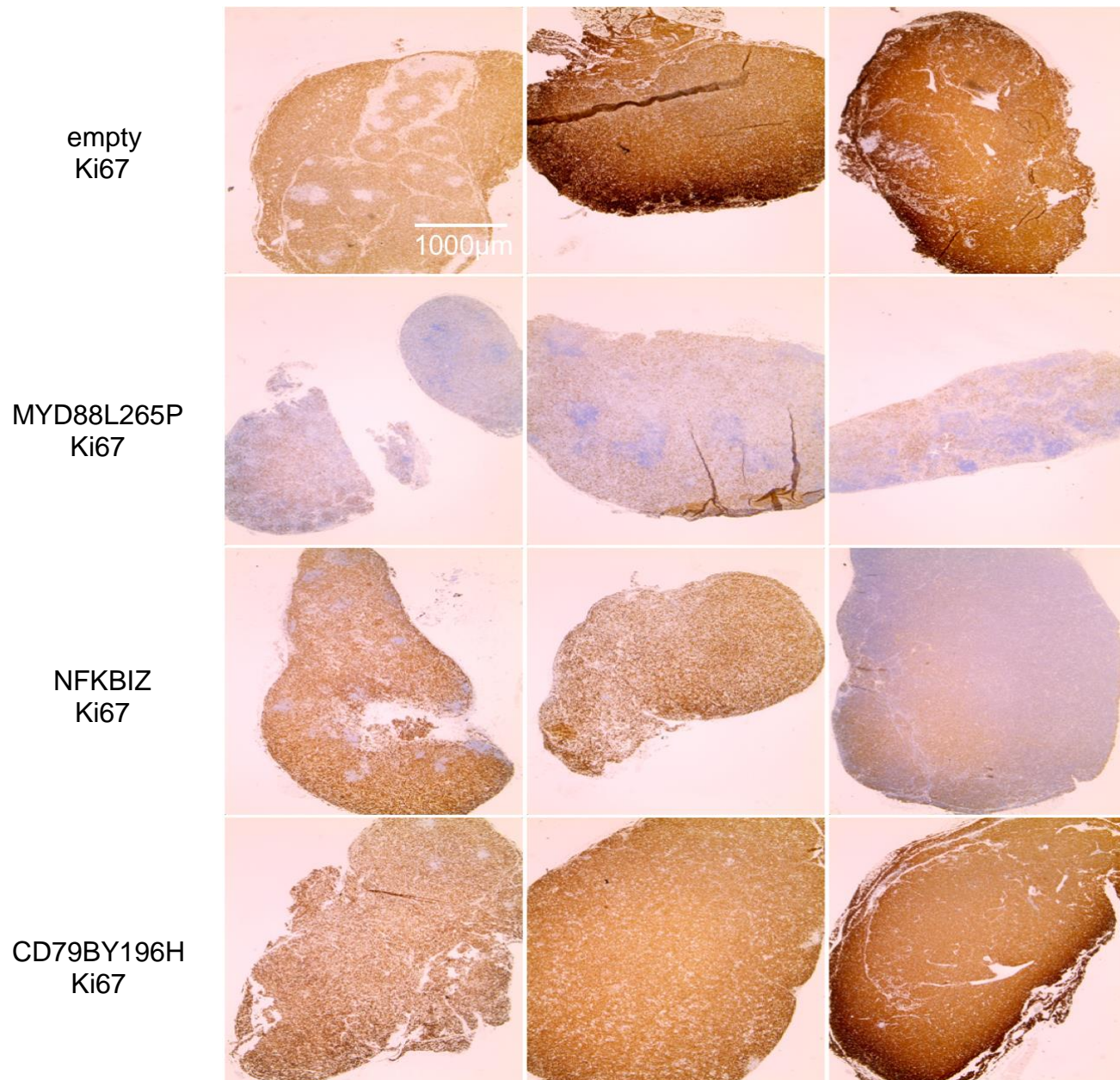


Figure 9: Ki67 stains from lymphomas in mice transplanted with MSCV-lesion-GFP transduced $E\mu$ -myc FLCs with either MSCV-empty-GFP or MSCV-MYD88L265P-GFP demonstrating overall architecture at 40x magnification are shown above. Compared to the analyzed 10 MSCV-empty-GFP transduced $E\mu$ -myc FLC lymphomas, that showed consistent Ki67 levels above 90%, all 11 analyzed lymphomas in mice transplanted with $E\mu$ -myc transgenic FLCs transduced with MSCV-MYD88L265P-GFP showed Ki67

indices below 60%. Lymphomas arising from MSCV-NFKBIZ-GFP transduced $\text{E}\mu\text{-myc}$ FLCs showed a mixed phenotype with the 7 analyzed lymphomas showing Ki67 indices between 50% and 90%.

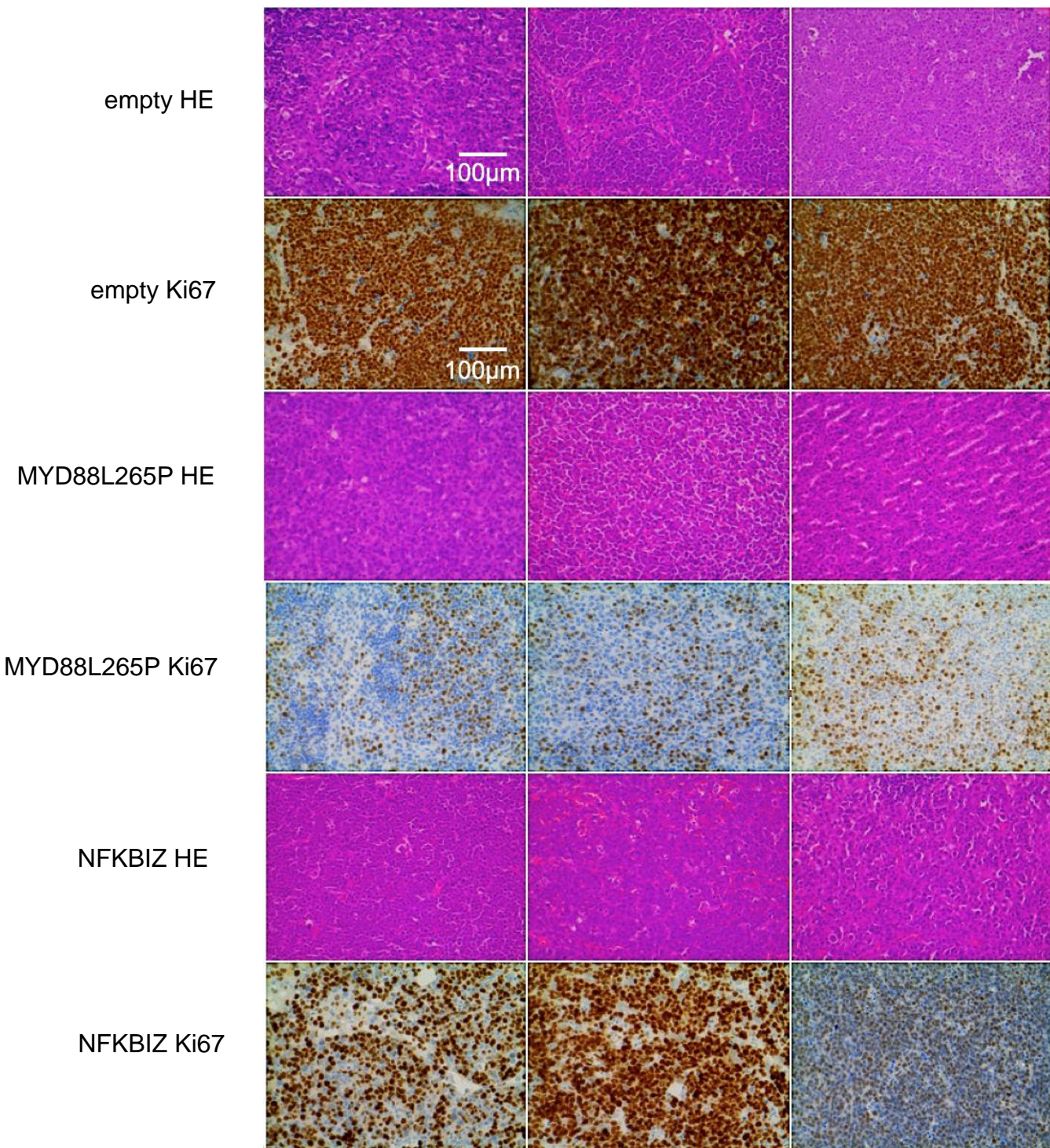


Figure 10: Immunohistochemical stains for FFPE sections of n=3 MSCV-empty-GFP transduced E μ -myc transgenic FLC lymphomas, n=3 MSCV-MYD88L265P-GFP transduced E μ -myc transgenic FLC lymphomas and n=3 MSCV-NFKBIZ-GFP transduced E μ -myc transgenic FLC lymphomas at 100x magnification.

In the next step, we analyzed CD11+F4/80+B220- macrophage, CD3+CD8+ and CD3+CD4+ -T-cell populations within total viable cells in GFP+ lymphomas from NFKBIZ, MYD88L265P and CD79BY196H driven MSCV- GFP transduced E μ -myc transgenic FLC lymphomas (Figure 11).

Immune cell subpopulations within lymphomas

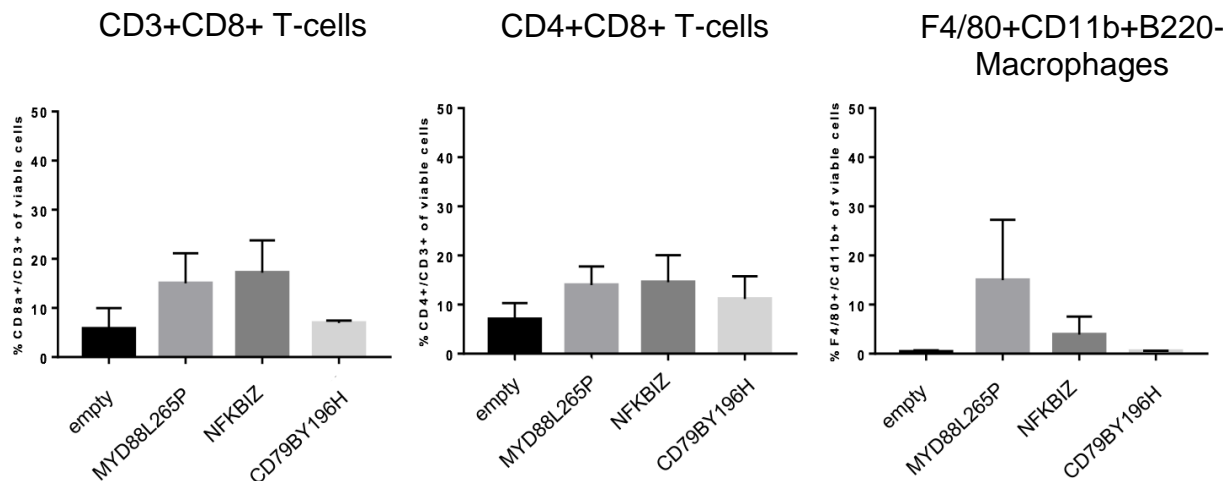


Figure 11: The amount of CD3+/CD8+ T-cells, CD3+C4+T-cells and CD11b+F4/80+B220- cells (shown as described from left to right) among total viable cells as determined by negativity for Ghost Red viability dye from MSCV-GFP transduced E μ -myc transgenic FLC lymphomas is depicted above. n=6 for empty, n=11 for MYD88L265P, n=5 nor NFKBIZ and n=3 for CD79BY196H. The empty vs. lesion comparison that passes the significance threshold after multiple testing correction using a one way ANOVA is empty vs. MYD88L265P for F4/80+CD11b+B220- cells ($p<0.0001$).

We found a significant increase in macrophage infiltration accounting on average for 15% of cells in MYD88L265P driven MSCV-MYD88L265P-GFP transduced E μ -myc

transgenic FLC lymphomas and only 2% in MSCV-empty -GFP transduced E μ -myc transgenic FLC lymphomas.

T-cell infiltration showed both for CD3+CD8+ and CD3+CD4+ a slight, yet not significant, increase in NFKBIZ and MYD88L265P driven MSCV-GFP transduced E μ -myc transgenic FLC lymphomas, indicating a different tumor-stroma crosstalk of MSCV-MYD88L265P-GFP and MSCV-NFKBIZ-GFP transduced E μ -myc transgenic FLC lymphomas compared to the empty group.

Transcriptome Analysis by RNA Sequencing in B220 and GFP purified NFKBIZ, MYD88L265P, PD-L1 and CD79BY196H-driven E μ -myc transgenic lymphomas

In the next step, we wanted to address how the different lesion driven lymphomas differ in their signaling architecture compared to empty control lymphomas.

In this section, the results for RNA Seq experiments of generated MSCV-PD-L1-GFP E μ -myc transgenic FLC lymphomas (Table 3 and Figure 17) that are directly driven by PD-L1 are already depicted.

To avoid a stroma bias due to different composition of stroma which was present between MYD88L265P and empty lymphomas (Figure 11), we purified MSCV-empty-GFP transduced E μ -myc transgenic FLC lymphomas for B220+ cells and MSCV-lesion-GFP transduced E μ -myc transgenic FLC lymphomas for GFP+ cells from which RNA was extracted for RNA sequencing.

All sorted GFP+ cells from MSCV-lesion-GFP transduced E μ -myc transgenic FLC lymphomas were also B220 positive. For MSCV-GFP transduced E μ -myc transgenic FLC lymphomas, we sequenced empty, MYD88L265P, NFKBIZ, PD-L1 and CD79BY196H driven (i.e. GFP enrichment to >70% of viable B220+ cells in mice presenting with lymphadenopathy) and empty lymphomas.

As a quality control, we observed that B220 counts were highly similar between all groups (Figure 12a).

Transcript levels of B220 in the different sequenced MSCV-lesion-GFP-transduced E μ -myc transgenic FLC lymphomas

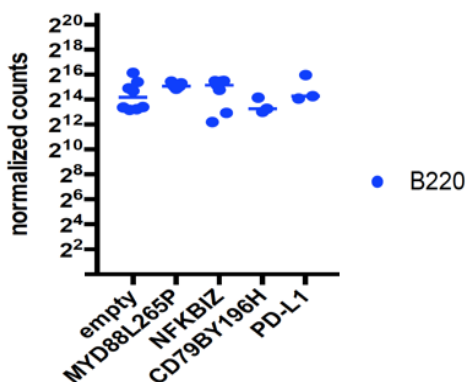


Figure 12a: B220 normalized count levels in sequenced MSCV-lesion-GFP transduced E μ -myc transgenic FLC lymphomas. Normalized counts were obtained by dividing the count matrix K_{ij} described by a generalized linear model of the negative binomial distribution family divided by a median-of-ratios constant K_r which is described by Love et al. in the methods section of “Moderated estimation of fold change and dispersion for RNA-seq data with DESeq2” (122).

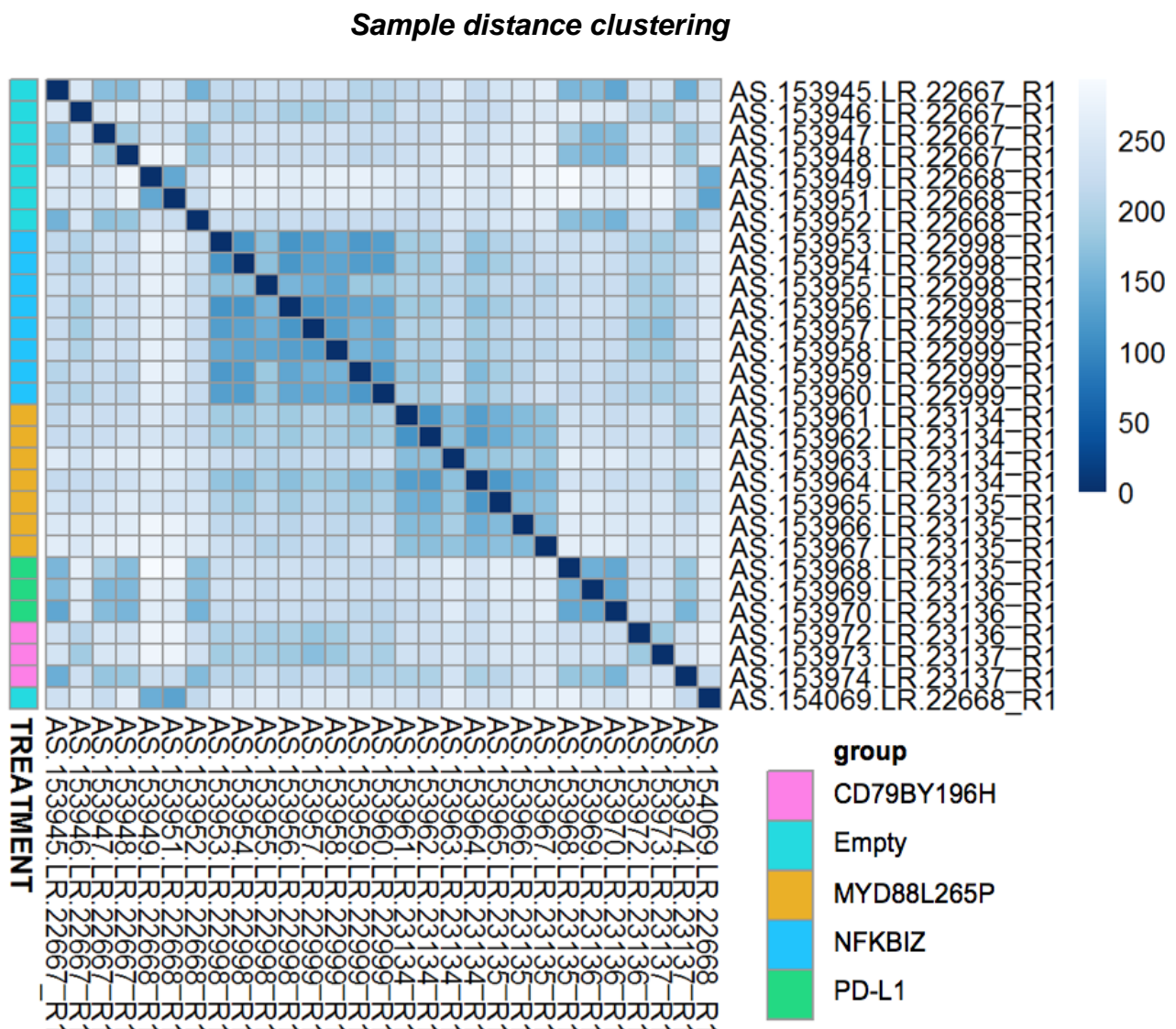


Figure 12b: Sample distances between sequenced FLC generated lymphomas showing strong clustering grouped by the driving oncogene. Number and letter codes next to the

graph show the sample attribution for the $n \times n$ Poisson dissimilarity matrix, with n_{ij} depicting the distance between two individual biological samples and $n_{i=j}$ denoting the matrix diagonal mapping the sample distance of each sample to itself and is necessarily, due to the properties of the Poisson dissimilarity measure, for sample $x_i = x_j = 0$. For further mathematical background and proofs and comparison to other clustering measures and algorithms, see D. Witten, 2011 (134). The blue, numbered bar denotes the sample Poisson distances in the matrix that are encoded by shadings of blue.

Histogram for counts of unadjusted p-values

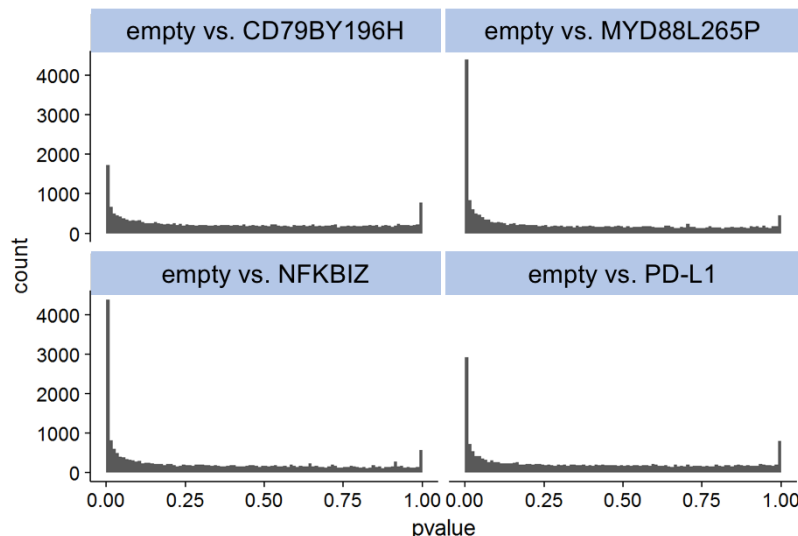


Figure 13: Probability density histogram for each group giving an empirical approximation of the true false discovery rate by reflecting the random baseline distribution of p-values for each gene. $n=8$ for empty E μ -myc transgenic lymphomas, $n=8$ for NFKBIZ E μ -myc tg lymphomas, $n=7$ for MYD88L265P E μ -myc transgenic lymphomas, $n=3$ for PD-L1 E μ -myc tg lymphomas and $n=3$ for CD79BY196H E μ -myc transgenic lymphomas.

Principal component analysis of transcriptome data

In the transcriptome data from MYD88L265P, NFKBIZ and PD-L1 driven MSCV-GFP transduced E μ -myc transgenic FLC lymphomas, we found the individual treatment groups to be highly similar and clearly clustering in the principal component analysis showing that the genetic lesion ab initio present in the FLCs induces a specific transcriptional program separating the intervention groups from each other (Figures 12b and 14).

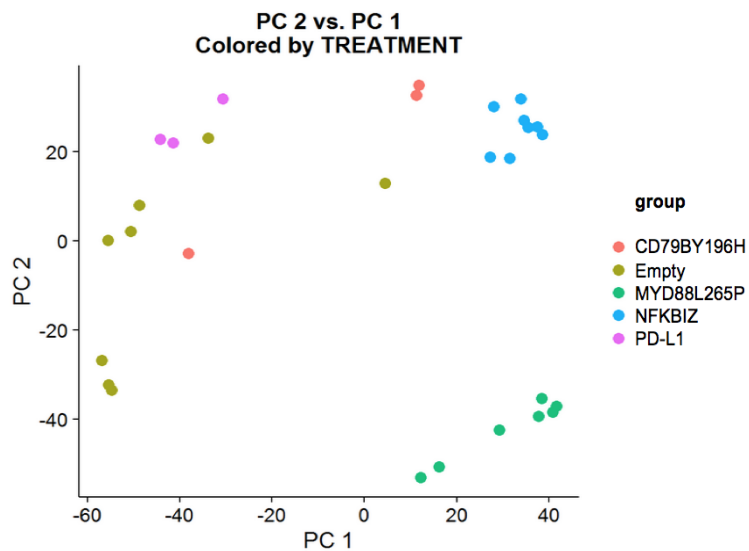


Figure 14: Plot illustrating inter-group variances in a principal component analysis showing high intra group homogeneity and good between group separation for MYD88L265P, NFKBIZ and PD-L1. n=8 for MSCV-empty-GFP transduced E μ -myc transgenic FLC lymphomas, n=8 for MSCV-NFKBIZ -GFP transduced E μ -myc transgenic FLC lymphomas, n=7 for MSCV-MYD88L265P-GFP transduced E μ -myc transgenic FLC lymphomas, n=3 for MSCV-PD-L1-GFP transduced E μ -myc transgenic FLC lymphomas and n=3 for MSCV-CD79BY196H-GFP transduced E μ -myc transgenic FLC lymphomas. Each dot represents a biological replicate.

As we could find several thousand significantly differentially regulated genes after multiple testing correction (Figure 13) we used the biological knowledge-based tool (DAVID,

(137)) for detecting functionally coherent gene clusters. We found the clusters depicted in Appendix 1 as central functional motives occurring in the respective genotypes.

Overlap of significantly differentially regulated genes between sequenced cohorts

NFKBIZ driven MSCV-NFKBIZ-GFP transduced E μ -myc transgenic FLC lymphomas proved to be similar to MYD88L265P driven MSCV-MYD88L265P-GFP transduced E μ -myc transgenic FLC lymphomas which can already be recognized by the high amount of significantly differentially regulated genes overlapping between both groups. (Figure 15). The PD-L1 driven MSCV-PD-L1-GFP transduced E μ -myc transgenic FLC lymphomas showed the common theme of downregulation (Appendix 1). Coming to transcription factor architecture, they showed 100-fold decreased levels of BCL6 compared to empty MSCV-empty-GFP transduced E μ -myc transgenic FLC lymphomas, decreased levels of AP1 signaling components and, in contrast to MYD88L265P driven MSCV-MYD88L265P-GFP transduced E μ -myc transgenic FLC lymphomas decreased levels of NFKBIZ and BLIMP1 (Appendix 1). Another interesting observation was the 24-fold reduction of PD-L2 expression in PD-L1 driven lymphomas which contrasted with an 8-fold upregulation compared to empty lymphomas in the MYD88L265P cohort (Appendix 1).

Overlap of significantly differentially regulated genes between groups

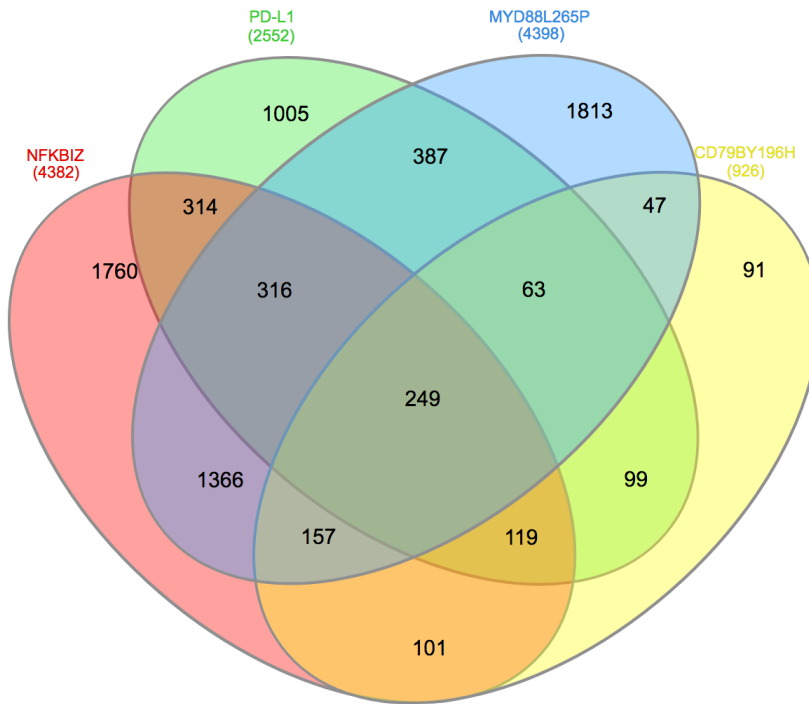


Figure 15: Venn diagram showing overlap of significantly up-and downregulated genes between lesion driven MSCV-lesion-GFP transduced E μ -myc transgenic FLC lymphomas compared to the MSCV-empty-GFP transduced E μ -myc transgenic FLC lymphoma control group. All genes that were differentially regulated with a multiple testing corrected p-value <0.05 compared to MSCV-empty-GFP transduced manifest E μ -myc lymphomas were included in the analysis and respective numbers are depicted behind the names of transduced genes. The Venn diagram was created using software provided by Heberle et al. (139).

Regarding significantly upregulated genes in the MYD88L265P driven MSCV-MYD88L265P-GFP transduced E μ -myc transgenic FLC lymphomas, they showed highly increased levels of many TLR receptors and pattern recognition receptors. PD-L1 and PD-L2 were significantly upregulated (Appendix 1). This was complemented by the observation that for MYD88L265P driven MYD88L265P driven MSCV-MYD88L265P-GFP transduced E μ -myc transgenic FLC lymphomas, the top scoring enriched clusters compared to empty E μ -myc FLC lymphomas are exemplified by the Gene Ontology and

KEGG terms “Graft-versus-host-disease” and “antigen-processing and presentation by MHCII” arguing for a strong influence of immune evasive processes in the biology of MYD88L265P driven lymphomas (Appendix 1). For NFKBIZ driven MSCV-NFKBIZ-GFP transduced E μ -myc transgenic FLC lymphomas, the top scoring enriched clusters compared to empty E μ -myc FLC lymphomas are exemplified by the Gene Ontology terms “kinase and transferase activity” and “transcription factor activity” which we also expected for a member of the NFkB family (Appendix 1).

Modelling MYD88L265P immune evasive mechanisms

To pursue the hypothesis of potentially induced T-cell evasion mechanisms exerted by MYD88L265P driven MSCV-MYD88L265P-GFP transduced E μ -myc transgenic FLC lymphomas, we decided to look for PD-L1 and PD-L2 on B220+ cells. We were able to detect strong PD-L1 surface expression on MYD88L265P driven MSCV-MYD88L265P-GFP transduced E μ -myc transgenic FLC lymphomas (Figure 16). To address the question whether this is just a bystander phenomenon or if PD-L1 overexpression is indeed able to exert an oncogenic effect on its own, we transduced E μ -myc transgenic FLCs with PD-L1. The RNA sequencing results for these lymphomas were already presented in the preceding section (Figures 12-15).

The experiment resulted in a phenotype less penetrant than NFKBIZ and MYD88L265P transduced E μ -myc transgenic FLC lymphomas, yet it yielded GFP+, B220+ and PD-L1 surface positive MSCV-PD-L1-GFP transduced E μ -myc transgenic FLC lymphomas (Table 3). The mice with GFP+ lymphomas succumbed to terminal disease after 60-70 days. Phenotypically, they had hugely enlarged thymuses compared to empty FLC lymphomas (not shown). The lymphomas generated in this setting displayed a completely disturbed lymph node architecture with immunoblastic appearance and Ki67 indices >99% in all three cases (Figure 17).

PD-L1 and PD-L2 expression on MSCV-lesion-GFP driven E μ -myc transgenic FLC lymphomas and MSCV-empty-GFP transduced E μ -myc transgenic FLC lymphomas

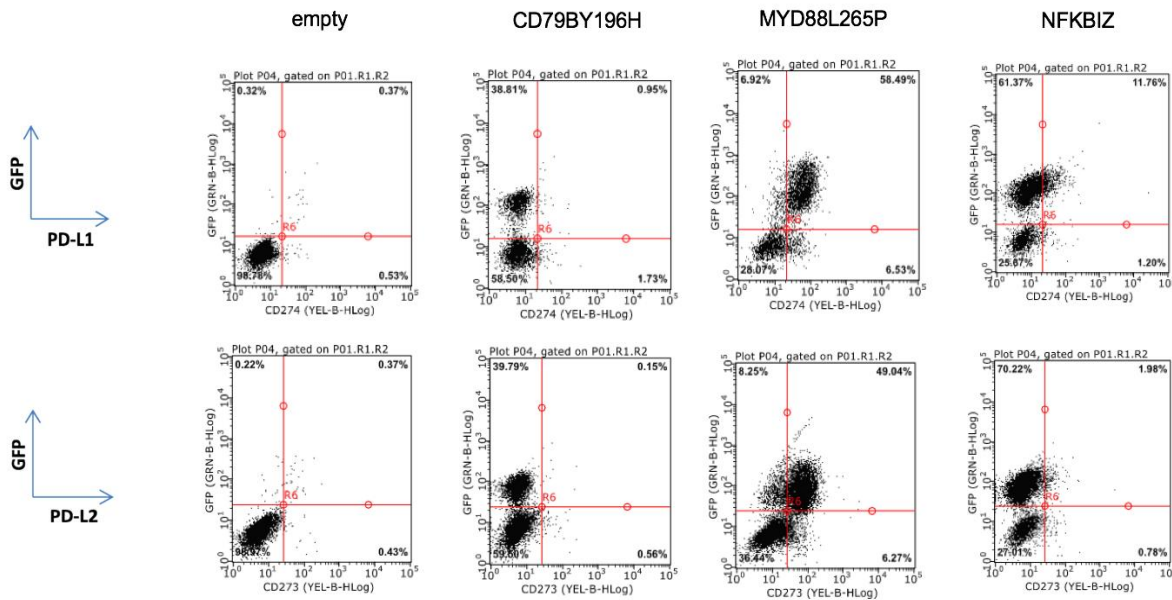


Figure 16: Surface PD-L1 and PD-L2 expression on B220+ cells for MYD88L265P, CD79BY196H, MYD88L265P and NFKBIZ driven MSCV-GFP transduced E μ -myc transgenic FLC lymphomas showing strongly increased PD-L1 and PD-L2 surface expression on MYD88L265P and slightly increased PD-L1 surface expression on NFKBIZ lymphomas, whereas empty and CD79BY196H showed no or minimal PD-L1 or PD-L2 staining.

Penetrance of PD-L1 driven MSCV-PD-L1-GFP transduced E μ -myc transgenic FLC lymphomas and PD-L1 surface expression on empty and PD-L1 MSCV-GFP transduced E μ -myc transgenic FLC lymphomas

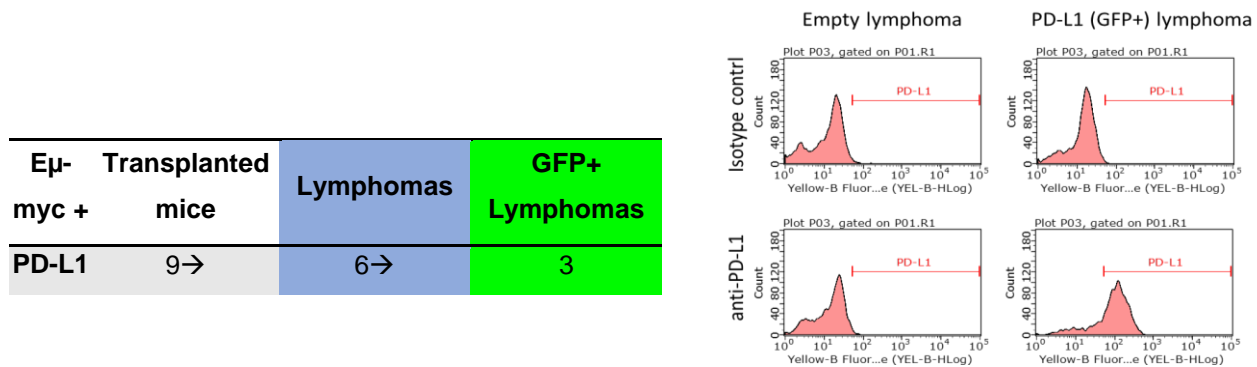


Table 3: The number of mice transplanted that did not meet the criterion of >20% of initial weight reduction until day 21 post irradiation, the number of these mice developing lymphadenopathy (blue column) and the number of animals whose lymphoma met the criterion of >70% of B220+ cells being GFP+ (green columns) are depicted. On the right, a histogram depicting positive PD-L1 surface staining on viable cells from MSCV-empty -GFP transduced E μ -myc transgenic FLC lymphomas and PD-L1 MSCV-PD-L1 -GFP transduced E μ -myc transgenic FLC lymphomas is shown.

HE and Ki67 stains of three independent PD-L1 driven lymphomas

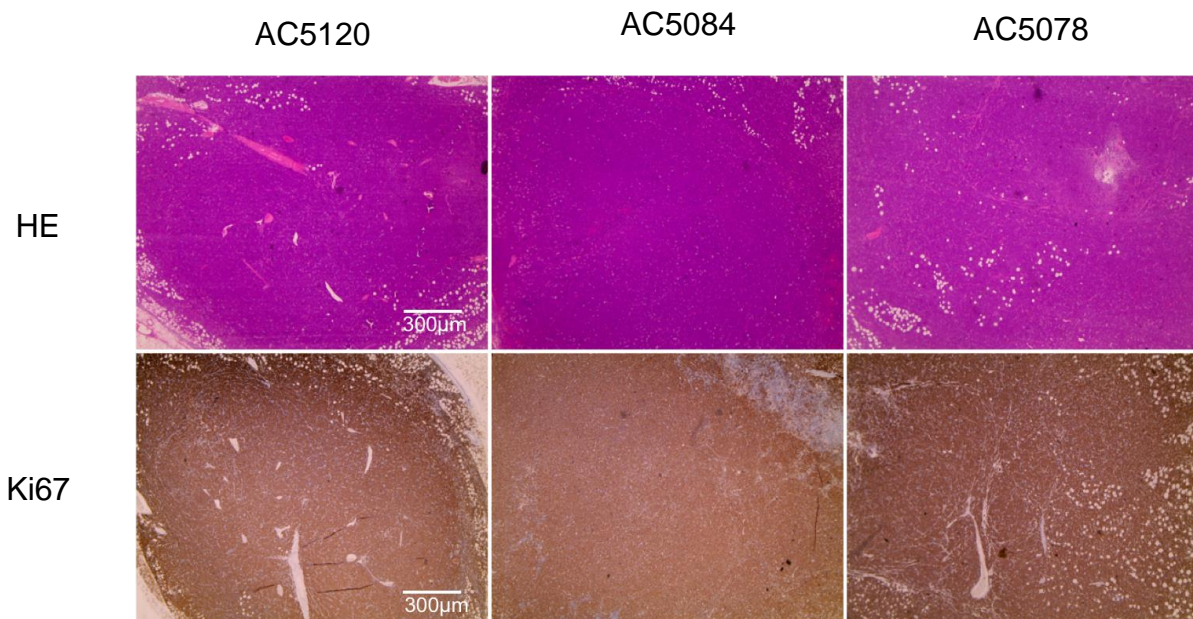


Figure 17: Ki67 and HE stains from the three generated PD-L1 driven MSCV-PD-L1 -GFP transduced E μ -myc transgenic FLC lymphomas. The numbers above the picture indicate the mouse from which the depicted respective lymphoma was excised.

Subsequently, we wanted to address the question whether PD-L1 is not a consequence but prerequisite for MYD88L265P oncogenic behavior.

We decided to address the question functionally by a genetic MYD88L265P overexpression and simultaneous PD-L1 knockdown. This means MYD88L265P overexpression and PD-L1 knockdown is achieved using the same plasmid. We

transduced E μ -myc transgenic FLCs with the plasmid described and used a MYD88L265Pshscrambled construct for the control group. This resulted in significantly prolonged survival of the MSCV-MYD88L265PshPD-L1-GFP transduced E μ -myc transgenic FLC transplanted mice (Figures 18 and 19), demonstrating a causal relationship between MYD88L265P driven lymphoma aggressiveness and PD-L1 surface expression. Additionally, MSCV-MYD88L265PshPD-L1-GFP transduced E μ -myc transgenic FLC lymphomas showed much higher Ki67 indices and completely anaplastic lymphoma architecture (Figure 20) compared to the MSCV-MYD88L265Pshscrambled-GFP transduced E μ -myc transgenic FLC lymphomas which was unexpected.

Survival impact of PD-L1 knockdown on MYD88L265P driven lymphomagenesis

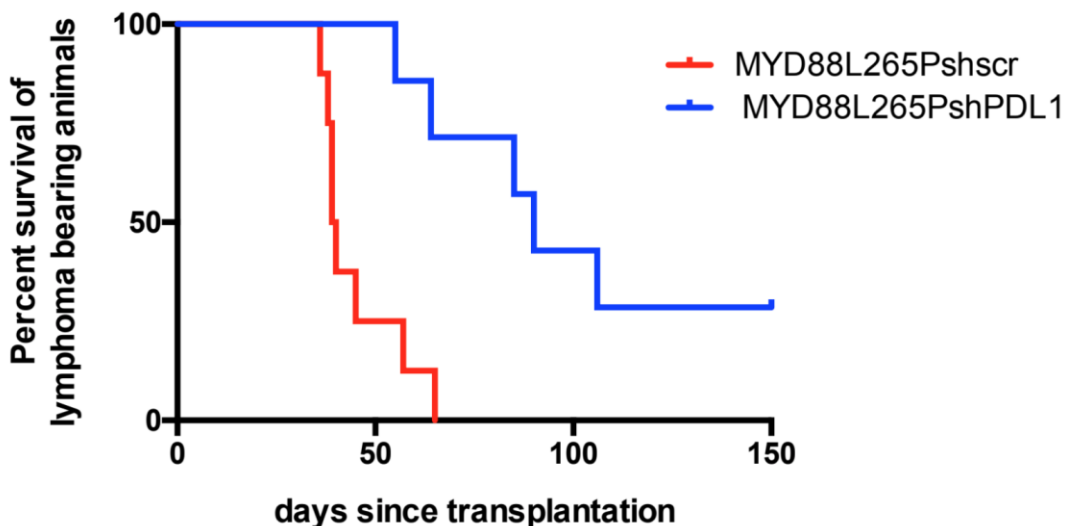


Figure 18: Kaplan-Meier plot depicting survival of mice transplanted with either MSCV-MYD88L265PshPD-L1-GFP transduced E μ -myc transgenic FLCs or the MSCV-MYD88L265Pshscrambled-GFP transduced E μ -myc transgenic FLCs. The curves are significantly different ($p=0.0012$ using the Log-Rank test). n=8 transplanted animals for MSCV-MYD88shscrambled-GFP E μ -myc transgenic fetal liver cell lymphomas. All animals developed GFP+ lymphoma. n=8 for MSCV-MYD88L265PshPD-L1GFP transduced E μ -myc transgenic fetal liver cell-transplanted animals. 6 of 8 animals developed lymphoma which were in all cases GFP positive.

Knockdown efficacy of MYD88L265PshPD-L1 vs. MYD88L265Pshscrambled

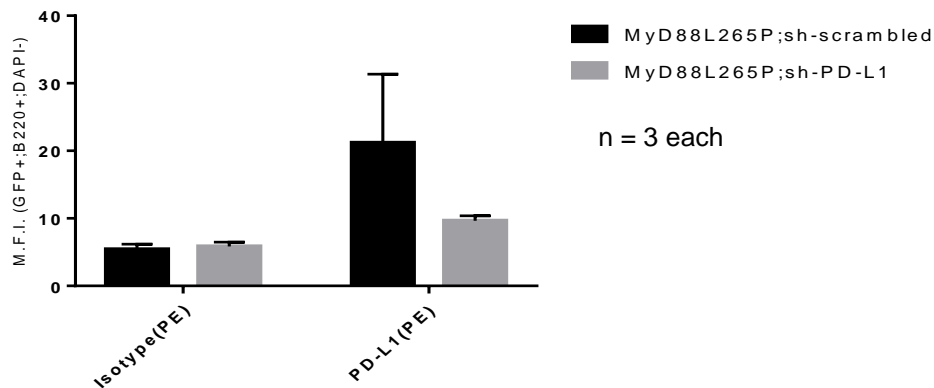


Figure 19: Demonstration of knockdown efficacy by mean fluorescence intensity on GFP+ cells measured by FACS. n=3 for both MSCV-MYD88L265Pshscrambled-GFP and MSCV-MYD88shPD-L1 E μ -myc transgenic FLC lymphomas.

Histopathological analysis of MSCV-MYD88L265Pshscrambled-GFP and MSCV-MYD88shPD-L1 E μ -myc transgenic FLC lymphomas

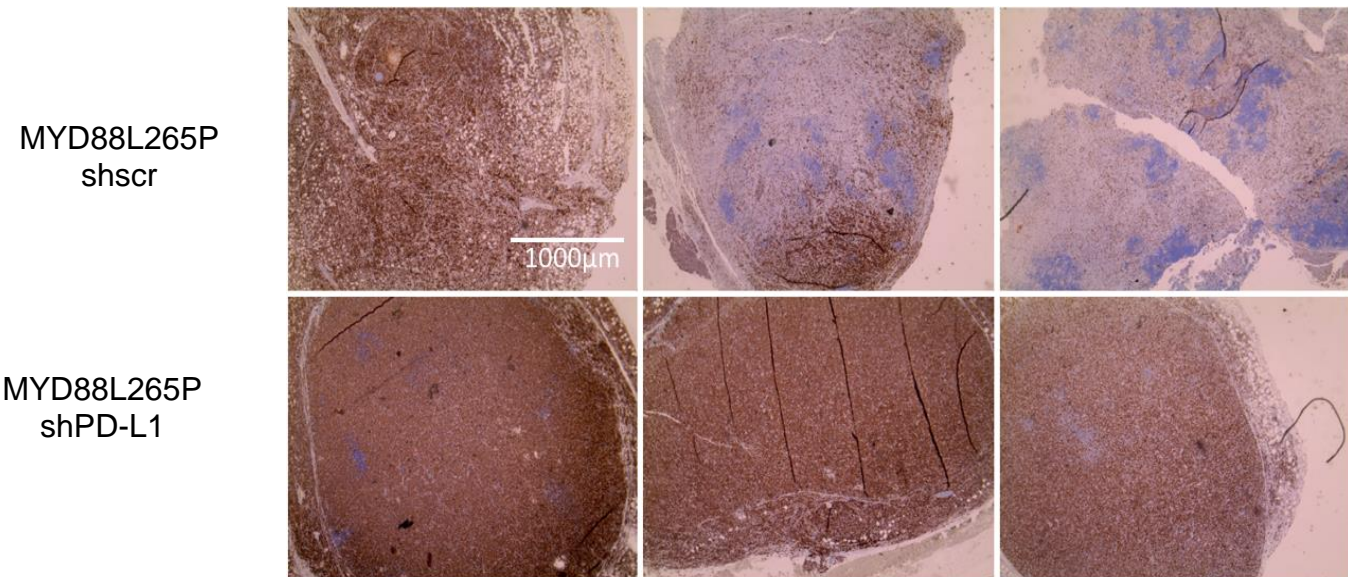


Figure 20: Ki67 stains of n=3 MYD88L265PshPD-L1 driven and MSCV-MYD88L265PshPD-L1-GFP transduced E μ -myc transgenic FLC lymphomas and n=3 MYD88L265Pshscrambled and MSCV-MYD88L265Pshscrambled-GFP transduced E μ -myc transgenic FLC lymphomas.

Oncogenic co-addictions of CARD11L244P

To answer the question why CARD11L244P was not able to drive lymphomas in co-operation with E μ -myc in our system, we looked for GFP+ cells residing in the spleens of the MSCV-CARD11L244P-GFP transduced E μ -myc transgenic FLC transplanted mice. We euthanized 2 animals with no signs of illness or physical distress and analyzed their spleens for residing GFP+ cells. To our surprise, 30% of B220+ cells were also GFP+ (not shown). Sorting the GFP+ against GFP- populations and ensuingly staining for senescence-associated beta galactosidase activity, we found that CARD11L244P transduced cells (98%) stained positive for senescence-associated beta galactosidase activity while only a minority (2.1%) of non-transduced cells stained positive (Figure 22).

In order to prospectively test whether oncogene induced senescence is a relevant barrier in CARD11L244P driven lymphomagenesis, we chose the oncogene induced senescence-incapable system of SUV39H1 -/- E μ -myc transgenic fetal liver cells (70) as a background for CARD11L244P overexpression (Figure 21). An exemplary result of the genotyping PCR from the fetuses of a single pregnant SUV39H1 -/- mouse for generation of SUV39H1 -/- E μ -myc transgenic fetal liver cells is presented in figure 21. From days 14 to 18, all four animals transplanted with the MSCV-CARD11L244P-GFP transduced E μ -myc transgenic FLC became terminally ill with moderately enlarged lymph nodes but being in extraordinary physical distress (Figure 23). Within this time frame, CARD11L244P-positive cells enriched from about 3% in the original transplanted FLC pool to over 60% of viable cells in the final lymphoma (Figure 24). Additional physical features were enlarged spleens (similar to those seen in normal E μ -myc FLC settings) and no other gross anatomical abnormalities.

Exemplary genotyping of used FLC of SUV39H1 -/- or SUV39H1 -/+ E μ -myc transgenic fetal liver cells

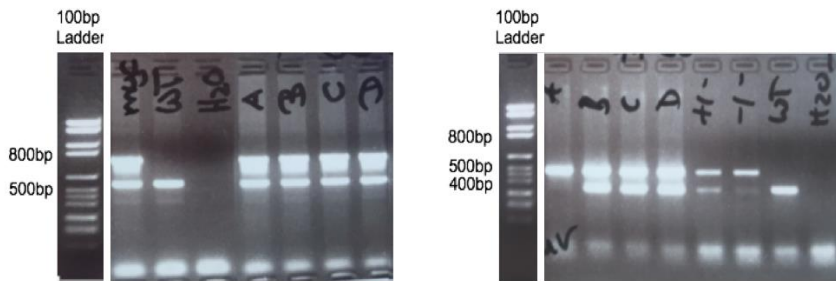


Figure 21: Genotyping gel for one litter of one of the FLCs used for the SUVA39H1 -/- E μ -myc transgenic fetal liver cell experiment. The mother of the genotyped fetuses was mouse 1195. The fetuses used for genotyping are denoted as a, b, c and d in the electrophoresis results depicted above. As PCR controls, DNA from tail biopsies of E μ -myc transgenic and wildtype mice was used. Fetus 1195a was used for transplant experiments. E μ -myc transgenic animals should display both a 830 bp product and a 530 bp internal tubulin control band.

Senescence associated beta galactosidase staining in GFP positive vs. GFP negative cells from MSCV-CARD11L244P-GFP transduced E μ -myc transgenic FLC and MSCV-empty-GFP transduced E μ -myc transgenic FLC transplanted C57BL6/N mice

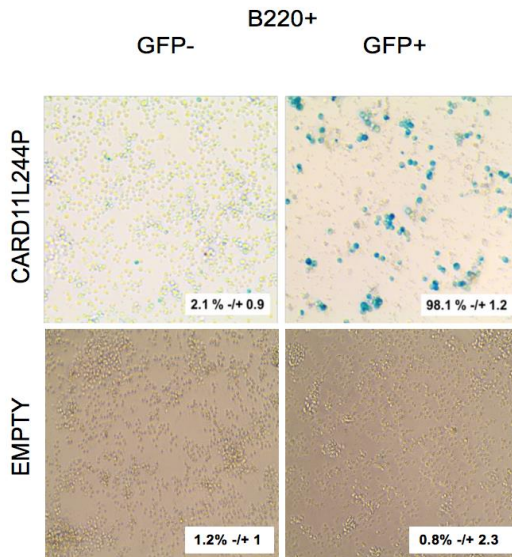


Figure 22: Representative senescence associated beta galactosidase staining in GFP positive and GFP negative splenocytes from MSCV-CARD11L244P-GFP transduced E μ -myc transgenic FLC and MSCV-empty-GFP transduced E μ -myc transgenic FLC transplanted C57BL6/N mice GFP+ and negative cells were separated by cell sorting.

Survival curve for C57BL6/N mice presenting with GFP positive lymphoma in MSCV-CARD11L244P-GFP or MSCV-empty-GFP transduced SUV39H1 -/- E μ -myc FLC-transplanted mice

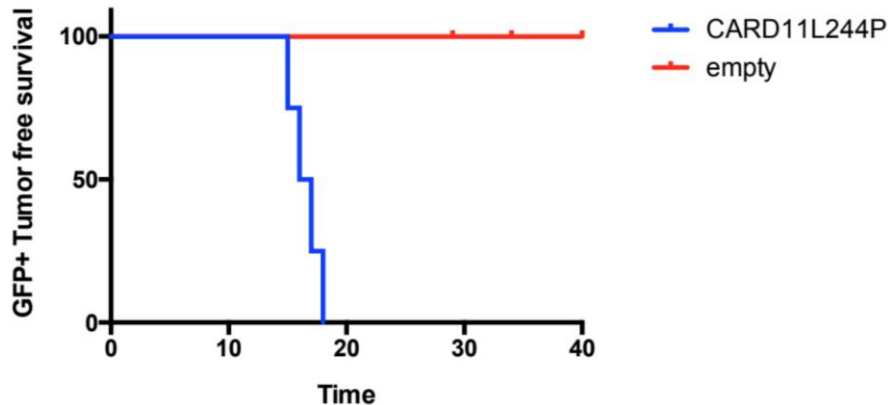


Figure 23: Kaplan Meier Plot showing survival of SUV39H1 -/- E μ -myc transgenic fetal liver cell transplanted animals that displayed palpable lymphadenopathy and GFP+ tumors in subsequent FACS analysis. n=4 for CARD11L244P and n=4 for empty.

GFP enrichment in total viable cells from spleens of MSCV-CARD11L244P -GFP transduced E μ -myc transgenic SUV39H1 -/- FLC transplanted C57BL6/N mice

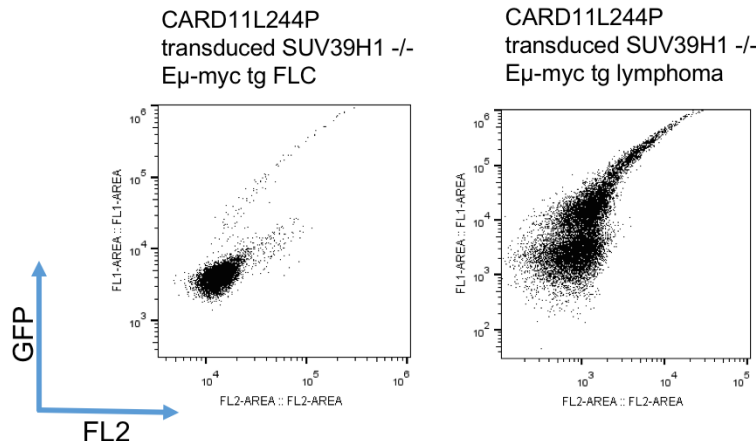


Figure 24: FACS plot demonstrating CARD11L244P-GFP enrichment in viable cells from originally transplanted SUV39H1 $^{-/-}$ E μ -myc tg FLC (approximately 2%) and the proportion in manifest lymphoma after 2 weeks (approximately 60%). Total cells were analyzed with discriminating true GFP positivity by analyzing FL1 (GFP) vs. FL2 intensity.

Phenotypic impact of genetic lesions in manifest E μ -myc transgenic primary lymphomas

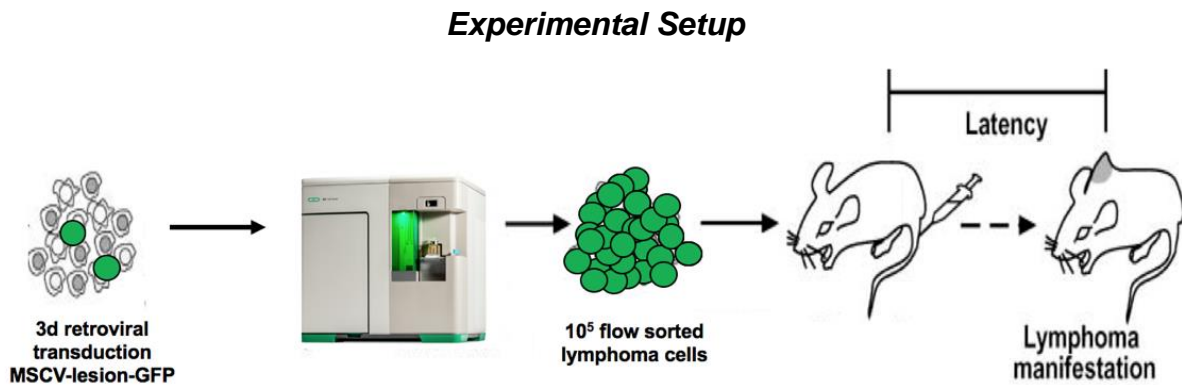


Figure 25: Illustration adapted from Schmitt et al. (88) presenting our experimental setup

In the next step, we contrasted the function of the lesions when acting as drivers in lymphomagenesis with their impact in manifest E μ -myc transgenic lymphomas that do not need an additional tumor driver anymore (illustrated in Figure 25).

The first observation made was that MSCV-MYD88L265P-GFP transduced manifest E μ -myc transgenic lymphoma transplanted animals developed tumors significantly later (Figure 26) than MSCV-empty-GFP transduced manifest E μ -myc transgenic lymphoma transplanted animals. Two primary manifest E μ -myc transgenic lymphomas became manifest when transduced with MSCV-empty-GFP but were not able to produce manifest disease in mice any more when transduced with MSCV-MYD88L265P-GFP (repeated 3 times for each manifest E μ -myc lymphoma in individual transductions, sorts and transplantations). Tumor onsets did not significantly differ between empty and CARD11L244P, NFKBIZ, CD79BY196H and I κ B α Δ N (not plotted). Histopathologically, the 6 MYD88L265P transduced manifest E μ -myc transgenic lymphomas that could still become manifest in mice showed highly decreased numbers of Ki67+ cells (Figures 27, 28, 29) and a significantly increased amount of cells staining positive for the senescence associated H3K9me3 mark (Figure 27 and 28) similar to the observations made in MSCV-MYD88L265P-GFP transduced E μ -myc transgenic FLC lymphomas.

Overall survival from transplantation to lymphoma manifestation in empty-GFP and MYD88L265P transduced and retransplanted E μ -myc transgenic manifest lymphomas

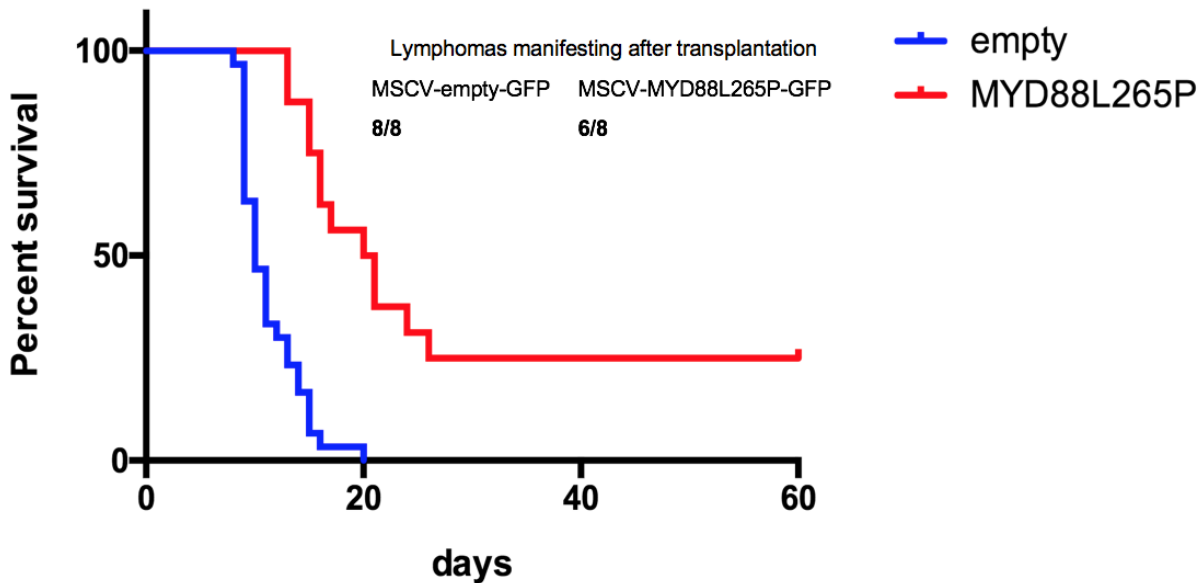


Figure 26: Kaplan Meier Plot for empty vs. MYD88L265P retransplanted manifest E μ -myc transgenic lymphomas. 8 primary manifest E μ -myc transgenic lymphomas were transduced as triplicates with either empty-GFP (n=24 plotted, with n=3 for each primary lymphoma) or doublets for MYD88L265P (n=16 plotted, with n=2 for each primary lymphoma). Different to the fetal liver cell lymphoma Kaplan-Meier plots, events are defined here as a mouse presenting with palpable lymphadenopathy and moribund appearance. The survival curves were analyzed using Log-Rank test and shown to be significantly different between MYD88L265P and empty transduced E μ -myc lymphomas using Log-Rank test ($p<0.0001$). No mouse died for any other reason than lymphoma within the timeframe shown.

This effect was not observed in the other transduced manifest E μ -myc transgenic lymphomas. Particularly MSCV-CD79BY196H-GFP and MSCV-IkB α Δ N-GFP transduced lymphomas were, concerning Ki67 and H3k9me3 indices, indistinguishable from MSCV-empty-GFP transduced manifest E μ -myc transgenic lymphomas (Figure 29).

Histopathological Analysis of MYD88L265P and empty transduced manifest Eμ-myc transgenic lymphomas I

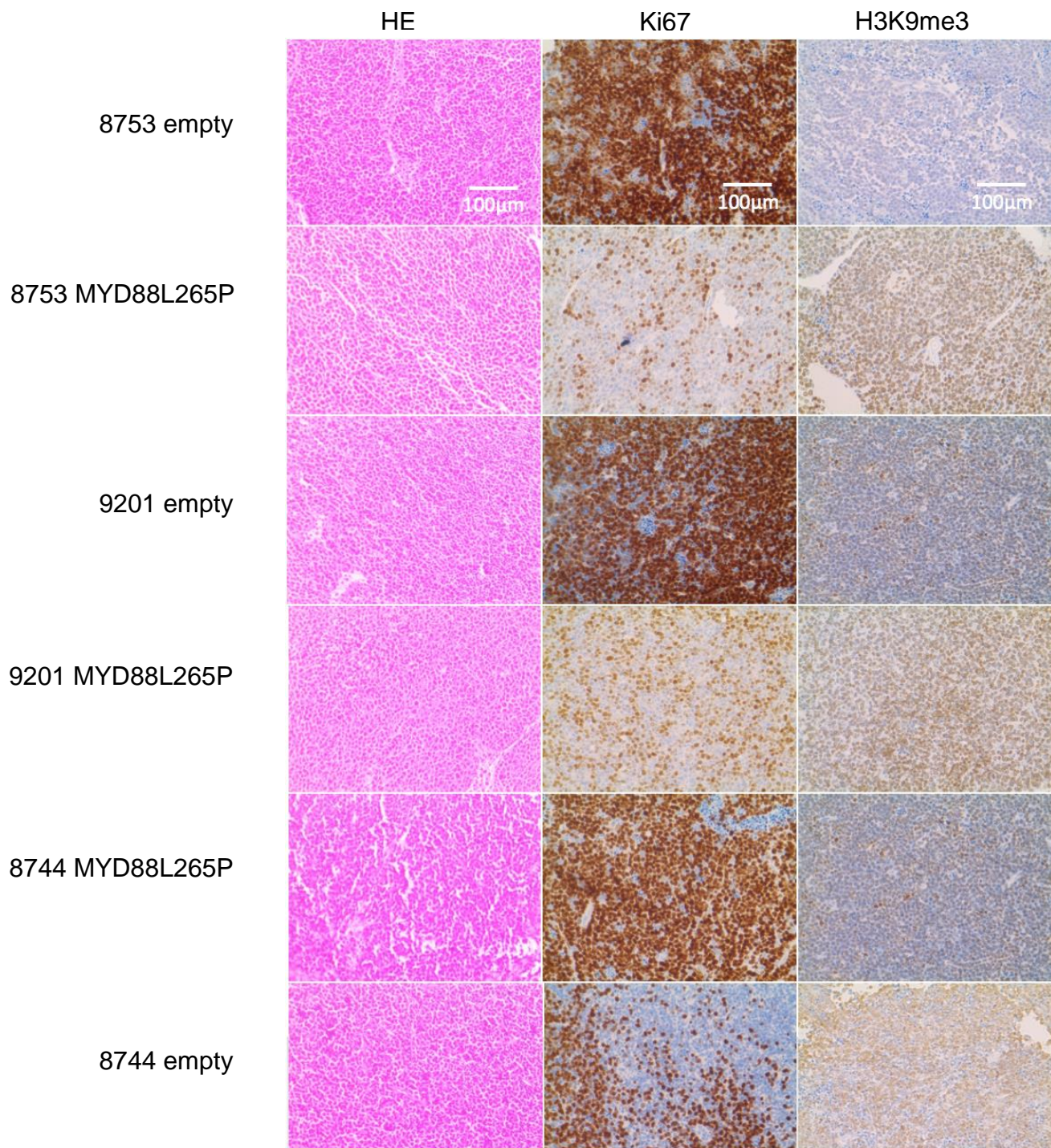


Figure 27: Photographs, 100x magnification. 1st row: 8753 empty HE, Ki67 and H3K9me3
2nd row: 8753 MYD88L265P HE, Ki67 and H3K9me3, 3rd row: 9201 empty HE, Ki67 and

H3K9me3 4th row: 9201 MYD88L265P: HE, Ki67 and H3K9me3 5th row: 8744 empty HE, Ki67 and H3K9me3, 6th row: 8744 MYD88L265P HE, Ki67 and H3K9me3.

Histopathological Analysis of MYD88L265P and empty transduced manifest Eμ-myc transgenic lymphomas II

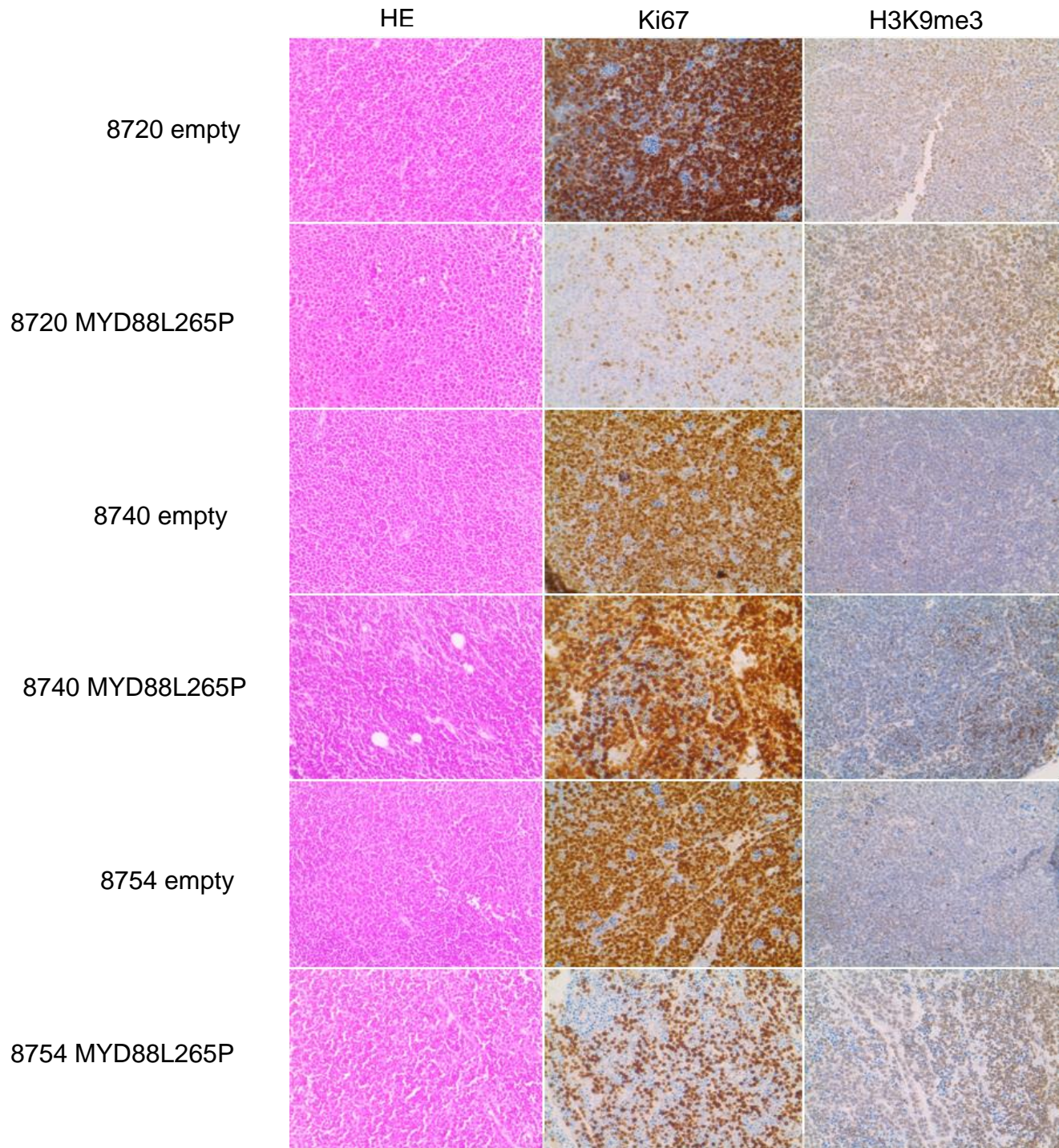


Figure 28: Photographs of 100x magnifications 1st row: 8720 empty HE, Ki67 and H3K9me3 2nd row: 8720 MYD88L265P HE, Ki67, H3K9me3 3rd: 8740 empty HE, Ki67, H3K9me3 4th row: 8740 MYD88L265P HE, Ki67, H3K9me3 5th row: 8754 empty HE, Ki67, H3K9me3 6th row: 8754 MYD88L265P HE, Ki67, H3K9me3. 8740 is the only examined sample that does not show any histopathological changes upon MYD88L265P transduction. HE stains show a highly similar overall appearance for all examined samples.

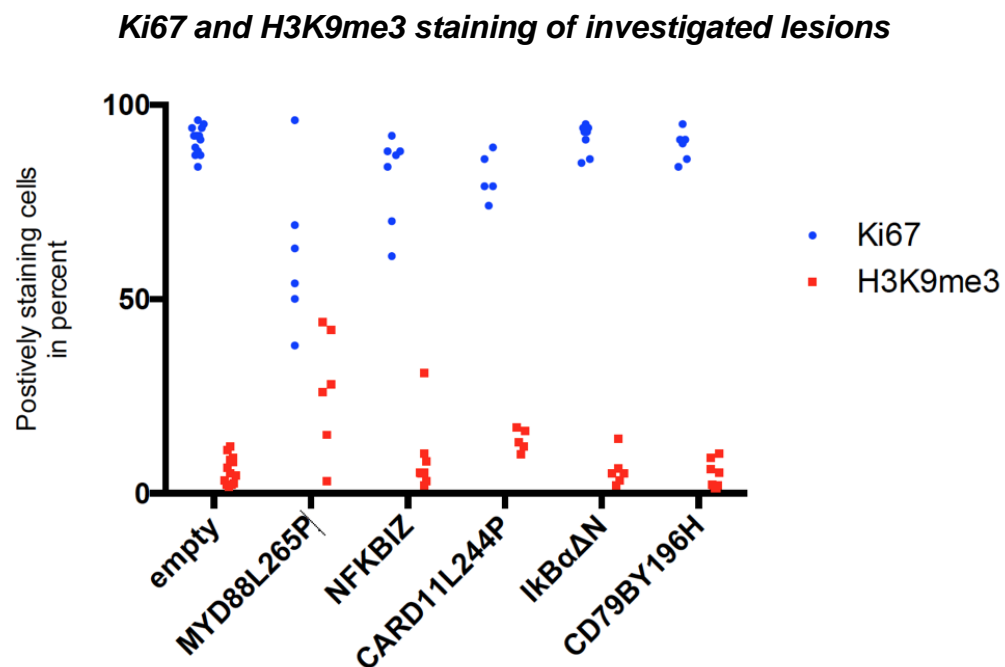


Figure 29: Histopathological evaluation of Ki67 and H3K9me3 in MSCV-lesion -GFP transduced manifest E μ -myc transgenic lymphoma. Using a one-way ANOVA, MSCV-MYD88L265P-GFP transduced manifest E μ -myc transgenic lymphoma proved to be significantly different from MSCV-empty-GFP transduced manifest E μ -myc lymphoma ($p<0.0001$). No other MSCV-lesion-transduced manifest E μ -myc lymphoma proved to be significantly different from empty after multiple testing correction. Each dot represents one evaluated lymphoma. All genotypes were evaluated for significance vs. empty but not among each other. Each dot represents one individual analyzed lymphoma for the respective marker.

Transcriptome Analysis by RNA Sequencing in manifest transduced E μ -myc transgenic lymphomas

As results from the previous sections, we found that MYD88L265P is a lymphoma driver in E μ -myc transgenic fetal liver cell lymphomas, exerting immune evasive mechanism as an oncogenic mechanism in the E μ -myc transgenic FLC approach. Yet it inhibited proliferation and lymphoma manifestation in already manifest E μ -myc transgenic primary lymphomas. Accordingly, we were interested in the molecular alterations that might lead to these opposite effects in E μ -myc transgenic lymphoma behavior. We approached this issue by using again RNA sequencing for transcriptome analysis of empty, scrambled, MYD88L265P, CD79BY196H, CARD11L244P, shA20, PD-L1 and I κ B α Δ N in manifest transduced E μ -myc transgenic lymphomas in total.

Samples were sequenced at a depth of approximately 5×10^7 aligned 50 base pair single end reads for each sample. The unadjusted p-value histograms for an evaluation of true positive hits are shown in Figure 30. Overall, the mutants were not able to dominate the transcriptome of manifest E μ -myc transgenic lymphomas, with the original E μ -myc transgenic lymphoma still being the principal distinguishing component and no clustering between MSCV-lesion-transduced E μ -myc transgenic lymphomas being observed when considering overall sample distances in contrast to FLC-generated mutant driven lymphomas (Figures 31 and 32).

Histogram for count of unadjusted p-values

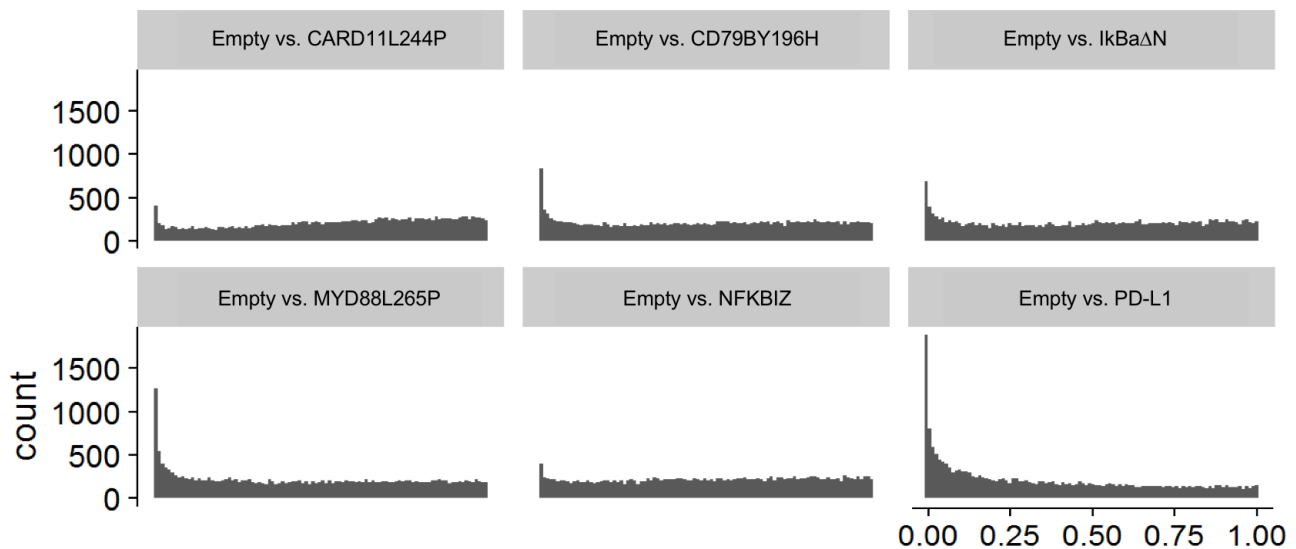


Figure 30: Probability density histograms for the sequenced groups. Each large square depicts a 0.125 interval for the 0-1 probability. A uniform distribution as in the comparison of shscrambled vs. empty (not shown) would be expected for random comparisons, whereas steep increases for small p-values indicate true positive hits. empty vs. CD79BY195H (n=8 for each), empty vs IκBaΔN-GFP (67) (n=8 for each), empty vs. NFKBIZ (n=8 for empty and N=7 for NFKBIZ), empty vs. PD-L1 (n=8 for empty and n=7 for PD-L1) and empty vs. MYD88L265P (n=8 for empty and n=6 for MYD88L265P).

Sample distance clustering

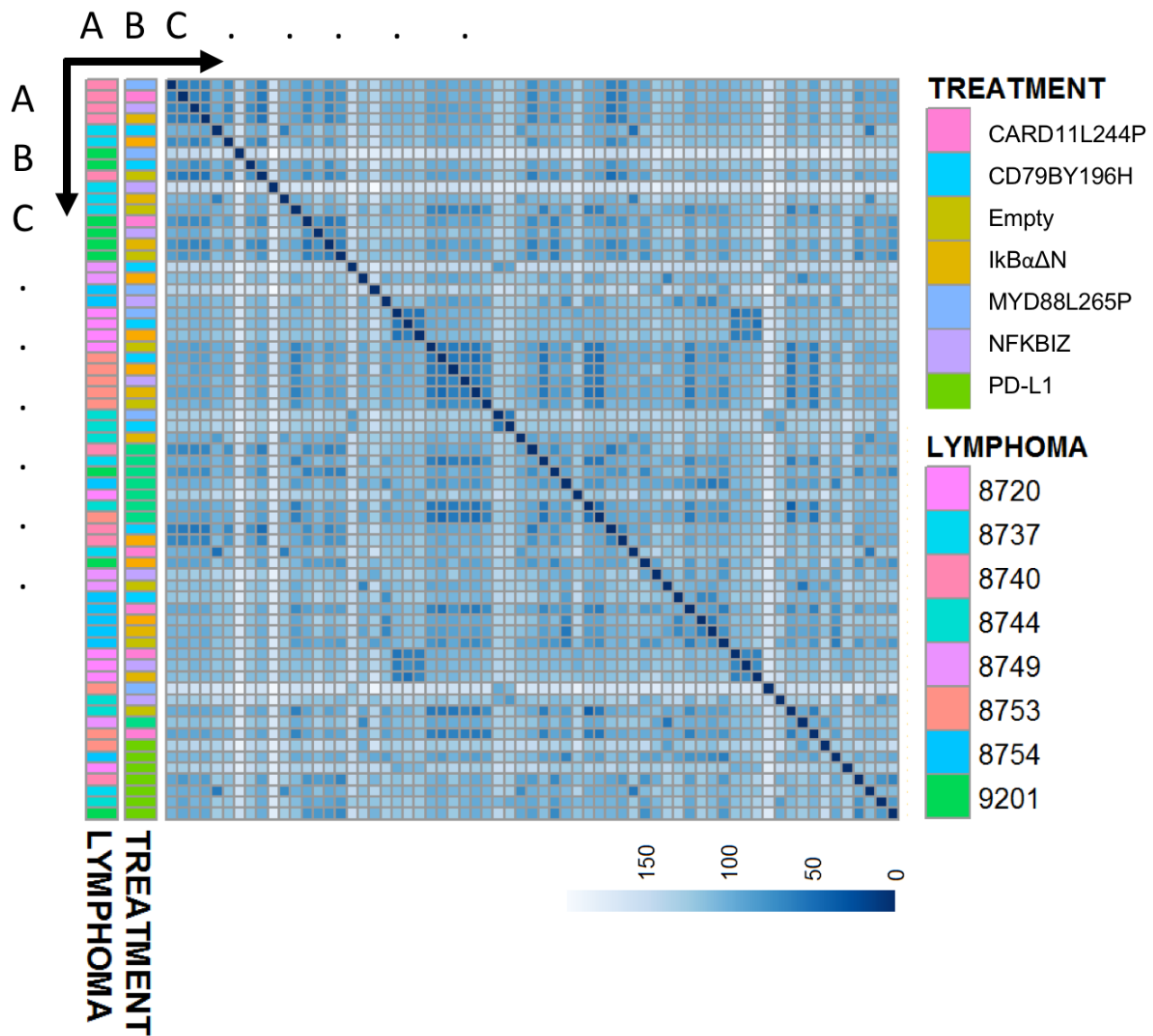


Figure 31: Sample distances between transduced manifest E μ -myc transgenic lymphomas showing strong clustering grouped by the driving oncogene. Letters and arrows next to the matrix indicate the principle behind constructing the $n \times n$ Poisson dissimilarity matrix with n_{ij} again depicting the distance between two individual biological samples and $n_{i=j}$ denoting the matrix diagonal mapping the sample distance of each sample to itself and is necessarily due to the properties of the Poisson dissimilarity measure for sample $x_i=x_j=0$. For further mathematical background, proofs and comparison to other clustering measures and algorithms see Witten, 2011 (134). The blue

bar denotes the sample Poisson distances in the matrix that are encoded by shadings of blue.

Principal component analysis of transcriptome data

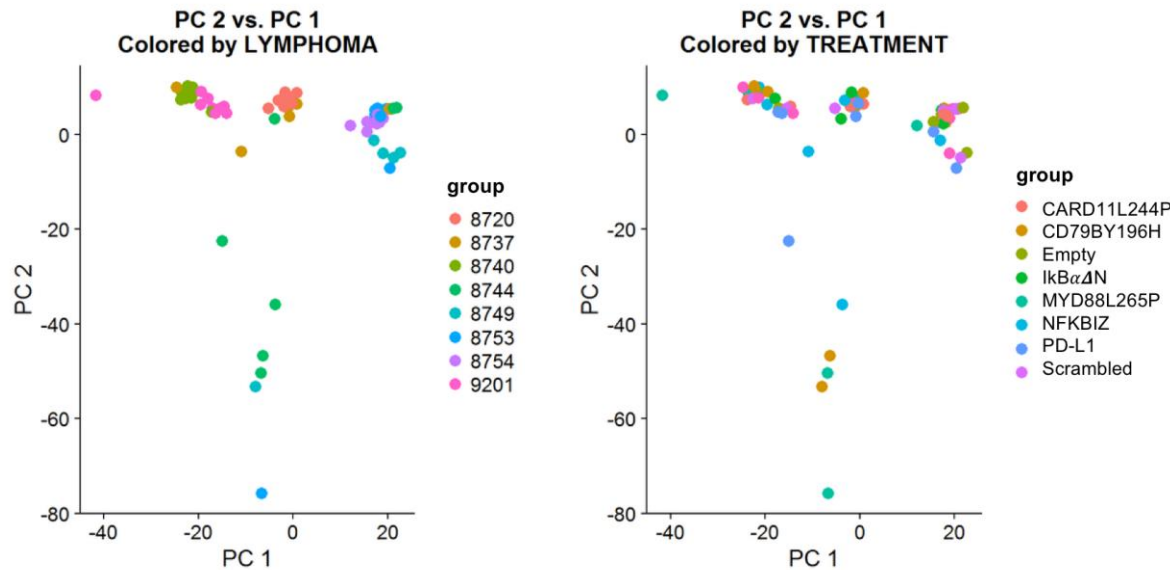


Figure 32: Principal component analysis depicting sample attribution in the left picture and transduced mutant in the right one. It can be seen, that the original manifest E μ -myc transgenic lymphoma remains the most determining clustering variable.

The I κ B $\alpha\Delta$ N “superrepressor” showed robust functionality (Figure 39 and Table 5) yet did not induce delayed E μ -myc transgenic lymphoma manifestation or proliferation. This clearly illustrates an independence of E μ -myc driven tumor growth of NFKBIA regulated genes. Among the genes significantly downregulated by I κ B $\alpha\Delta$ N we found e.g. JAK3, BCL3, NOTCH1, NOTCH2, PIM1, FOS, CD180, S1pr1 and TLR8, (Appendix 2). Yet this transcriptional signature did not result in inhibition of proliferation opposed to MYD88L265P hyperactivation.

To understand the main components of cellular signaling disturbed by MYD88L265P, we examined the significantly differentially regulated genes using again the DAVID web tool (137). This time, clusters named “kinase activity” and “innate immune system process”

represented the highest enriched functional clusters within the 646 significantly changing genes between MSCV-MYD88L265P-GFP and MSCV-empty-GFP transduced manifest E μ -myc transgenic lymphomas (Appendix 2).

Reduced Ki67 seen in the histological stains (Figures 28 and Figures 27) could also be recapitulated in the RNA seq data. This is reflected by features like reduced cyclin D and E levels and strongly reduced levels of E2F8 and E2F7 that were significantly downregulated in MYD88L265P lymphomas, whereas RGCC, as a detrimental checkpoint arrest signal transducer (140), was strongly upregulated (Appendix 2).

Overlap of significantly differentially regulated genes

The significantly differentially regulated genes compared to the empty vector control E μ -myc lymphoma that overlapped in the different lesion transduced cohorts are depicted in Figure 33. NFKBIZ showed very few differentially regulated genes, with almost all of them overlapping with MYD88L265P differentially regulated genes adding evidence to the strong functional relation of both mutants.

PIM1, BCL3, NFKB2 and BCAR3 were significantly upregulated in MYD88L265P transduced lymphomas and significantly downregulated in either CD79BY196H or I κ B α Δ N transduced lymphomas. Therefore, since neither CD79BY196H nor I κ B α Δ N shows decreased Ki67 indices in contrast to MYD88L265P transduced lymphomas, these genes might contribute to the proliferation-inhibiting phenotype seen in MYD88L265P transduced manifest E μ -myc transgenic lymphomas.

Overlap of significantly differentially regulated genes between groups

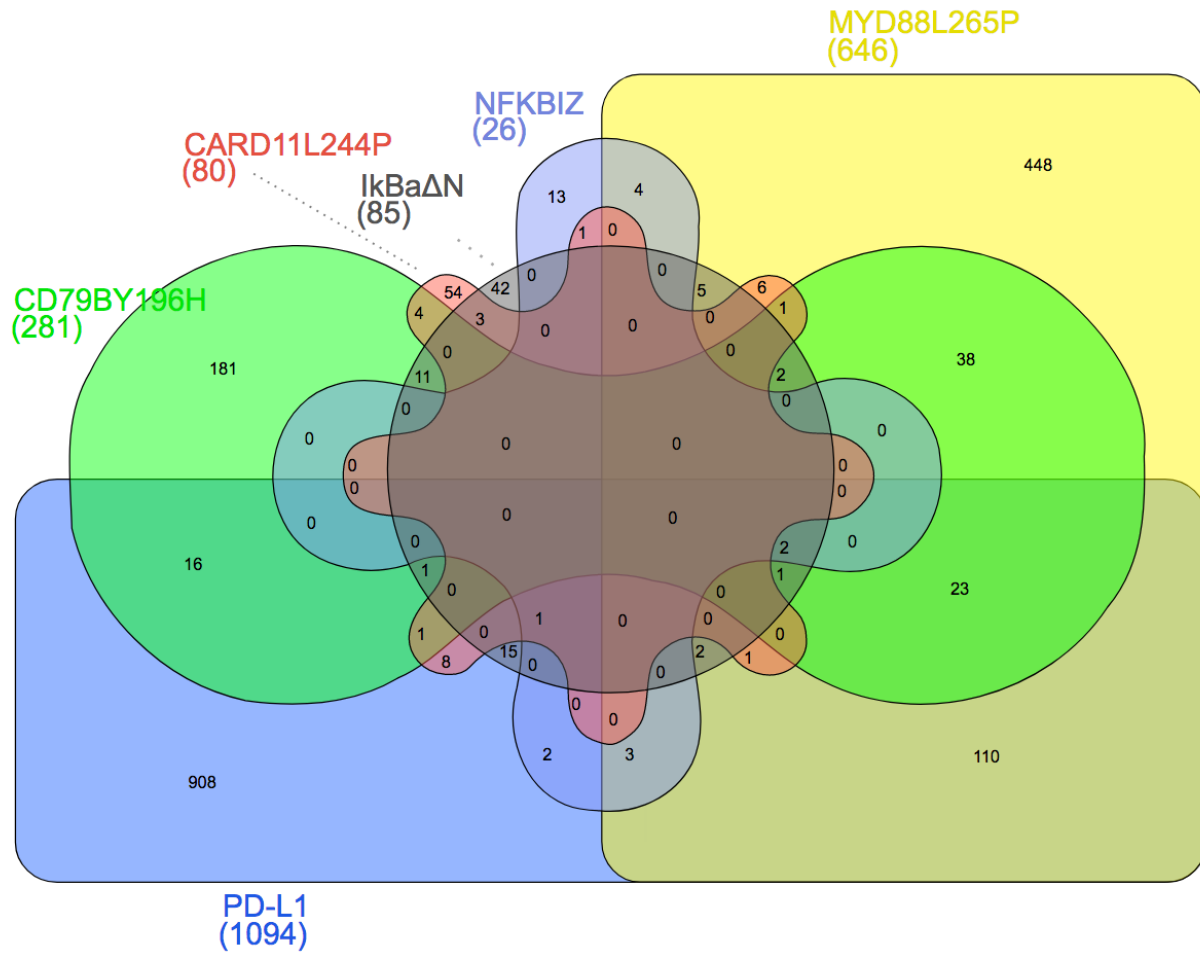


Figure 33: Significantly differentially expressed genes between mutants vs. empty and overlap of these genes between different mutants in MSCV-GFP transduced E μ -myc transgenic manifest lymphomas. PD-L1 transduced manifest E μ -myc transgenic lymphomas are already presented in this graph. BCL3, BCAR3, NFKB2 and PIM1 are upregulated in MYD88L265P lymphomas and downregulated in CD79BY196H and NFKBIA, respectively.

All genes that were differentially regulated with a multiple testing-corrected p-value <0.05 compared to MSCV-empty-GFP transduced manifest E μ -myc lymphomas were included in the analysis and respective numbers are depicted behind the names of transduced genes. The Venn diagram was created using software provided by Heberle et al. (139).

MYD88L265P immune evasion mechanisms in manifest lymphomas

On manifest MYD88L265P transduced E μ -myc transgenic lymphomas, we were not able to detect either PD-L1 or PD-L2 surface staining (data not shown). The composition of infiltrating immune cells was not altered compared to empty transduced manifest E μ -myc lymphomas contrasting MSCV-MYD88L265P-GFP transduced E μ -myc transgenic FLC lymphomas (T-cell stainings shown in Figure 34). Therefore, we looked for immune-evasive markers from RNA seq data applying a “T-cell activation” and a “T-cell evasion” transcriptional signature (Appendix 3)

T-cell infiltration in empty GFP and MYD88L265P transduced lymphomas

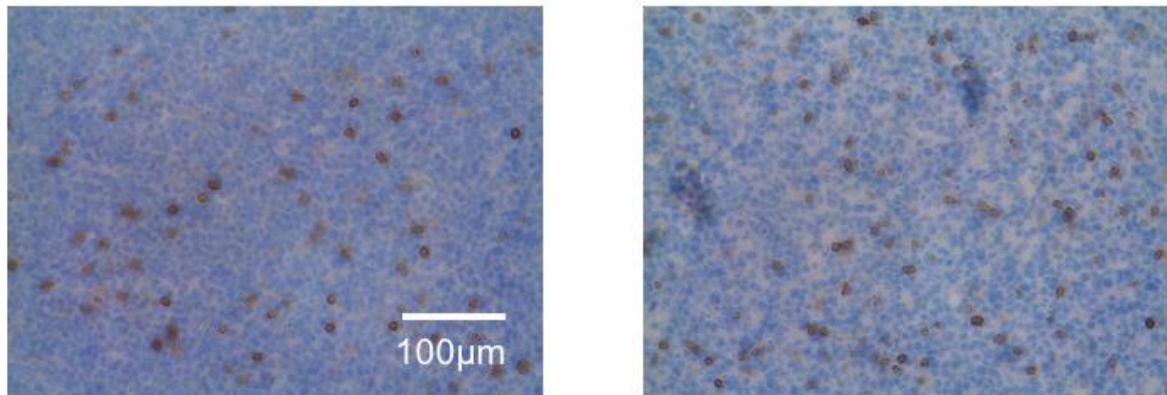


Figure 34: Representative images for CD3 HRP-stained tissue sections from empty transduced manifest E μ -myc transgenic lymphomas on the left side and MYD88L265P transduced E μ -myc lymphomas on the right side. No significantly different T-cell infiltration was observed. n=8 for empty and n=6 for MYD88L265P transduced E μ -myc lymphomas.

Within a gene list of 22 genes six genes from a T-cell evasion signature (141) seven were significantly upregulated (Appendix 3). Among those, prominent inhibitors like CTLA-4 that are found on T-cells were found (Appendix 3). From our T-cell activation signature, only two genes were significantly differentially regulated (Appendix 3). Significant

downregulation of other T-Cell activators like LAT2 and LCK was observed. PD-L1 was also not found to be transcriptionally differentially regulated in MYD88L265P transduced manifest lymphomas.

Since we could not detect upregulation of PD-L1 or PD-L2 on manifest MYD88L265P transduced E μ -myc transgenic lymphoma compared to the empty control, but many transcripts that are crucial for B-T-cell interaction and regulation (for example CTLA4, IL10, PRDM1, CD244, Appendix 3), we wondered what effect “forced” expression of PD-L1 would have on manifest E μ -myc driven lymphomas. The same lymphoma set used for the other transduction experiments was used again for this experiment. The lymphomas were transduced with MSCV-PD-L1-GFP and retransplanted into C57BL6/N mice as described. The lymphoma material generated from the retransplantations was subjected to RNA sequencing.

Differentially regulated genes in PD-L1 transduced manifest E μ -myc lymphomas

MSCV-PD-L1-GFP transduction and surface expression in manifest E μ -myc transgenic lymphoma cells and retransplantation into immunocompetent C57BL6/N mice resulted in a downregulation of many genes associated with maintenance of genomic integrity (BRCA1, BRCA2, FANC1) compared to MSCV-empty-GFP transduced manifest E μ -myc lymphomas (Figure 35 and Appendix 2). Upregulation of MHC class two family members, CD27, LAT, CD247, TNFSF9, IFNGR2 are rather indicative of an induction of T/B-cell attraction and interaction (Appendix 2). PD-L1 overexpression strongly increases expression of NFKBIZ, similar to MYD88L265P.

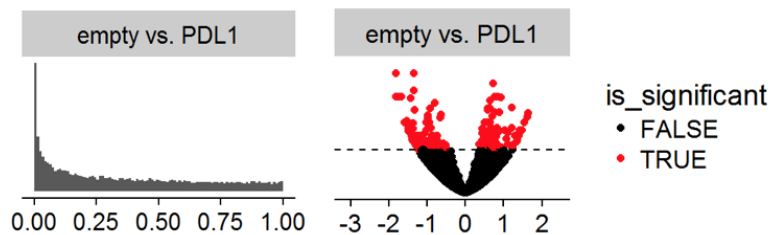


Figure 35: Volcano Plot for empty vs PD-L1 and histogram of distribution of unadjusted p-values for empty vs. PD-L1. 1102 genes passed the significance threshold $p<0.05$. n=7 for PD-L1 and n=8 for empty.

These findings contrast the transcriptional signatures found in MSCV-PD-L1-GFP driven E μ -myc transgenic FLC lymphomas that show a transcriptional signature strongly resembling T-cell inhibition, co-stimulation ablation and MHC II avoidance. This shows an acute effect of PD-L1 surface expression being characterized by augmentation of genes associated with cell division and DNA replication (Appendix 2). Mouse survival was not affected by PD-L1 overexpression on manifest E μ -myc transgenic lymphomas (not shown).

Alteration of cellular NF κ B signaling by genetic lesions

Within the 646 significantly differentially regulated genes in MSCV-MYD88L265P-GFP transduced manifest E μ -myc lymphomas compared to MSCV-empty-GFP transduced manifest E μ -myc lymphomas, we found 8 other components that have so far been observed to be dysregulated at high frequencies in DLBCL as either deletions (e.g. NFKBIA) or being overexpressed or amplified (e.g. NFKB2, NFKBIZ) (36, 46). Since these 8 genes are crucial components of the NF κ B signaling cascade, we wanted to know how the overall signaling architecture of NF κ B signaling in our E μ -myc driven lymphomas is altered by MYD88L265P and the other genetic lesions.

Differentially regulated NF κ B players from RNA Seq data in MYD88L265P vs. empty lymphomas

Contrast	baseMean	log2FoldChange	pvalue	padj	chr	mgi_symbol
empty vs. MYD88L265P	628.7145656	-1.086354762	8.54421E-05	0.006352996	7	Bcl3
empty vs. MYD88L265P	2240.920119	-0.749546564	0.001108145	0.033677506	19	Nfkcb2
empty vs. MYD88L265P	4627.758348	-0.733826662	6.39243E-05	0.005321354	12	Nfkbia
empty vs. MYD88L265P	1112.610306	-0.726450225	0.000759687	0.02737911	7	Nfkbid
empty vs. MYD88L265P	1300.885964	-0.725424647	0.000904938	0.029937212	17	Nfkbie
empty vs. MYD88L265P	1584.358591	-1.242242064	5.5352E-05	0.004817197	16	Nfkbiz
empty vs. MYD88L265P	2917.132895	-0.894265651	2.22604E-05	0.002525649	17	Pim1
empty vs. MYD88L265P	2001.636607	-1.16188801	1.46564E-05	0.001810417	10	Tnfaip3

Table 4: NFkB family members and DLBCL Hotspots by RNA Seq data of MYD88L265P on transcriptional regulation of other DLBCL “hot spot” loci as described recently in primary E μ -myc transgenic murine lymphoma (36, 42, 46).

The changes in NFKBIZ levels observed in MSCV-MYD88L265P-GFP transduced manifest E μ -myc lymphomas and LPS stimulation of on MSCV-empty-GFP transduced manifest E μ -myc lymphomas were specifically analyzed by reverse quantitative PCR and showed augmented NFKBIZ levels both in the MYD88L265P transduced manifest E μ -myc lymphomas and even stronger upon LPS stimulation in the MSCV-empty-GFP transduced manifest E μ -myc lymphoma control group (Figure 36)

NFKBIZ mRNA is upregulated by LPS and MYD88L265P in manifest E μ -myc lymphomas

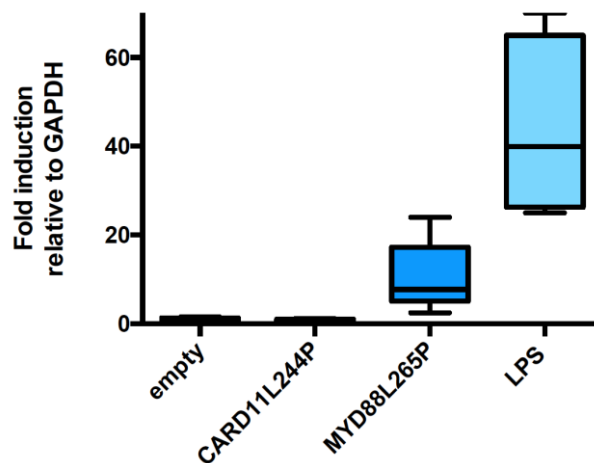


Figure 36: Relative NFKBIZ levels in CARD11L244P, MYD88L265P and empty LPS treated lymphomas showing a strong induction by MYD88L265P and an even stronger upregulation by 2 hours 50 μ g/ml LPS stimulation. n=6 for empty, CARD11L244P, MYD88L265P and n=4 for LPS. Experiments were carried out in technical triplicates.

For determining the impact of our mutants on cellular NFkB signaling in a broad perspective, we chose to use an NFkB consensus site binding ELISA that can detect DNA binding activity of p65 (RelA), p52 (NFKB2), p50 and RelB in murine cells (106). Five lymphomas were tested for each NFkB subunit in triplicates in the mutant settings and 7 lymphomas were tested in the control group. The results (Figure 37) show that

MYD88L265P exerts an NFkB activating function via p52. p52 (synonymous for NFKB2) and is also directly transcriptionally upregulated by MYD88L265P (table 4). NFKBIZ transduction augments p65 binding (Figures 37, 38 and Table 5).

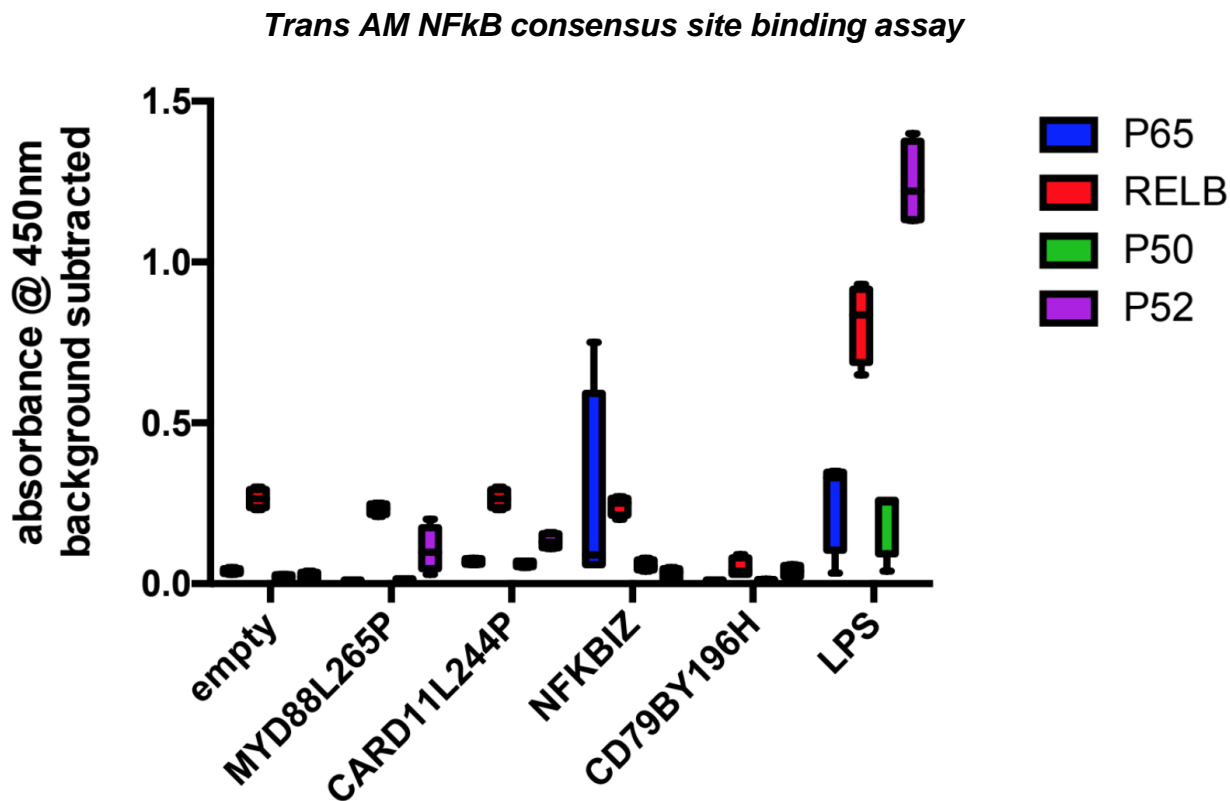


Figure 37: Differential binding of different NFkB subunits to the repeated NFkB consensus sequence (142) in mutant lymphomas relative to empty transduced lymphomas is shown. n=5 different lymphomas for each mutant and n=7 for empty.

I wanted to cross-check these results for p65 using another methodology with a potentially higher sensitivity. For achieving this goal, I established a p65 nuclear translocation FACS-microscopy-based assay using p65 nuclear translocation as a parameter for NFkB activation (Figure 38)

Analysis Interface for Image Stream Flow Microscopy

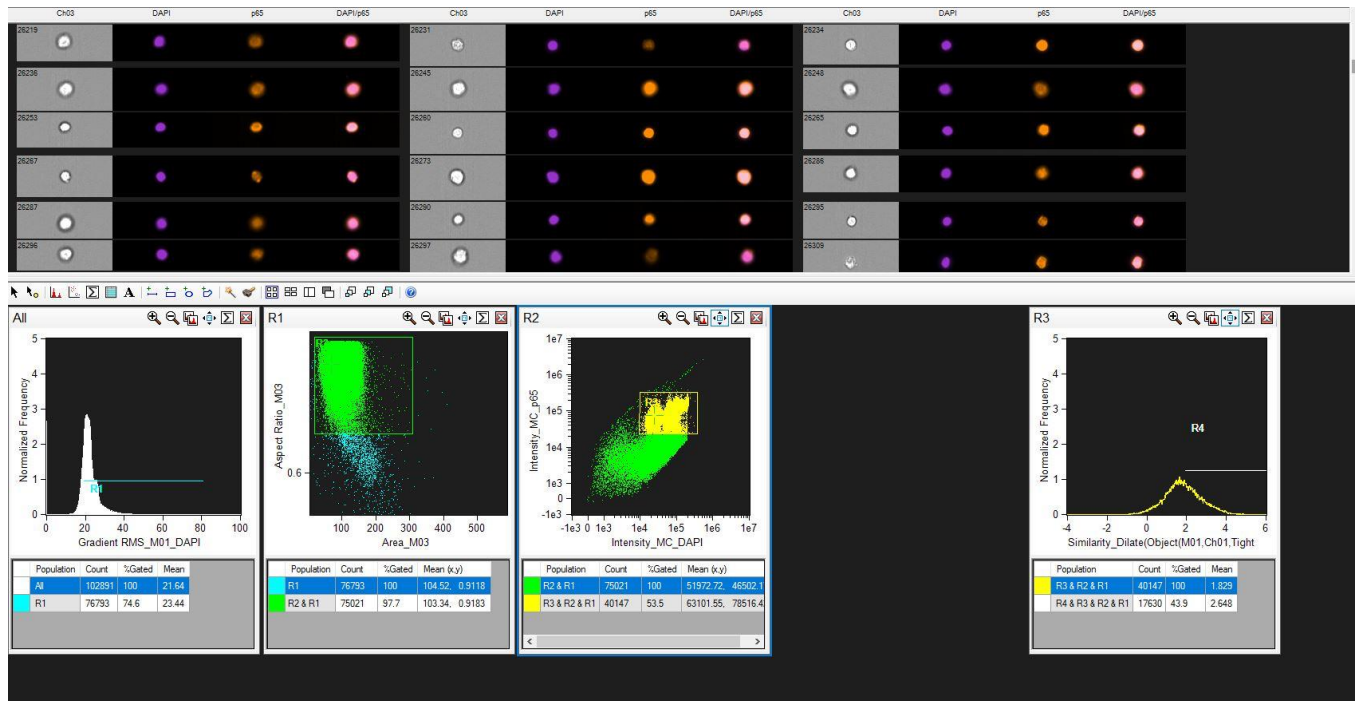


Figure 38: Gating strategy and analysis interface for Image Stream IDEAS data analysis depicting both the microscopic image for each cell in the fluorescence channels used and the overall classic FACS plots.

p65 nuclear localization histograms

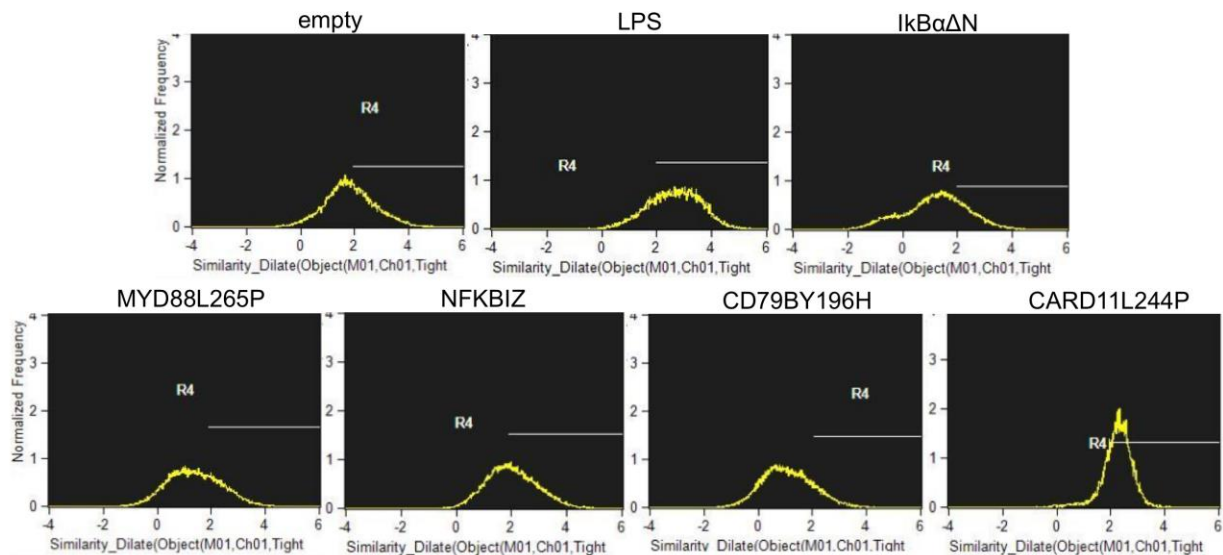


Figure 39: Histograms for nuclear translocation showing the correlation between the nucleus (detected via DAPI stain) and p65 staining for each acquired cell.

p65 nuclear localization statistics for MSCV-lesion transduced manifest E μ -myc transgenic lymphomas

<i>lesion</i>	<i>% of recorded events in R3</i>	<i>Mean translocation</i>	<i>% of recorded events in R4</i>
<i>Empty</i>	54	1.829	43.9
<i>LPS</i>	79	2.627	75.2
<i>IkB$\alpha\Delta N$</i>	78	1.201	25.9
<i>MYD88L265P</i>	54	1.375	31
<i>CARD11L244P</i>	78	2.243	77.9
<i>CD79BY196H</i>	60	1.095	16.4
<i>NFKBIZ</i>	78	2.006	53.1

Table 5: Statistics for nuclear translocation for each mutant, n=7 for empty and n=5 for each genetic lesion.

5 lymphomas were analyzed again for each group and 20 000 ungated events were acquired for each lymphoma. The gating strategy is depicted in Figure 38. Firstly, events in microscopic focus were included in gate R1. Afterwards, doublets were excluded. Thirdly, only cells that stained positive for both DAPI and p65 were finally included in the analysis. Cells with a correlation coefficient >2 were taken into gate 4 and regarded as “completely translocated”. The amount of originally recorded events that were finally analyzed in the analysis gate 3 for nuclear translocation was between 50-80% for individual samples and groups.

To examine the impact of the respective mutants in the MSCV-lesion-GFP transduced E μ -myc transgenic fetal liver cell lymphoma setting, we determined a target set of E μ -myc-specific NFkB targets by using all significantly downregulated transcripts from I kB $\alpha\Delta N$ transduced manifest E μ -myc transgenic lymphomas as an “NFkB E μ -myc specific fingerprint”. Comparing this target set to significantly differentially regulated transcripts of mutant induced FLC lymphomas, we found an NFkB upregulation fingerprint for MSCV-MYD88L265P-GFP, an up-and down regulation by MSCV-NFKBIZ-GFP, indifference by MSCV-CD79BY196H-GFP and consistent downregulation by MSCV-PD-

L1-GFP driven transduced E μ -myc transgenic FLC lymphomas compared to MSCV-empty-GFP transduced E μ -myc transgenic FLC lymphomas.

Heatmap of NF κ B Fingerprint in MSCV-lesion-GFP transduced E μ -myc transgenic FLC lymphomas compared to MSCV-empty-GFP transduced E μ -myc transgenic FLC lymphomas

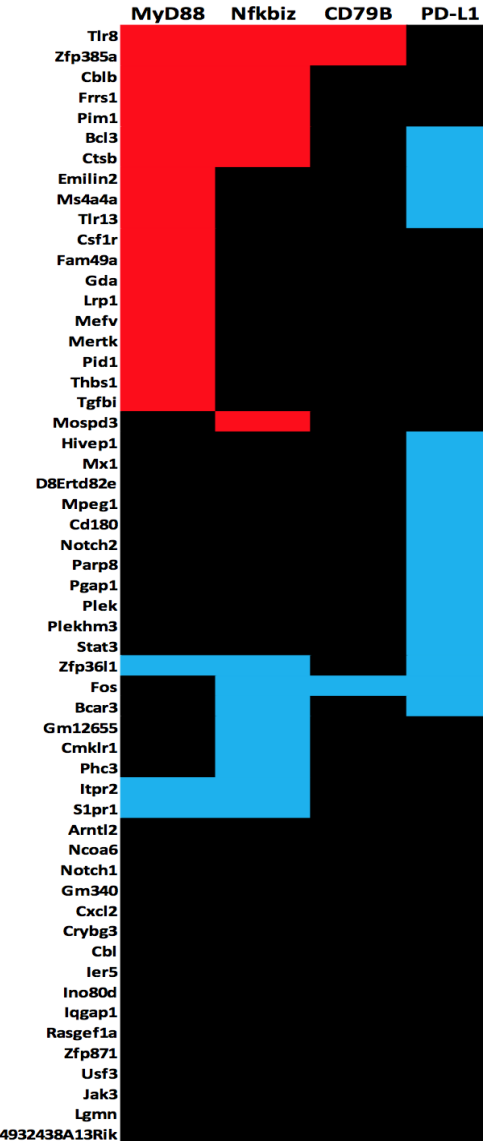


Figure 40: Transcripts shown on the left side denote significantly downregulated transcripts by I κ B $\alpha\Delta$ N transduced manifest E μ -myc transgenic lymphomas (n=7 I κ B $\alpha\Delta$ N

vs. n=8 empty). Significantly differential transcripts (cut-off p<0.05 after multiple testing correction) from MSCV-lesion-GFP transduced E μ -myc transgenic FLC lymphomas compared to MSCV-empty-GFP transduced E μ -myc transgenic FLC lymphomas were compared to this gene set showing differentially upregulated transcripts within the respective genotype in red and significantly downregulated transcripts in the respective genotype in blue. Black denotes no significant change.

In the manifest E μ -myc transgenic lymphomas, we also wanted to investigate the impact of NFKBIZ and MYD88L265P lesions on B-cell receptor activity due to a recent report from the Horikawa group demonstrating crosstalk and co-operativity between MYD88L265P and the B-cell receptor (143). We decided to use pBTK at Tyr223 as a surrogate parameter for B-cell receptor activity. Both lesion showed increased BTK phosphorylation compared to the empty vector control lymphomas

BTK Tyrosine 223 phosphorylation in NFKBIZ and MYD88L265P transduced manifest E μ -myc relative to empty E μ -myc lymphomas

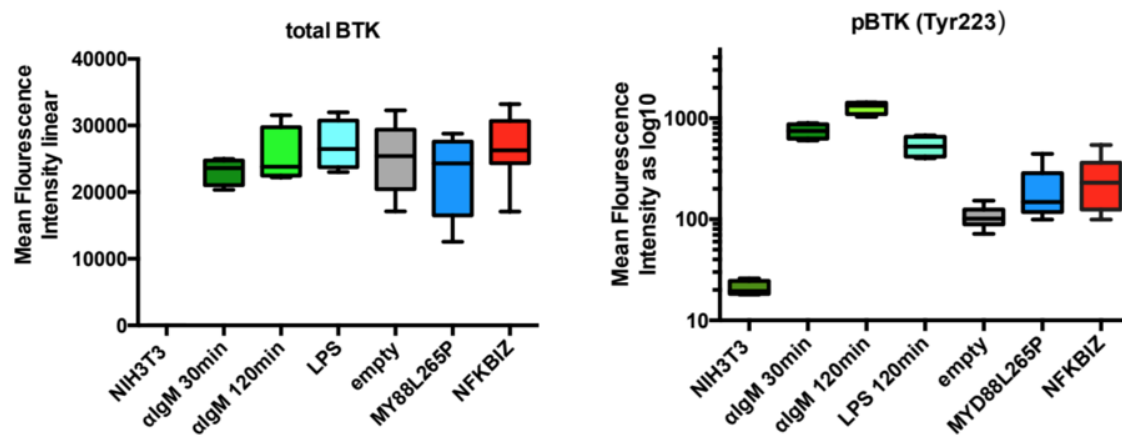


Figure 41: Total BTK levels in IgM treated empty, LPS-treated empty, unstimulated empty, unstimulated MYD88L265P and unstimulated NFKBIZ transduced manifest E μ -myc lymphomas measured using Luminex are shown. In NIH3T3 control cells, BTK is not detectable. The total BTK loading for all other settings is not significantly different (tested by one way ANOVA without multiple testing correction). In the same wells, pBTK was also

measured using another bead region. The controls differed significantly from empty transduced lymphomas ($p<0.0001$) and exhibited strong BTK phosphorylation after 2 hours LPS stimulation and even higher levels after 2 hours anti IgM stimulation. NFKBIZ and MYD88L265P transduced manifest E μ -myc lymphomas showed a significantly increased BTK phosphorylation when tested using a one way ANOVA with multiple testing correction against empty transduced E μ -myc lymphomas ($p=0.0007$ for NFKBIZ and $p=0.04$ for MYD88L265P). $n=3$ for IgM and LPS treatment, $n=5$ for empty and $n=4$ for MYD88L265P and $n=4$ for NFKBIZ. 3 technical replicates were acquired for each sample.

Metabolic Alterations driven by genetic lesions

Paired with the E μ -myc-genetic lesion interaction project, we performed a metabolomics study to investigate how mutants might alter the metabolic phenotype of MSCV-lesion-GFP transduced manifest E μ -myc transgenic lymphomas.

We performed this experiment due to the fact that different DLBCL metabolism-related findings had been made, primarily by the group of M. Shipp. Firstly, her group described an “Ox/Phos” human DLBCL subgroup from microarray studies that is signified by elevated transcripts associated with the cytochrome c oxidase, the NADPH dehydrogenase as well as other mitochondrial membrane proteins (29). Secondly, a follow-up study of these findings by the group of N. Danial demonstrated greater mitochondrial contribution to cellular energy balance in the “Ox/Phos” group and a greater role of fatty acid oxidation compared to the other subgroups (27). Thirdly, M. Shipp’s group reported that the SYK/PI3K axis in B-cell receptor dependent human DLBCL subgroups heavily impacts cholesterol synthesis and metabolism (74).

Using a methodology that can resolve a large array of cellular metabolites from amino acids to sterols, we asked the question: can the introduction of NFKBIZ, CD79BY196H, MYD88L265P, CARD11L244P or I k B $\alpha\Delta N$ into an already manifest E μ -myc transgenic manifest lymphoma change the metabolic composition of these lymphomas to e.g. increased or decreased sterol, nuclei acid or amino acid levels compared to the empty vector transduced controls?

To answer this question, we subjected MSCV-lesion-GFP transduced E μ -myc transgenic manifest lymphomas to extensive GC/LC MS metabolic profiling comprising approximately 2600 metabolites (Table 6).

We analyzed inguinal lymph nodes from animals that were immediately extracted after animals were euthanized. One inguinal lymph node was immediately snap frozen in liquid nitrogen after removal. The other inguinal lymph node was used for pathologic evaluation to ensure that only lymphoma and no surrounding or non-lymphoma tissue was extracted. For the experiment, pieces of approximately 15 mg were cut from whole lymph node biopsies and weighed afterwards. This was followed by metabolite extraction and metabolite measurement. Finally measured metabolite levels were normalized for weight cut from the tissues. For most evaluated genotypes, technical replicates from independent transductions, sorts and transplantations were analyzed.

Number of biological and technical replicates in lesion transduced E μ -myc transgenic manifest lymphomas used for metabolomics

	8720	8737	8740	8744	8749	8753	8754	9201	MYCtg/p53ko	spleen	thymus
empty	9	5	6	4	6	4	4	5	0	0	0
shscrambled	1	1	4	4	5	1	1	1	0	0	0
MYD88L265P	2	0	1	1	0	0	1	1	0	0	0
CARD11L244P	2	1	1	1	0	1	2	2	0	0	0
NFKBIZ	1	2	1	2	1	1	1	2	0	0	0
IkBAN	1	2	1	3	1	3	2	1	0	0	0
p53+/-	0	0	0	0	0	0	0	0	11	0	0
spleen	0	0	0	0	0	0	0	0	0	5	0
thymus	0	0	0	0	0	0	0	0	0	0	5

Table 6: The table shows the input matrix for the metabolite snapshot experiment. 102 lesion transduced manifest E μ -myc transgenic lymphomas, 11 manifest p53 +/- E μ -myc transgenic lymphomas, 5 spleens and 5 thymuses from wildtype mice were analyzed. Each number denotes from how many individual animals we used lymph nodes for measurement.

Experimental setup

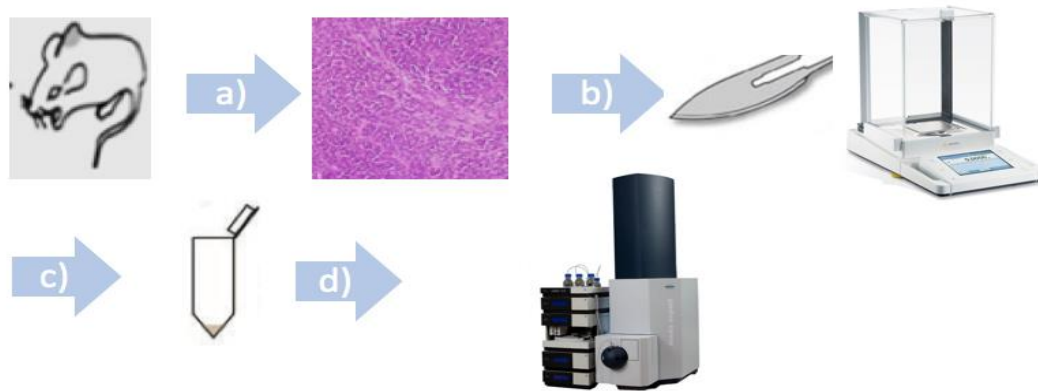


Figure 42: Illustration presenting our experimental setup for the metabolomics investigations of manifest lesion transduced E μ -myc transgenic lymphomas.

We chose spleens and thymuses from wildtype B57BL/6 mice and lymphomas from p53 -/+ E μ -myc transgenic manifest lymphomas (87) as control groups. The metabolite levels were normalized for weights cut from whole lymph nodes, spleens and thymus, respectively (Figure 29).

In the principal component analysis (144) spleen and thymus lymphomas were clearly separated from MSCV-empty-GFP transduced E μ -myc transgenic manifest lymphomas (Figure 43). The separation between MSCV-empty-GFP and MSCV-lesion-GFP transduced E μ -myc transgenic manifest lymphomas is rather weak. The PCA depicting samples grouped according to the originally transduced lymphoma was highly similar to the PCA obtained for transcriptome data as depicted in figure 32a (data for metabolome not shown). This indicates a stable metabolic phenotype despite functionally highly active mutations like MYD88L265P. Only in MSCV-NFKBIZ-GFP transduced manifest E μ -myc transgenic lymphomas metabolites significantly differing compared to MSCV-empty-GFP transduced lymphomas (Figure 45) were found. The variance in the empty group is unexpectedly large (Figure 46). This is not the case for thymus and spleen samples which were processed in the same way.

Overall principal component analysis of all analysed groups

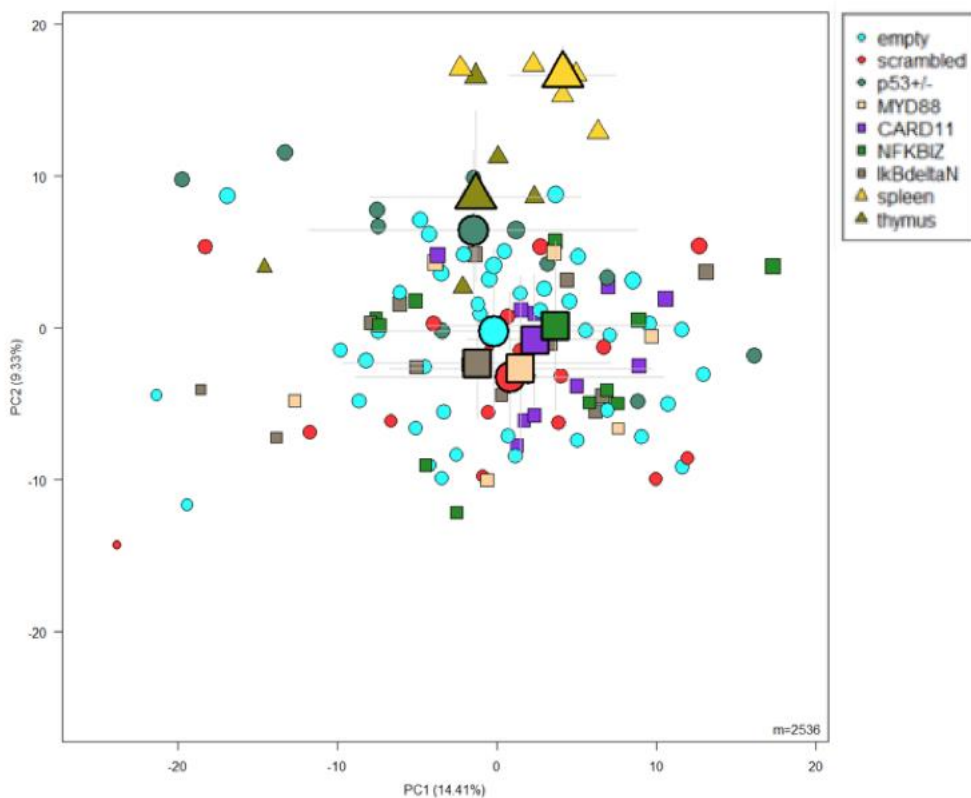


Figure 43: Overall PCA for all analyzed samples. Small dots represent single transduced E μ -myc transgenic lymphomas/spleens/thymuses and large symbols, the overall geometric mean.

P-value histograms of overall data for samples measured depicted in table 6

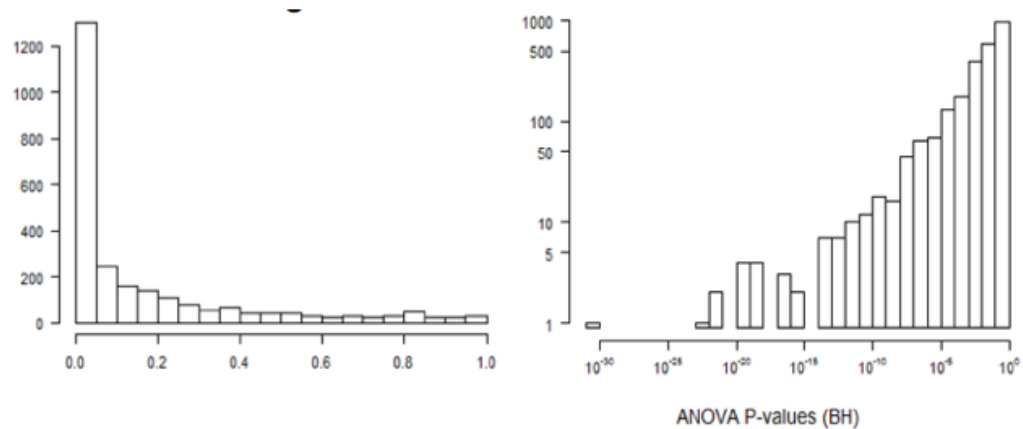


Figure 44: The histograms show the p-value distribution not multiple testing corrected and Benjamini-Hochberg multiple testing corrected.

Restricted principal component analysis and p-value histograms for transduced manifest E μ -myc lymphomas

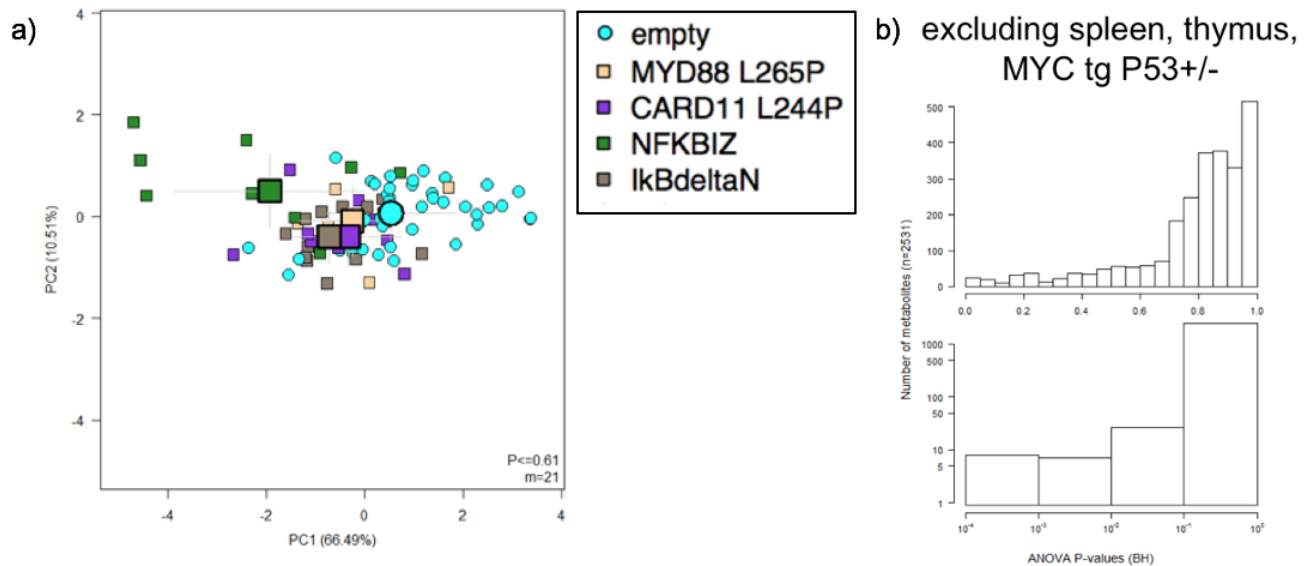


Figure 45: Restricted principal component analysis for transduced manifest E μ -myc lymphomas using only metabolites as underlying data that passed a <0.01 significance threshold after multiple testing. Small dots represent single lymphomas and large symbols, the overall geometric mean. b) the histogram shows the p-value distribution (already multiple testing corrected) for analyzed metabolites.

Restricted principal component analysis for MSCV-empty-GFP transduced and MSCV-NFKBIZ-GFP transduced manifest E μ -myc transgenic lymphomas and box-whisker plots for one exemplary metabolite

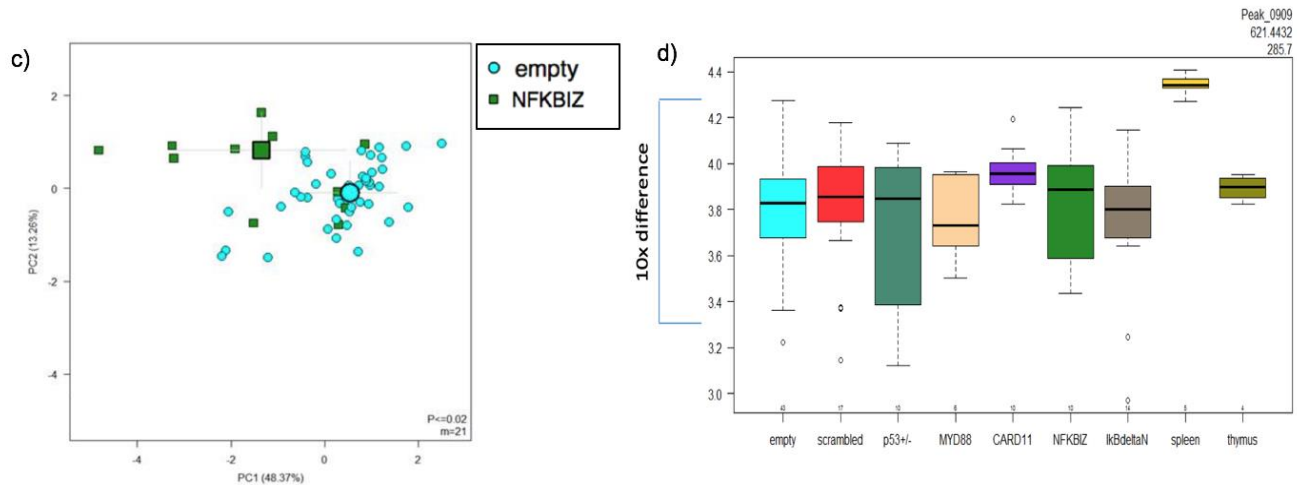


Figure 46: In the left, a restricted principal component analysis depicting only NFKBIZ and empty transduced manifest E μ -myc lymphomas. On the right box-whisker plots for one mass spectrometry peak are exemplarily shown. The plot is representative for most analyzed metabolites showing the large intra-group variances of metabolite levels. The variances within spleen and thymus groups are much smaller.

Metabolites showing significantly different levels between NFKBIZ and empty transduced manifest E μ -myc lymphomas

Retention Time	m/z	Name
24	296.0666	"Choline glycerophosphate"
24	175.1186	"Arginine"
25	398.0338	"unknown"
25	254.0186	"Shikimate 5-phosphate"
54	112.051	"Cytosine"
55	228.0976	"Deoxycytidine"
86	126.0674	"5-Methylcytosine"
26	258.1101	"5-Methylcytidine"

Table 7: The eight metabolites that pass a significance threshold of 0.01 after multiple testing correction in the comparison of MSCV-empty-GFP vs. MSCV-NFKBIZ-GFP transduced manifest E μ -myc transgenic lymphomas.

A few consistent effects could however be observed for NFKBIZ samples. Employing a restricted PCA that only takes into account Benjamini-Hochberg multiple testing corrected significantly differentially regulated metabolites we could isolate a set of 21 metabolites that give an acceptable metabolic separation for empty vs NFKBIZ (Figure 46) transduced lymphomas. Among those the top 8 passed a significance threshold of 0.01. Among them 4 metabolites from cytosine metabolism were found (Figure 47 and Table 7).

Box-Whisker Plots for relative levels of cytosine metabolites measured in empty and NFKBIZ transduced manifest E μ -myc lymphomas

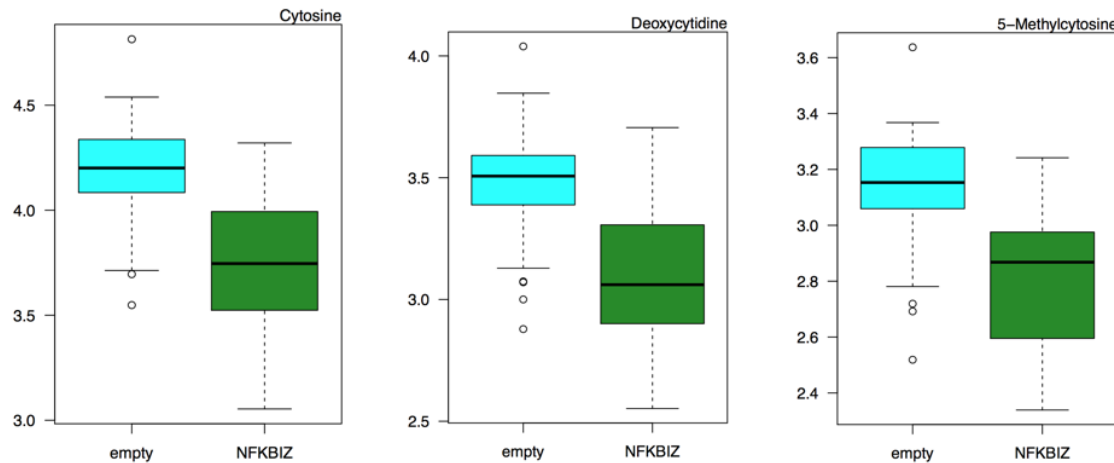


Figure 47: Box-Whisker Plots for cytosine and two related metabolites that were found to be significantly different between empty and NFKBIZ transduced lymphomas. The 5-95% confidence interval is depicted. The black bars within the boxes denote the median.

Discussion

The fetal liver cell approach

MYD88L265P and NFKBIZ showed highly penetrant phenotypes concerning formation of aggressive lymphomas in concert with E μ -myc (47). CD79BY196H does not show the same degree of penetrance. The dependence of all these mutants on an additional oncogene for lymphomagenesis is demonstrated by the fact that no lesion driven lymphomas are formed when wildtype fetal liver cells not containing the E μ -myc transgene are transduced within the observation period of 300 days.

From RNA sequencing studies on B220+ purified empty vector and lesion driven lymphomas we found that NFKBIZ (37) and MYD88L265P (34) driven lymphomas constitute transcriptionally distinguishable lymphoma entities in this system (134). This means that MYD88L265P driven lymphomas constitute, in co-operation with E μ -myc, a very homogenous lymphoma entity that can be distinguished from other lesion driven E μ -myc FLC lymphomas and empty-E μ -myc FLC lymphomas via transcriptome profiling. The same applies to NFKBIZ driven E μ -myc FLC lymphomas. This led to distinct “NFKBIZ-lymphoma” signaling patterns in mutant driven lymphomas that were different from those of “MYD88L265P-lymphoma”. That both lesions constituted biologically different entities is supported by the difference in fundamental parameters like immune-cell infiltration (macrophages increased in MYD88L265P driven lymphomas), proliferation markers (Ki67 indices decreased in both NFKBIZ and MYD88L265P driven lymphomas) and specific vulnerabilities (PD-L1 surface expression on MYD88L265P driven lymphomas) (70, 145).

The possibility to detect MYD88L265P and NFKBIZ clusters is especially remarkable, as aggressive lymphomas are subject to extensive gene expression profiling studies (8, 30). MYD88L265P mutations and NFKBIZ amplifications were originally identified to be highly enriched in a subgroup of DLBCL that transcriptionally resembles activated B-cells (ABC subgroup of DLBCL) (18, 34, 37). ABC DLBCL was shown to be a particularly aggressive lymphoma subgroup (47, 146).

Regarding tailored treatment options, certain aspects of MYD88L265P driven lymphomas were noteworthy. Firstly, although the most aggressive and penetrant lesion, these lymphomas exhibited the lowest amount of Ki67-positive cells from all cohorts in our FLC transplantation approach. The second feature of the MYD88L265P driven lymphomas was the increased amount of macrophages found in these lymphomas. The third aspect was the expression of PD-L1 and PD-L2. Neither PD-L1 nor PD-L2 expression could be detected on any of the manifest empty-E μ -myc FLC lymphomas nor on more than 10% of the lymphoma cells formed by another lesion. This observation might be, of course, in close relation with the increased macrophage infiltration that was observed in MY88L265P driven lymphomas. However, neither isolated MYD88L265P driven lymphomas (achieved by the simultaneous knockdown of PD-L1) nor PD-L1 driven lymphomas (which do not simultaneously overexpress MYD88) show this phenotype. This observation clarifies that only the interplay of both lesions expressed in B220+ cells is sufficient for this very distinct and aggressive “MYD88L265P” phenotype affecting proliferation and lymphoma-immune interaction in the E μ -myc fetal liver cell system. This finding is of particular interest, as checkpoint inhibitor treatment strategies are currently investigated in many trials as a second line treatment for aggressive lymphomas (147, 148).

The contribution of PD-L1 to the aggressiveness of MYD88L265P driven lymphomas was illustrated by the prolongation of survival by knockdown of PD-L1 on MYD88L265P driven lymphomas. However, 6 of 8 transplanted animals nevertheless succumbed to MYD88L265P driven lymphomas, demonstrating that efficient ablation of PD-L1 expression is not sufficient to completely ablate MYD88L265P driven lymphomagenesis in our system. This experiment illustrated that PD-L1 is an important, but dispensable mechanism in MYD88L265P E μ -myc driven lymphomagenesis. We could observe from RNA seq data that the top KEGG and Gene Ontology Term annotation clusters for MYD88L265P driven lymphomas compared to empty E μ -myc lymphomas were “antigen processing and presentation of exogenous peptide antigen via MHC class II” and “Graft versus Host disease” (149, 150). This finding indicates a much broader array of immune

evasive mechanisms exploited by MYD88L265P driven lymphomas than could be investigated in this dissertation (151).

A recent report by the Felsher group showed that in a T-ALL model MYC functions via direct transcriptional activation of PD-L1 and partly maintains thereby tumorigenesis (152). In general, direct activation of PD-L1 via MYC seems to be of limited importance in the E μ -myc system which lacks additional genetic lesions like MYD88L265P. This is underlined by the observations that we can detect minimal PD-L1 surface expression on empty E μ -myc lymphomas (153). Additionally, also a constitutive knockdown of PD-L1 in the experimental approach of transducing E μ -myc transgenic fetal liver cells with MYD88L265PshPD-L1 did not prevent enrichment of these cells in the resulting lymphomas.

PD-L1 itself proved to be more than just a bystander phenomenon in our system. An oncogenic driver in co-operation with E μ -myc in our system, PD-L1 exhibited interesting effects on the lymphoma signaling mechanisms apart from being a mere “T-cell-lightning-rod” on tumor cells (154). From the RNA seq data of PD-L1 driven E μ -myc lymphomas, we could observe that a large array of additional immune evasive mechanisms are evoked in the B220+ cells of MYD88L265P driven E μ -myc FLC lymphomas with “Graft versus host disease” and “antigen processing via MHC Class II” being examples of the top scoring annotation cluster lists from the KEGG and Gene Ontology annotation clusters (exemplified by genes like MHCII, TAP, ICOSL and CD80) (149, 155, 156). B220+ cells from PD-L1 driven E μ -myc lymphomas showed a reduction of BCL6 (157) levels to less than 1% of those found in empty E μ -myc lymphomas within RNA Seq data. This notion might justify further investigations in direction towards the interplay of BCL6 and PD-L1 in other murine lymphoma systems, as both have the capacity to drive lymphomas in murine tumors and are highly prevalent lesions in aggressive lymphomas (61) NFKBIZ, which is a rather new lesion in the field of lymphoma biology (37, 158, 159), showed equally powerful penetrance and aggressiveness as MYD88L265P in our system. One of the findings from our study concerning NFKBIZ was its significant upregulation in both MYD88L265P driven E μ -myc FLC lymphomas but also in manifest MYD88L265P

transduced E μ -myc lymphomas. Vice versa, a similarly strong crosstalk was not observed. As NFKBIZ can be found in lymphomas as an amplification, already simple transcriptional upregulation might have a lymphoma-promoting impact (37). Despite this potential assistance of NFKBIZ in MYD88L265P driven lymphomagenesis, the cluster of NFKBIZ E μ -myc driven lymphomas proved to be clearly distinguishable from MYD88L265P driven lymphomas. Hence, they do not just represent subsets in a MYD88L265P lymphoma cluster.

In contrast to NFKBIZ and MYD88L265P, we could not generate CARD11L244P driven lymphomas in the E μ -myc FLC system, yet we found GFP positive cells in the spleens of seemingly healthy CARD11L244P E μ -myc fetal liver cell transplanted mice. All of the GFP positive cells in the spleens of seemingly healthy CARD11L244P E μ -myc fetal liver cell transplanted mice showed to be senescent. Thus, we generated the hypothesis of oncogene-induced senescence as a barrier in CARD11L244P driven lymphomagenesis (105). As GFP positive lymphomas formed in CARD11L244P E μ -myc fetal liver cell transplanted mice in the absence of an oncogene induced senescence barrier (SUV39H1 -/- E μ -myc system), we could further strengthen this hypothesis (70).

This finding is complementary to a recent report by the Ruland Group showing a hyperproliferative phenotype of CARD11L244I lesion in a murine model of CD19 dependent model of mutant CARD11 overexpression (160) without additional genetic lesions.

Our approach also demonstrated that MYD88265P, NFKBIZ and CARD11L244P can function as tumor driving lesions when they are present as constitutively LTR-driven overexpressed lesions in hematopoietic stem cells with MYC as a second hit that enters our system when MYC overexpression is induced via the IgM enhancer (59) in the course of B-cell-lineage commitment (E μ -myc transgene) which is interesting in the context of the currently rapidly evolving investigations into the role of clonal hematopoiesis in hematologic malignancies (161, 162).

The manifest E μ -myc lymphoma approach

MYD88L265P was the lesion with the most prominent phenotypic effect in the setting of retrovirally transduced manifest E μ -myc lymphomas with genetic lesions of interest and retransplantation into immunocompetent C57BL6/N mice.

Contrasting its lymphomagenic effect in concert with E μ -myc in the fetal liver cell approach, MYD88L265P transduced manifest E μ -myc lymphomas showed delayed or even completely ablated lymphoma formation (ablated in two of eight tested lymphomas) (163, 164). It was striking that MYD88L265P transduced manifest E μ -myc lymphomas frequently shared the feature of Ki67 indices <60% with their MYD88L265P driven fetal liver cell counterparts. However, the molecular basis is probably different to the MYD88L265P effects in the fetal liver cell approach. The MYD88L265P transduced manifest E μ -myc lymphomas neither show surface PD-L1 or PD-L2 expression nor do we see any significant upregulation of PD-L1 or PD-L2 in the RNA seq data. MYD88L265P overexpression without PD-L1 surface expression in the fetal liver cell setting did not show an effect towards reduced Ki67 indices. Therefore, the increased H3K9me3, reduced Ki67 stains and delayed lymphoma onsets probably rather reflect an oncogene induced senescence phenotype that were also observed in CARD11L244P transduced cells in the E μ -myc fetal liver cell approach (105).

The top scoring gene ontology annotation term for the RNA seq data for MYD88L265P transduced manifest E μ -myc lymphomas was “innate immune system processes” as we expected. As a consequence, the extent to which toll-like-receptor activation might be a therapeutic option in MYC overexpressing lymphomas (58, 165) should be addressed in future investigations.

Manifest empty vector transduced E μ -myc show no or minimal surface PD-L1 expression. Introducing PD-L1 in this setting leads to the upregulation of inflammatory signaling markers like NFKBIZ, NFKBID, IKBKE, LAT, AIM2 and TNFSF9 and genes associated with DNA replication and cell division in RNA seq data. Contrasting the KEGG and gene ontology terms of PD-L1 driven fetal liver cell lymphomas, the top annotation clusters in the setting of manifest PD-L1 transduced E μ -myc lymphomas were “DNA templated

transcription” and “cell cycle”. This potential impact of PD-L1 as a proliferation driver in manifest E μ -myc lymphomas deserves further attention (154, 166).

Retransplanted NFKBIZ transduced manifest E μ -myc lymphomas did not show any alterations in survival compared to empty vector transduced manifest E μ -myc lymphomas, contrasting the highly penetrant lymphomagenic properties of NFKBIZ compared to empty in the E μ -myc fetal liver cell lymphoma approach.

NFKBIZ transduced manifest E μ -myc lymphomas showed very few transcriptional changes compared to empty vector transduced E μ -myc lymphomas contrasting the transcriptional changes contrasting again the observations of NFKBIZ vs. empty in the E μ -myc fetal liver cell lymphoma approach. In the RNA Seq data retrovirally overexpressed NFKBIZ was the only gene that could be declared with certainty to be differentially regulated compared to the manifest empty transduced E μ -myc lymphomas. On the protein level, we found NFKBIZ to induce significant p65 nuclear translocation and increased p65 DNA binding compared to the empty vector control transduced manifest E μ -myc lymphomas (TransAM DNA binding ELISA and FACS-Microscopy p65 nuclear translocation) (167). A closer look at effects of MYD88L265P and NFKBIZ signaling in the system was prompted by a recent report of the Horikawa group demonstrating the augmenting effect of MYD88L265P on B-cell receptor signaling in their system (143). Examining the impact of MYD88L265P and NFKBIZ on BCR signaling via accessing BTK Tyr223 phosphorylation we could observe increased B-cell receptor signaling in both settings against the background of low baseline BTK phosphorylation in the empty vector transduced lymphomas (168). Yet, despite low baseline BTK Tyr223 phosphorylation in the empty vector control lymphomas, they showed a strongly increased phosphorylation upon both IgM and LPS stimulation. As the unstimulated empty, MYD88L265P and NFKBIZ transduced manifest E μ -myc lymphoma protein lysates were directly prepared from ex vivo material, their phosphorylation status most like represents a physiologic situation.

Lastly, we investigated the effect of the chosen genetic lesion on the lymphoma metabolism as we aimed to gain metabolic insights into the oncogene induced senescence phenotype observed in MYD88L265P transduced manifest E μ -myc lymphomas and the NFkB augmenting phenotype in NFKBIZ transduced manifest

E μ -myc lymphomas (75, 169). The lesions had very little impact on the metabolic phenotype of the transduced lymphomas (170). Contrasting the very homogenous phenotype in spleen and thymus controls E μ -myc transgenic lymphomas displayed frequently ten-fold differences in the levels of central metabolites like glutamate between individual lymphomas. This was never observed in healthy control tissues. Only in NFKBIZ transduced E μ -myc a few significantly downregulated metabolites from cytosine metabolism could be identified compared to empty. Thus, we could conclude that MYC driven lymphomas show a large divergence in their metabolic phenotype not observed in normal lymphatic tissues. Yet none of the transduced genes we investigated (MYD88L265P, NFKBIZ, CARD11L244P, CD79BY196H and I κ B $\alpha\Delta$ N) could significantly change the overall metabolic phenotype compared to the empty transduced controls contrasting E μ -myc P53 +/- lymphomas that were clearly distinguishable from E μ -myc P53 +/+ lymphomas. Therefore, the genetic lesions we investigated showed a minor impact on metabolite levels in a MYC driven lymphoma system with no significant impact of the investigated lesions on sterol, fatty acid or TCA cycle metabolites. Yet we detected a very specific effect of the transcription factor NFKBIZ on cytosine metabolism which involves 5-Methylcytosine that is also the main substrate for TET2 (172, 173). Finally, it should be noted that the retransplantations and technical replicates made for studies of lesion-transduced manifest E μ -myc lymphomas were not only used for the investigations presented in this thesis but also for an ensuing study evaluating the impact of these lesions on the central nervous system tropism of E μ -myc lymphomas and its molecular biology (174).

In summary, we demonstrated that the same genetic lesions vary considerably in their biological impact depending on an early introduction as driver lesion in E μ -myc FLCs or late addition as add-ons in already manifest E μ -myc lymphomas.

We showed the varying penetrance of different genetic lesions in E μ -myc co-operated lymphomagenesis in the FLC model with MYD88L265P and NFKBIZ displaying a highly penetrant and aggressive phenotype. Furthermore, we elucidated the immune evasive mechanisms which MYD88L265P exploits in lymphomagenesis. Likewise, we described oncogene-induced senescence in CARD11L244P driven lymphomagenesis. Finally, we

showed the profound transcriptional changes exerted by the investigated lesions in lymphomagenesis and the paucity of transcriptional changes when introduced in already manifest E μ -myc lymphomas.

Bibliography

1. Lenz G, Staudt LM. Aggressive lymphomas. *New England Journal of Medicine.* 2010;362(15):1417-1429.
2. Conley ME, Dobbs AK, Farmer DM, Kilic S, Paris K, Grigoriadou S, Coustan-Smith E, Howard V, Campana D. Primary B cell immunodeficiencies: comparisons and contrasts. *Annual review of immunology.* 2009;27:199-227.
3. Smith-Garvin JE, Koretzky GA, Jordan MS. T cell activation. *Annual review of immunology.* 2009;27:591-619.
4. Korfel A, Chamberlain M, Neuwelt E, Thiel E, Doolittle N, Schlegel U, Dreyling M, Rubenstein J, Fischer L, Björkholm M, Martus P, Weller M, Glantz M. Therapy for Secondary CNS Involvement in Malignant Lymphomas: No Standard Yet! *Journal of Clinical Oncology.* 2016;34(15):1829-1830.
5. Fisher SG, Fisher RI. The epidemiology of non-Hodgkin's lymphoma. *Oncogene.* 2004;23(38):6524. 6524-34
6. Bouska A, Bi C, Lone W, Zhang W, Kedwaii A, Heavican T, Lachel CM, Yu J, Ferro R, Eldorhamy N, Greiner TC, Vose J, Weisenburger DD, Gascoyne RD, Rosenwald A, Ott G, Campo E, Rimsza LM, Jaffe ES, Braziel RM, Siebert R, Miles RR, Dave S, Reddy A, Delabie J, Staudt LM, Song JY, McKeithan TW, Fu K, Green M, Chan WC, Iqbal J. Adult high-grade B-cell lymphoma with Burkitt lymphoma signature: genomic features and potential therapeutic targets. *Blood.* 2017;130(16):1819-1831.
7. Dave SS, Fu K, Wright GW, Lam LT, Kluin P, Boerma E-J, Greiner TC, Weisenburger DD, Rosenwald A, Ott G, Müller-Hermelink H-K, Gascoyne RD, Delabie J, Rimsza LM, Braziel RM, Grogan TM, Campo E, Jaffe ES, Dave BJ, Sanger W, Bast M, Vose JM, Armitage JO, Connors JM, Smeland EB, Kvaloy S, Holte H, Fisher RI, Miller TP, Montserrat E, Wilson WH, Bahl M, Zhao H, Yang L, Powell J, Simon R, Chan WC, Staudt LM. Molecular Diagnosis of Burkitt's Lymphoma. *New England Journal of Medicine.* 2006;354(23):2431-2442.
8. Hummel M, Bentink S, Berger H, Klapper W, Wessendorf S, Barth TFE, Bernd H-W, Cogliatti SB, Dierlamm J, Feller AC, Hansmann M-L, Haralambieva E, Harder L, Hasenclever D, Kühn M, Lenze D, Lichter P, Martin-Subero JI, Möller P, Müller-Hermelink H-K, Ott G, Parwaresch RM, Pott C, Rosenwald A, Rosolowski M,

- Schwaenen C, Stürzenhofecker B, Szczepanowski M, Trautmann H, Wacker H-H, Spang R, Loeffler M, Trümper L, Stein H, Siebert R. A Biologic Definition of Burkitt's Lymphoma from Transcriptional and Genomic Profiling. *New England Journal of Medicine*. 2006;354(23):2419-2430.
9. Taub R, Kirsch I, Morton C, Lenoir G, Swan D, Tronick S, Aaronson S, Leder P. Translocation of the c-myc gene into the immunoglobulin heavy chain locus in human Burkitt lymphoma and murine plasmacytoma cells. *Proceedings of the National Academy of Sciences*. 1982;79(24):7837-7841.
10. Gross R, Wulf G. Klinische und experimentelle Erfahrungen mit zyklischen und nichtzyklischen Phosphamidestern des N-Losl in der Chemotherapie von Tumoren. *Strahlentherapie*. 1959;41:361-367.
11. Ziegler JL. Treatment results of 54 American patients with Burkitt's lymphoma are similar to the African experience. *New England Journal of Medicine*. 1977;297(2):75-80.
12. Pfreundschuh M, Trümper L, Österborg A, Pettengell R, Trneny M, Imrie K, Ma D, Gill D, Walewski J, Zinzani P-L, Stahel R, Kvaloy S, Shpilberg O, Jaeger U, Hansen M, Lehtinen T, López-Guillermo A, Corrado C, Scheliga A, Milpied N, Mendila M, Rashford M, Kuhnt E, Loeffler M. CHOP-like chemotherapy plus rituximab versus CHOP-like chemotherapy alone in young patients with good-prognosis diffuse large-B-cell lymphoma: a randomised controlled trial by the MabThera International Trial (MInT) Group. *The Lancet Oncology*. 2006;7(5):379-391.
13. Coiffier B, Thieblemont C, Van Den Neste E, Lepeu G, Plantier I, Castaigne S, Lefort S, Marit G, Macro M, Sebban C, Belhadj K, Bordessoule D, Fermé C, Tilly H. Long-term outcome of patients in the LNH-98.5 trial, the first randomized study comparing rituximab-CHOP to standard CHOP chemotherapy in DLBCL patients: a study by the Groupe d'Etudes des Lymphomes de l'Adulte. *Blood*. 2010;116(12):2040-2045.
14. Hitz F, Connors JM, Gascoyne RD, Hoskins P, Moccia AA, Savage KJ, Sehn LH, Shenkier T, Klasa R. Outcome of patients with chemotherapy refractory and early progressive diffuse large B cell lymphoma after R-CHOP treatment. *Blood*. 2010;116(21):1751-1751.

15. Swerdlow SH, Campo E, Pileri SA, Harris NL, Stein H, Siebert R, Advani R, Ghielmini M, Salles GA, Zelenetz AD, Jaffe ES. The 2016 revision of the World Health Organization classification of lymphoid neoplasms. *Blood*. 2016;127(20):2375-2390.
16. Craig FE, Foon KA. Flow cytometric immunophenotyping for hematologic neoplasms. *Blood*. 2008;111(8):3941-3967.
17. Schmitz R, Young RM, Ceribelli M, Jhavar S, Xiao W, Zhang M, Wright G, Shaffer AL, Hodson DJ, Buras E, Liu X, Powell J, Yang Y, Xu W, Zhao H, Kohlhammer H, Rosenwald A, Kluin P, Müller-Hermelink HK, Ott G, Gascoyne RD, Connors JM, Rimsza LM, Campo E, Jaffe ES, Delabie J, Smeland EB, Ogwang MD, Reynolds SJ, Fisher RI, Braziel RM, Tubbs RR, Cook JR, Weisenburger DD, Chan WC, Pittaluga S, Wilson W, Waldmann TA, Rowe M, Mbulaiteye SM, Rickinson AB, Staudt LM. Burkitt Lymphoma Pathogenesis and Therapeutic Targets from Structural and Functional Genomics. *Nature*. 2012;490(7418):116-120.
18. Alizadeh AA, Eisen MB, Davis RE, Ma C, Lossos IS, Rosenwald A, Boldrick JC, Sabet H, Tran T, Yu X, Powell JI, Yang L, Marti GE, Moore T, Hudson Jr J, Lu L, Lewis DB, Tibshirani R, Sherlock G, Chan WC, Greiner TC, Weisenburger DD, Armitage JO, Warnke R, Levy R, Wilson W, Grever MR, Byrd JC, Botstein D, Brown PO, Staudt LM. Distinct types of diffuse large B-cell lymphoma identified by gene expression profiling. *Nature*. 2000;403:503-511
19. Bullinger L, Döhner K, Bair E, Fröhling S, Schlenk RF, Tibshirani R, Döhner H, Pollack JR. Use of gene-expression profiling to identify prognostic subclasses in adult acute myeloid leukemia. *New England Journal of Medicine*. 2004;350(16):1605-1616.
20. Rosenwald A, Wright G, Chan WC, Connors JM, Campo E, Fisher RI, Gascoyne RD, Muller-Hermelink HK, Smeland EB, Giltnane JM, Hurt EM, Zhao H, Averett L, Yang L, Wilson WH, Jaffe ES, Simon R, Klausner RD, Powell J, Duffey PL, Longo DL, Greiner TC, Weisenburger DD, Sanger WG, Dave BJ, Lynch JC, Vose J, Armitage JO, Montserrat E, López-Guillermo A, Grogan TM, Miller TP, LeBlanc M, Ott G, Kvaloy S, Delabie J, Holte H, Krajci P, Stokke T, Staudt LM. The Use of Molecular Profiling to Predict Survival after Chemotherapy for Diffuse Large-B-Cell Lymphoma. *New England Journal of Medicine*. 2002;346(25):1937-1947.

21. Lam K-P, Kühn R, Rajewsky K. In vivo ablation of surface immunoglobulin on mature B cells by inducible gene targeting results in rapid cell death. *Cell*. 1997;90(6):1073-1083.
22. Casola S, Otipoby KL, Alimzhanov M, Humme S, Uyttersprot N, Kutok JL, Carroll MC, Rajewsky K. B cell receptor signal strength determines B cell fate. *Nature Immunology* 2004;5(3):317-327.
23. Pasparakis M, Schmidt-Suprian M, Rajewsky K. IκB Kinase Signaling Is Essential for Maintenance of Mature B Cells. *The Journal of Experimental Medicine*. 2002;196(6):743-752.
24. Davis RE, Ngo VN, Lenz G, Tolar P, Young RM, Romesser PB, Kohlhammer H, Lamy L, Zhao H, Yang Y, Xu W, Shaffer AL, Wright G, Xiao W, Powell J, Jiang JK, Thomas CJ, Rosenwald A, Ott G, Muller-Hermelink HK, Gascoyne RD, Connors JM, Johnson NA, Rimsza LM, Campo E, Jaffe ES, Wilson WH, Delabie J, Smeland EB, Fisher RI, Braziel RM, Tubbs RR, Cook JR, Weisenburger DD, Chan WC, Pierce SK, Staudt LM. Chronic active B-cell-receptor signalling in diffuse large B-cell lymphoma. *Nature*. 2010;463(7277):88-92.
25. Wilson WH, Young RM, Schmitz R, Yang Y, Pittaluga S, Wright G, Lih CJ, Williams PM, Shaffer AL, Gerecitano J, de Vos S, Goy A, Kenkre VP, Barr PM, Blum KA, Shustov A, Advani R, Fowler NH, Vose JM, Elstrom RL, Habermann TM, Barrientos JC, McGreivy J, Fardis M, Chang BY, Clow F, Munneke B, Moussa D, Beaupre DM, Staudt LM. Targeting B cell receptor signaling with ibrutinib in diffuse large B cell lymphoma. *Nature Medicine* 2015;21(8):922-926.
26. Shipp MA, Ross KN, Tamayo P, Weng AP, Kutok JL, Aguiar RCT, Gaasenbeek M, Angelo M, Reich M, Pinkus GS, Ray TS, Koval MA, Last KW, Norton A, Lister TA, Mesirov J, Neuberg DS, Lander ES, Aster JC, Golub TR. Diffuse large B-cell lymphoma outcome prediction by gene-expression profiling and supervised machine learning. *Nature Medicine*. 2002;8:68-74
27. Caro P, Kishan AU, Norberg E, Stanley IA, Chapuy B, Ficarro SB, Polak K, Tonnerer D, Gounaris J, Yin H, Zhou F, Green MR, Chen L, Monti S, Marto JA, Shipp MA, Danial NN. Metabolic signatures uncover distinct targets in molecular subsets of diffuse large B cell lymphoma. *Cancer Cell*. 2012;22(4):547-560.

28. Norberg E, Lako A, Chen PH, Stanley IA, Zhou F, Ficarro SB, Chapuy B, Chen L, Rodig S, Shin D, Choi DW, Lee S, Shipp MA, Marto JA, Danial NN. Differential contribution of the mitochondrial translation pathway to the survival of diffuse large B-cell lymphoma subsets. *Cell Death Differ.* 2016;251-262
29. Monti S, Savage KJ, Kutok JL, Feuerhake F, Kurtin P, Mihm M, Wu B, Pasqualucci L, Neuberg D, Aguiar RC, Dal Cin P, Ladd C, Pinkus GS, Salles G, Harris NL, Dalla-Favera R, Habermann TM, Aster JC, Golub TR, Shipp MA. Molecular profiling of diffuse large B-cell lymphoma identifies robust subtypes including one characterized by host inflammatory response. *Blood.* 2005;105(5):1851-1861.
30. Lenz G, Wright G, Dave SS, Xiao W, Powell J, Zhao H, Xu W, Tan B, Goldschmidt N, Iqbal J, Vose J, Bast M, Fu K, Weisenburger DD, Greiner TC, Armitage JO, Kyle A, May L, Gascoyne RD, Connors JM, Troen G, Holte H, Kvaloy S, Dierickx D, Verhoef G, Delabie J, Smeland EB, Jares P, Martinez A, Lopez-Guillermo A, Montserrat E, Campo E, Braziel RM, Miller TP, Rimsza LM, Cook JR, Pohlman B, Sweetenham J, Tubbs RR, Fisher RI, Hartmann E, Rosenwald A, Ott G, Muller-Hermelink H-K, Wrench D, Lister TA, Jaffe ES, Wilson WH, Chan WC, Staudt LM. Stromal Gene Signatures in Large-B-Cell Lymphomas. *New England Journal of Medicine.* 2008;359(22):2313-2323.
31. Younes A. Prognostic Significance of Diffuse Large B-Cell Lymphoma Cell of Origin: Seeing the Forest and the Trees. *Journal of Clinical Oncology.* 2015;33(26):2835-2836.
32. Staiger AM, Ziepert M, Horn H, Scott DW, Barth TFE, Bernd H-W, Feller AC, Klapper W, Szczepanowski M, Hummel M, Stein H, Lenze D, Hansmann M-L, Hartmann S, Möller P, Cogliatti S, Lenz G, Trümper L, Löffler M, Schmitz N, Pfreundschuh M, Rosenwald A, Ott G. Clinical Impact of the Cell-of-Origin Classification and the MYC/BCL2 Dual Expresser Status in Diffuse Large B-Cell Lymphoma Treated Within Prospective Clinical Trials of the German High-Grade Non-Hodgkin's Lymphoma Study Group. *Journal of Clinical Oncology.* 2017;JCO.2016.2070.3660.2515-2526
33. Lenz G, Davis RE, Ngo VN, Lam L, George TC, Wright GW, Dave SS, Zhao H, Xu W, Rosenwald A, Ott G, Muller-Hermelink HK, Gascoyne RD, Connors JM, Rimsza LM, Campo E, Jaffe ES, Delabie J, Smeland EB, Fisher RI, Chan WC, Staudt LM.

Oncogenic CARD11 Mutations in Human Diffuse Large B Cell Lymphoma. *Science*. 2008;319(5870):1676-1679.

34. Ngo VN, Young RM, Schmitz R, Jhavar S, Xiao W, Lim KH, Kohlhammer H, Xu W, Yang Y, Zhao H, Shaffer AL, Romesser P, Wright G, Powell J, Rosenwald A, Muller-Hermelink HK, Ott G, Gascoyne RD, Connors JM, Rimsza LM, Campo E, Jaffe ES, Delabie J, Smeland EB, Fisher RI, Braziel RM, Tubbs RR, Cook JR, Weisenburger DD, Chan WC, Staudt LM. Oncogenically active MYD88 mutations in human lymphoma. *Nature*. 2011;470(7332):115-119.
35. Kato M, Sanada M, Kato I, Sato Y, Takita J, Takeuchi K, Niwa A, Chen Y, Nakazaki K, Nomoto J, Asakura Y, Muto S, Tamura A, Iio M, Akatsuka Y, Hayashi Y, Mori H, Igarashi T, Kurokawa M, Chiba S, Mori S, Ishikawa Y, Okamoto K, Tobinai K, Nakagama H, Nakahata T, Yoshino T, Kobayashi Y, Ogawa S. Frequent inactivation of A20 in B-cell lymphomas. *Nature*. 2009;459(7247):712-716.
36. Compagno M, Lim WK, Grunn A, Nandula SV, Brahmachary M, Shen Q, Bertoni F, Ponzoni M, Scandurra M, Califano A, Bhagat G, Chadburn A, Dalla-Favera R, Pasqualucci L. Mutations of multiple genes cause deregulation of NF- κ B in diffuse large B-cell lymphoma. *Nature*. 2009;459(7247):717-721.
37. Nogai H, Wenzel SS, Hailfinger S, Grau M, Kaergel E, Seitz V, Wollert-Wulf B, Pfeifer M, Wolf A, Frick M, Dietze K, Madle H, Tzankov A, Hummel M, Dorken B, Scheidereit C, Janz M, Lenz P, Thome M, Lenz G. IkappaB-zeta controls the constitutive NF-kappaB target gene network and survival of ABC DLBCL. *Blood*. 2013;122(13):2242-2250.
38. Pasqualucci L, Compagno M, Houldsworth J, Monti S, Grunn A, Nandula SV, Aster JC, Murty VV, Shipp MA, Dalla-Favera R. Inactivation of the PRDM1/BLIMP1 gene in diffuse large B cell lymphoma. *Journal of Experimental Medicine*. 2006;203(2):311-317.
39. Pasqualucci L, Migliazza A, Basso K, Houldsworth J, Chaganti R, Dalla-Favera R. Mutations of the BCL6 proto-oncogene disrupt its negative autoregulation in diffuse large B-cell lymphoma. *Blood*. 2003;101(8):2914-2923.
40. Piva R, Deaglio S, Famà R, Buonincontri R, Scarfò I, Bruscaggin A, Mereu E, Serra S, Spina V, Brusa D. The Krüppel-like factor 2 transcription factor gene is

- recurrently mutated in splenic marginal zone lymphoma. *Leukemia*. 2015;29(2):503-507.
41. Morin RD, Mendez-Lago M, Mungall AJ, Goya R, Mungall KL, Corbett RD, Johnson NA, Severson TM, Chiu R, Field M, Jackman S, Krzywinski M, Scott DW, Trinh DL, Tamura-Wells J, Li S, Firme MR, Rogic S, Griffith M, Chan S, Yakovenko O, Meyer IM, Zhao EY, Smailus D, Moksa M, Chittaranjan S, Rimsza L, Brooks-Wilson A, Spinelli JJ, Ben-Neriah S, Meissner B, Woolcock B, Boyle M, McDonald H, Tam A, Zhao Y, Delaney A, Zeng T, Tse K, Butterfield Y, Birol I, Holt R, Schein J, Horsman DE, Moore R, Jones SJM, Connors JM, Hirst M, Gascogne RD, Marra MA. Frequent mutation of histone-modifying genes in non-Hodgkin lymphoma. *Nature*. 2011;476:298-303.
42. Pasqualucci L, Trifonov V, Fabbri G, Ma J, Rossi D, Chiarenza A, Wells VA, Grunn A, Messina M, Elliot O, Chan J, Bhagat G, Chadburn A, Gaidano G, Mullighan CG, Rabidan R, Dalla-Favera R. Analysis of the coding genome of diffuse large B-cell lymphoma. *Nature Genetics*. 2011;43:830-837.
43. Schmitt CA, Fridman JS, Yang M, Lee S, Baranov E, Hoffman RM, Lowe SW. A Senescence Program Controlled by p53 and p16INK4a Contributes to the Outcome of Cancer Therapy. *Cell*. 2002;109(3):335-346.
44. Bouchard C, Lee S, Paulus-Hock V, Loddenkemper C, Eilers M, Schmitt CA. FoxO transcription factors suppress Myc-driven lymphomagenesis via direct activation of Arf. *Genes & Development*. 2007;21(21):2775-2787.
45. Reimann M, Loddenkemper C, Rudolph C, Schildhauer I, Teichmann B, Stein H, Schlegelberger B, Dörken B, Schmitt CA. The Myc-evoked DNA damage response accounts for treatment resistance in primary lymphomas in vivo. *Blood*. 2007;110(8):2996-3004.
46. Lohr JG, Stojanov P, Lawrence MS, Auclair D, Chapuy B, Sougnez C, Cruz-Gordillo P, Knobochel B, Asmann YW, Slager SL, Novak AJ, Dogan A, Ansell SM, Link BK, Zou L, Gould J, Saksena G, Stransky N, Rangel-Escareño C, Fernandez-Lopez JC, Hidalgo-Miranda A, Melendez-Zajgla J, Hernández-Lemus E, Schwarz-Cruz y Celis A, Imaz-Rosshandler I, Ojesina AI, Jung J, Pedamallu CS, Lander ES, Habermann TM, Cerhan JR, Shipp MA, Getz G, Golub TR. Discovery and prioritization of somatic

mutations in diffuse large B-cell lymphoma (DLBCL) by whole-exome sequencing. Proceedings of the National Academy of Sciences. 2012;109(10):3879-3884.

47. Reddy A, Zhang J, Davis NS, Moffitt AB, Love CL, Waldrop A, Leppa S, Pasanen A, Meriranta L, Karjalainen-Lindsberg M-L, Nørgaard P, Pedersen M, Gang AO, Høgdall E, Heavican TB, Lone W, Iqbal J, Qin Q, Li G, Kim SY, Healy J, Richards KL, Fedoriw Y, Bernal-Mizrachi L, Koff JL, Staton AD, Flowers CR, Paltiel O, Goldschmidt N, Calaminici M, Clear A, Gribben J, Nguyen E, Czader MB, Ondrejka SL, Collie A, Hsi ED, Tse E, Au-Yeung RKH, Kwong Y-L, Srivastava G, Choi WWL, Evens AM, Pilichowska M, Sengar M, Reddy N, Li S, Chadburn A, Gordon LI, Jaffe ES, Levy S, Rempel R, Tzeng T, Happ LE, Dave T, Rajagopalan D, Datta J, Dunson DB, Dave SS. Genetic and Functional Drivers of Diffuse Large B Cell Lymphoma. *Cell*. 2017;171(2):481-494.e415.

48. Basso K, Margolin AA, Stolovitzky G, Klein U, Dalla-Favera R, Califano A. Reverse engineering of regulatory networks in human B cells. *Nature Genetics*. 2005;37(4):382-390.

49. Calado DP, Sasaki Y, Godinho SA, Pellerin A, Kochert K, Sleckman BP, de Alboran IM, Janz M, Rodig S, Rajewsky K. The cell-cycle regulator c-Myc is essential for the formation and maintenance of germinal centers. *Nature Immunology*. 2012;13(11):1092-1100.

50. Johnson NA, Slack GW, Savage KJ, Connors JM, Ben-Neriah S, Rogic S, Scott DW, Tan KL, Steidl C, Sehn LH, Chan WC, Iqbal J, Meyer PN, Lenz G, Wright G, Rimsza LM, Valentino C, Brunhoeber P, Grogan TM, Brazil RM, Cook JR, Tubbs RR, Weisenburger DD, Campo E, Rosenwald A, Ott G, Delabie J, Holcroft C, Jaffe ES, Staudt LM, Gascoyne RD. Concurrent expression of MYC and BCL2 in diffuse large B-cell lymphoma treated with rituximab plus cyclophosphamide, doxorubicin, vincristine, and prednisone. *Journal of Clinical Oncology*. 2012;30(28):3452-3459.

51. Scott DW, Mottok A, Ennishi D, Wright GW, Farinha P, Ben-Neriah S, Kridel R, Barry GS, Hother C, Abrisqueta P, Boyle M, Meissner B, Telenius A, Savage KJ, Sehn LH, Slack GW, Steidl C, Staudt LM, Connors JM, Rimsza LM, Gascoyne RD. Prognostic Significance of Diffuse Large B-Cell Lymphoma Cell of Origin Determined by

Digital Gene Expression in Formalin-Fixed Paraffin-Embedded Tissue Biopsies. *Journal of Clinical Oncology*. 2015;33(26):2848-2856.

52. Perry AM, Alvarado-Bernal Y, Laurini JA, Smith LM, Slack GW, Tan KL, Sehn LH, Fu K, Aoun P, Greiner TC. MYC and BCL2 protein expression predicts survival in patients with diffuse large B-cell lymphoma treated with rituximab. *British journal of haematology*. 2014;165(3):382-391.
53. Chapuy B, McKeown MR, Lin CY, Monti S, Roemer MG, Qi J, Rahl PB, Sun HH, Yeda KT, Doench JG, Reichert E, Kung AL, Rodig SJ, Young RA, Shipp MA, Bradner JE. Discovery and characterization of super-enhancer-associated dependencies in diffuse large B cell lymphoma. *Cancer Cell*. 2013;24(6):777-790.
54. Shaffer III AL, Young RM, Staudt LM. Pathogenesis of human B cell lymphomas. *Annual review of immunology*. 2012;30:565-610.
55. Schmitt CA. Senescence, apoptosis and therapy—cutting the lifelines of cancer. *Nature Reviews Cancer*. 2003;3(4):286-295.
56. Däbritz JHM, Yu Y, Milanovic M, Schönlein M, Rosenfeldt MT, Dörr JR, Kaufmann AM, Dörken B, Schmitt CA. CD20-targeting immunotherapy promotes cellular senescence in B-cell lymphoma. *Molecular cancer therapeutics*. 2016;15(5):1074-1081.
57. Milanovic M, Fan DNY, Belenki D, Däbritz JHM, Zhao Z, Yu Y, Dörr JR, Dimitrova L, Lenze D, Monteiro Barbosa IA, Mendoza-Parra MA, Kanashova T, Metzner M, Pardon K, Reimann M, Trumpp A, Dörken B, Zuber J, Gronemeyer H, Hummel M, Dittmar G, Lee S, Schmitt CA. Senescence-associated reprogramming promotes cancer stemness. *Nature*. 2017;553:96-100
58. Jing H, Kase J, Dörr JR, Milanovic M, Lenze D, Grau M, Beuster G, Ji S, Reimann M, Lenz P, Hummel M, Dörken B, Lenz G, Scheidereit C, Schmitt CA, Lee S. Opposing roles of NF-κB in anti-cancer treatment outcome unveiled by cross-species investigations. *Genes & Development*. 2011;25(20):2137-2146.
59. Adams J, Harris A, Pinkert C, Corcoran L, Alexander W, Cory S, Palmiter R, Brinster R. The c-myc oncogene driven by immunoglobulin enhancers induces lymphoid malignancy in transgenic mice. *Nature*. 1985;318(6046):533-538.

60. Knittel G, Liedgens P, Korovkina D, Seeger JM, Al-Baldawi Y, Al-Maarri M, Fritz C, Vlantis K, Bezhanova S, Scheel AH, Wolz OO, Reimann M, Moller P, Lopez C, Schlesner M, Lohneis P, Weber AN, Trumper L, German International Cancer Genome Consortium Molecular Mechanisms in Malignant Lymphoma by Sequencing Project C, Staudt LM, Ortmann M, Pasparakis M, Siebert R, Schmitt CA, Klatt AR, Wunderlich FT, Schafer SC, Persigehl T, Montesinos-Rongen M, Odenthal M, Buttner R, Frenzel LP, Kashkar H, Reinhardt HC. B-cell-specific conditional expression of Myd88p.L252P leads to the development of diffuse large B-cell lymphoma in mice. *Blood*. 2016;127(22):2732-2741.
61. Zhang B, Calado DP, Wang Z, Fröhler S, Köchert K, Qian Y, Koralov SB, Schmidt-Suprian M, Sasaki Y, Unitt C, Rodig S, Chen W, Dalla-Favera R, Alt FW, Pasqualucci L, Rajewsky K. An oncogenic role for alternative NF-κB signaling in DLBCL revealed upon deregulated BCL6 expression. *Cell Reports*. 2015;11(5):715-726.
62. Calado DP, Zhang B, Srinivasan L, Sasaki Y, Seagal J, Unitt C, Rodig S, Kutok J, Tarakhovsky A, Schmidt-Suprian M, Rajewsky K. Constitutive canonical NF-κB activation cooperates with disruption of BLIMP1 in the pathogenesis of activated B cell-like diffuse large cell lymphoma. *Cancer Cell*. 2010;18(6):580-589.
63. Goff S, Traktman P, Baltimore D. Isolation and properties of Moloney murine leukemia virus mutants: use of a rapid assay for release of virion reverse transcriptase. *Journal of virology*. 1981;38(1):239-248.
64. Schmitt CA, McCurrach ME, de Stanchina E, Wallace-Brodeur RR, Lowe SW. INK4a/ARF mutations accelerate lymphomagenesis and promote chemoresistance by disabling p53. *Genes & Development*. 1999;13(20):2670-2677.
65. Schmitt CA, Rosenthal CT, Lowe SW. Genetic analysis of chemoresistance in primary murine lymphomas. *Nature Medicine*. 2000;6(9):1029-1035.
66. Wulczyn FG, Naumann M, Scheidereit C. Candidate proto-oncogene bcl-3 encodes a subunit-specific inhibitor of transcription factor NF-κB. *Nature*. 1992;358(6387):597-599.
67. Brockman JA, Scherer DC, McKinsey TA, Hall SM, Qi X, Lee WY, Ballard DW. Coupling of a signal response domain in I kappa B alpha to multiple pathways for NF-kappa B activation. *Molecular and cellular biology*. 1995;15(5):2809-2818.

68. Hinz M, Lemke P, Anagnostopoulos I, Hacker C, Krappmann D, Mathas S, Dörken B, Zenke M, Stein H, Scheidereit C. Nuclear Factor κB–dependent Gene Expression Profiling of Hodgkin's Disease Tumor Cells, Pathogenetic Significance, and Link to Constitutive Signal Transducer and Activator of Transcription 5a Activity. *The Journal of Experimental Medicine*. 2002;196(5):605-617.
69. Gerdes J, Lemke H, Baisch H, Wacker H-H, Schwab U, Stein H. Cell cycle analysis of a cell proliferation-associated human nuclear antigen defined by the monoclonal antibody Ki-67. *The Journal of Immunology*. 1984;133(4):1710-1715.
70. Reimann M, Lee S, Loddenkemper C, Dorr JR, Tabor V, Aichele P, Stein H, Dorken B, Jenuwein T, Schmitt CA. Tumor stroma-derived TGF-beta limits myc-driven lymphomagenesis via Suv39h1-dependent senescence. *Cancer Cell*. 2010;17(3):262-272.
71. Haugstetter A, Loddenkemper C, Lenze D, Gröne J, Standfuss C, Petersen I, Dörken B, Schmitt C. Cellular senescence predicts treatment outcome in metastasised colorectal cancer. *British journal of cancer*. 2010;103(4):505-509.
72. Consortium M, Shi L, Reid LH, Jones WD, Shippy R, Warrington JA, Baker SC, Collins PJ, de Longueville F, Kawasaki ES, Lee KY, Luo Y, Sun YA, Willey JC, Setterquist RA, Fischer GM, Tong W, Dragan YP, Dix DJ, Frueh FW, Goodsaid FM, Herman D, Jensen RV, Johnson CD, Lobenhofer EK, Puri RK, Schrf U, Thierry-Mieg J, Wang C, Wilson M, Wolber PK, Zhang L, Amur S, Bao W, Barbacioru CC, Lucas AB, Bertholet V, Boysen C, Bromley B, Brown D, Brunner A, Canales R, Cao XM, Cebula TA, Chen JJ, Cheng J, Chu TM, Chudin E, Corson J, Corton JC, Croner LJ, Davies C, Davison TS, Delenstarr G, Deng X, Dorris D, Eklund AC, Fan XH, Fang H, Fulmer-Smentek S, Fuscoe JC, Gallagher K, Ge W, Guo L, Guo X, Hager J, Haje PK, Han J, Han T, Harbottle HC, Harris SC, Hatchwell E, Hauser CA, Hester S, Hong H, Hurban P, Jackson SA, Ji H, Knight CR, Kuo WP, LeClerc JE, Levy S, Li QZ, Liu C, Liu Y, Lombardi MJ, Ma Y, Magnuson SR, Maqsodi B, McDaniel T, Mei N, Myklebost O, Ning B, Novoradovskaya N, Orr MS, Osborn TW, Papallo A, Patterson TA, Perkins RG, Peters EH, Peterson R, Philips KL, Pine PS, Pusztai L, Qian F, Ren H, Rosen M, Rosenzweig BA, Samaha RR, Schena M, Schroth GP, Shchegrova S, Smith DD, Staedtler F, Su Z, Sun H, Szallasi Z, Tezak Z, Thierry-Mieg D, Thompson KL,

Tikhonova I, Turpaz Y, Vallanat B, Van C, Walker SJ, Wang SJ, Wang Y, Wolfinger R, Wong A, Wu J, Xiao C, Xie Q, Xu J, Yang W, Zhang L, Zhong S, Zong Y, Slikker W, Jr. The MicroArray Quality Control (MAQC) project shows inter- and intraplatform reproducibility of gene expression measurements. *Nature Biotechnology*. 2006;24(9):1151-1161.

73. Wang JQ, Jeelall YS, Humberg P, Batchelor EL, Kaya SM, Yoo HM, Goodnow CC, Horikawa K. Synergistic cooperation and crosstalk between MYD88 L265P and mutations that dysregulate CD79B and surface IgM. *The Journal of Experimental Medicine*. 2017;2759-2776.

74. Chen L, Monti S, Juszczynski P, Ouyang J, Chapuy B, Neuberg D, Doench John G, Bogusz Agata M, Habermann Thomas M, Dogan A, Witzig Thomas E, Kutok Jeffery L, Rodig Scott J, Golub T, Shipp Margaret A. SYK Inhibition Modulates Distinct PI3K/AKT- Dependent Survival Pathways and Cholesterol Biosynthesis in Diffuse Large B Cell Lymphomas. *Cancer Cell*. 2013;23(6):826-838.

75. Dorr JR, Yu Y, Milanovic M, Beuster G, Zasada C, Dabritz JH, Lisec J, Lenze D, Gerhardt A, Schleicher K, Kratzat S, Purfurst B, Walenta S, Mueller-Klieser W, Graler M, Hummel M, Keller U, Buck AK, Dorken B, Willmitzer L, Reimann M, Kempa S, Lee S, Schmitt CA. Synthetic lethal metabolic targeting of cellular senescence in cancer therapy. *Nature*. 2013;501(7467):421-425.

76. Jaeger C, Hoffmann F, Schmitt CA, Lisec J. Automated Annotation and Evaluation of In-Source Mass Spectra in GC/Atmospheric Pressure Chemical Ionization-MS-Based Metabolomics. *Analytical Chemistry*. 2016;88(19):9386-9390.

77. Riedelsheimer C, Lisec J, Czedik-Eysenberg A, Sulpice R, Flis A, Grieder C, Altmann T, Stitt M, Willmitzer L, Melchinger AE. Genome-wide association mapping of leaf metabolic profiles for dissecting complex traits in maize. *Proceedings of the National Academy of Sciences*. 2012;109(23):8872-8877.

78. Lisec J, Schauer N, Kopka J, Willmitzer L, Fernie AR. Gas chromatography mass spectrometry-based metabolite profiling in plants. *Nat Protoc*. 2006;1(1):387-396.

79. Oliver Fiehn JK, Peter Dörmann, Thomas Altmann, Richard N. Trethewey, and Lothar Willmitzer. Metabolite profiling for plant functional genomics. *Nature Biotechnology*. 2000;1157-1161

80. Fraser D. Understanding animal welfare. *Acta Veterinaria Scandinavica*. 2008;50(1):S1.
81. Luskey BD, Rosenblatt M, Zsebo K, Williams DA. Stem cell factor, interleukin-3, and interleukin-6 promote retroviral-mediated gene transfer into murine hematopoietic stem cells. *Blood*. 1992;80(2):396-402.
82. Johnson M, Zaretskaya I, Raytselis Y, Merezhuk Y, McGinnis S, Madden TL. NCBI BLAST: a better web interface. *Nucleic Acids Research*. 2008;36(suppl_2):W5-W9.
83. Kofoed EM, Vance RE. Innate immune recognition of bacterial ligands by NAIPs determines inflammasome specificity. *Nature*. 2011;477:592-594
84. Gentleman RC, Carey VJ, Bates DM, Bolstad B, Dettling M, Dudoit S, Ellis B, Gautier L, Ge Y, Gentry J, Hornik K, Hothorn T, Huber W, Iacus S, Irizarry R, Leisch F, Li C, Maechler M, Rossini AJ, Sawitzki G, Smith C, Smyth G, Tierney L, Yang JY, Zhang J. Bioconductor: open software development for computational biology and bioinformatics. *Genome biology*. 2004;5(10):R80.
85. Huber W, Carey VJ, Gentleman R, Anders S, Carlson M, Carvalho BS, Bravo HC, Davis S, Gatto L, Girke T, Gottardo R, Hahne F, Hansen KD, Irizarry RA, Lawrence M, Love MI, MacDonald J, Obenchain V, Oles AK, Pages H, Reyes A, Shannon P, Smyth GK, Tenenbaum D, Waldron L, Morgan M. Orchestrating high-throughput genomic analysis with Bioconductor. *Nature Methods*. 2015;12(2):115-121.
86. Mekada K, Abe K, Murakami A, Nakamura S, Nakata H, Moriwaki K, Obata Y, Yoshiki A. Genetic Differences among C57BL/6 Substrains. *Experimental Animals*. 2009;58(2):141-149.
87. Jacks T, Remington L, Williams BO, Schmitt EM, Halachmi S, Bronson RT, Weinberg RA. Tumor spectrum analysis in p53-mutant mice. *Current biology*. 1994;4(1):1-7.
88. Schmitt CA, Fridman JS, Yang M, Baranov E, Hoffman RM, Lowe SW. Dissecting p53 tumor suppressor functions in vivo. *Cancer cell*. 2002;1(3):289-298.
89. Lachner M, O'Carroll D, Rea S, Mechtler K, Jenuwein T. Methylation of histone H3 lysine 9 creates a binding site for HP1 proteins. *Nature*. 2001;410(6824):116-120.

90. Todaro GJ, Green H. Quantitative studies of the growth of mouse embryo cells in culture and their development into established lines. *The Journal of cell biology*. 1963;17(2):299-313.
91. Swift S, Lorens J, Achacoso P, Nolan GP. Rapid production of retroviruses for efficient gene delivery to mammalian cells using 293T cell-based systems. *Current protocols in immunology*. 2001:10.17. 14-10.17. 29.
92. Pear WS, Miller JP, Xu L, Pui JC, Soffer B, Quackenbush RC, Pendergast AM, Bronson R, Aster JC, Scott ML. Efficient and rapid induction of a chronic myelogenous leukemia-like myeloproliferative disease in mice receiving P210 bcr/abl-transduced bone marrow. *Blood*. 1998;92(10):3780-3792.
93. Taylor RG, Walker DC, McInnes R. E. coli host strains significantly affect the quality of small scale plasmid DNA preparations used for sequencing. *Nucleic acids research*. 1993;21(7):1677-1678.
94. Wixson S, Smiler K. Anesthesia and Analgesia in Rodents: American College of Laboratory Animal Medicine 1990 Forum. Academic Press, San Diego, London; 1997.
95. Sambrook J, Russell DW. The inoue method for preparation and transformation of competent E. coli:“ultra-competent” cells. *CSH Protoc*. 2006;2006(1).prot3944
96. Kozak M. Point mutations define a sequence flanking the AUG initiator codon that modulates translation by eukaryotic ribosomes. *Cell*. 1986;44(2):283-292.
97. Kasowski M, Grubert F, Heffelfinger C, Hariharan M, Asabere A, Waszak SM, Habegger L, Rozowsky J, Shi M, Urban AE, Hong M-Y, Karczewski KJ, Huber W, Weissman SM, Gerstein MB, Korbel JO, Snyder M. Variation in Transcription Factor Binding Among Humans. *Science*. 2010;328(5975):232-235.
98. Pear WS, Nolan GP, Scott ML, Baltimore D. Production of high-titer helper-free retroviruses by transient transfection. *Proceedings of the National Academy of Sciences*. 1993;90(18):8392-8396.
99. Naviaux RK, Costanzi E, Haas M, Verma IM. The pCL vector system: rapid production of helper-free, high-titer, recombinant retroviruses. *Journal of virology*. 1996;70(8):5701-5705.

100. Sambrook J, Russell DW. Calcium-phosphate-mediated transfection of eukaryotic cells with plasmid DNAs. *Cold Spring Harbor Protocols*. 2006;2006(1):pdb.prot3871.
101. Ema H, Morita Y, Yamazaki S, Matsubara A, Seita J, Tadokoro Y, Kondo H, Takano H, Nakauchi H. Adult mouse hematopoietic stem cells: purification and single-cell assays. *Nature Protocols*. 2006;1(6):2979-2987.
102. Zhong JF, Zhan Y, Anderson WF, Zhao Y. Murine hematopoietic stem cell distribution and proliferation in ablated and nonablated bone marrow transplantation. *Blood*. 2002;100(10):3521-3526.
103. Duran-Struuck R, Dysko RC. Principles of bone marrow transplantation (BMT): providing optimal veterinary and husbandry care to irradiated mice in BMT studies. *Journal of the American Association for Laboratory Animal Science*. 2009;48(1):11-22.
104. Shapiro HM. Practical flow cytometry: John Wiley & Sons; 2005. 242-256
105. Braig M, Lee S, Loddenkemper C, Rudolph C, Peters AH, Schlegelberger B, Stein H, Dorken B, Jenuwein T, Schmitt CA. Oncogene-induced senescence as an initial barrier in lymphoma development. *Nature*. 2005;436(7051):660-665.
106. Renard P, Ernest I, Houbion Ae, Art M, Le Calvez H, Raes M, Remacle J. Development of a sensitive multi-well colorimetric assay for active NF κ B. *Nucleic Acids Research*. 2001;29(4):e21-e21.
107. George TC, Fanning SL, Fitzgerald-Bocarsly P, Medeiros RB, Highfill S, Shimizu Y, Hall BE, Frost K, Basiji D, Ortyn WE, Morrissey PJ, Lynch DH. Quantitative measurement of nuclear translocation events using similarity analysis of multispectral cellular images obtained in flow. *J Immunol Methods*. 2006;311(1-2):117-129.
108. Maguire O, Collins C, O'Loughlin K, Miecznikowski J, Minderman H. Quantifying nuclear p65 as a parameter for NF- κ B activation: Correlation between ImageStream cytometry, microscopy, and Western blot. *Cytometry A*. 2011;79(6):461-469.
109. Adler J, Parmryd I. Quantifying colocalization by correlation: the Pearson correlation coefficient is superior to the Mander's overlap coefficient. *Cytometry Part A*. 2010;77(8):733-742.

110. Ahlgren P, Jarneving B, Rousseau R. Requirements for a cocitation similarity measure, with special reference to Pearson's correlation coefficient. *Journal of the American Society for Information Science and Technology*. 2003;54(6):550-560.
111. Debacq-Chainiaux F, Erusalimsky JD, Campisi J, Toussaint O. Protocols to detect senescence-associated beta-galactosidase (SA- β gal) activity, a biomarker of senescent cells in culture and in vivo. *Nature protocols*. 2009;4(12):1798-1806.
112. Olive DM. Quantitative methods for the analysis of protein phosphorylation in drug development. *Expert review of proteomics*. 2004;1(3):327-341.
113. Aoki Y, Isselbacher KJ, Pillai S. Bruton tyrosine kinase is tyrosine phosphorylated and activated in pre-B lymphocytes and receptor-ligated B cells. *Proceedings of the National Academy of Sciences*. 1994;91(22):10606-10609.
114. Anders S, Huber W. Differential expression analysis for sequence count data. *Genome biology*. 2010;11(10):R106.
115. Busby MA, Stewart C, Miller CA, Grzeda KR, Marth GT. Scotty: a web tool for designing RNA-Seq experiments to measure differential gene expression. *Bioinformatics*. 2013;29(5):656-657.
116. Coffman RL, Weissman IL. B220: a B cell-specific member of the T200 glycoprotein family. *Nature*. 1981;289(5799):681-683.
117. Quail MA, Kozarewa I, Smith F, Scally A, Stephens PJ, Durbin R, Swerdlow H, Turner DJ. A large genome center's improvements to the Illumina sequencing system. *Nature Methods*. 2008;5(12):1005-1010.
118. Tariq MA, Kim HJ, Jejelowo O, Pourmand N. Whole-transcriptome RNAseq analysis from minute amount of total RNA. *Nucleic acids research*. 2011;39(18):e120-e120.
119. Tarazona S, Garcia-Alcalde F, Dopazo J, Ferrer A, Conesa A. Differential expression in RNA-seq: a matter of depth. *Genome Res*. 2011;21(12):2213-2223.
120. Conesa A, Madrigal P, Tarazona S, Gomez-Cabrero D, Cervera A, McPherson A, Szcześniak MW, Gaffney DJ, Elo LL, Zhang X. A survey of best practices for RNA-seq data analysis. *Genome biology*. 2016;17(1):13.

121. Dobin A, Davis CA, Schlesinger F, Drenkow J, Zaleski C, Jha S, Batut P, Chaisson M, Gingeras TR. STAR: ultrafast universal RNA-seq aligner. *Bioinformatics*. 2013;29(1):15-21.
122. Love MI, Huber W, Anders S. Moderated estimation of fold change and dispersion for RNA-seq data with DESeq2. *Genome biology*. 2014;15(12):1.
123. Ginestet C. ggplot2: elegant graphics for data analysis. *Journal of the Royal Statistical Society: Series A (Statistics in Society)*. 2011;174(1):245-246.
124. Smith CA, Want EJ, O'Maille G, Abagyan R, Siuzdak G. XCMS: Processing Mass Spectrometry Data for Metabolite Profiling Using Nonlinear Peak Alignment, Matching, and Identification. *Analytical Chemistry*. 2006;78(3):779-787.
125. Nelder JA, Wedderburn RWM. Generalized Linear Models. *Journal of the Royal Statistical Society Series A (General)*. 1972;135(3):370-384.
126. Wu H, Wang C, Wu Z. A new shrinkage estimator for dispersion improves differential expression detection in RNA-seq data. *Biostatistics*. 2012;kxs033.232-243
127. Deutsch JM. Quantum statistical mechanics in a closed system. *Physical Review A*. 1991;43(4):2046-2049.
128. Benjamini Y, Hochberg Y. Controlling the false discovery rate: a practical and powerful approach to multiple testing. *Journal of the royal statistical society Series B (Methodological)*. 1995:289-300.
129. Kaplan EL, Meier P. Nonparametric estimation from incomplete observations. *Journal of the American statistical association*. 1958;53(282):457-481.
130. Peto R, Peto J. Asymptotically efficient rank invariant test procedures. *Journal of the Royal Statistical Society Series A (General)*. 1972:185-207.
131. Fisher RA. On the probable error of a coefficient of correlation deduced from a small sample. *Metron*. 1921;1:3-32.
132. Atkin P, de Paula J. Atkins' physical chemistry. WH Freeman and Company Books. 2006:747-755.
133. Fleisch DA. A student's guide to vectors and tensors: Cambridge University Press; 2011.97-157
134. Witten DM. Classification and clustering of sequencing data using a Poisson model. *The Annals of Applied Statistics*. 2011:2493-2518.

135. Acland A, Agarwala R, Barrett T, Beck J, Benson DA, Bollin C, Bolton E, Bryant SH, Canese K, Church DM. Database resources of the national center for biotechnology information. *Nucleic acids research*. 2014;42(Database issue):D7-17.
136. Di Eugenio B, Glass M. The kappa statistic: A second look. *Computational linguistics*. 2004;30(1):95-101.
137. Huang DW, Sherman BT, Tan Q, Collins JR, Alvord WG, Roayaei J, Stephens R, Baseler MW, Lane HC, Lempicki RA. The DAVID Gene Functional Classification Tool: a novel biological module-centric algorithm to functionally analyze large gene lists. *Genome biology*. 2007;8(9):R183.
138. Hosack DA, Dennis G, Sherman BT, Lane HC, Lempicki RA. Identifying biological themes within lists of genes with EASE. *Genome biology*. 2003;4(10):R70.
139. Heberle H, Meirelles GV, da Silva FR, Telles GP, Minghim R. InteractiVenn: a web-based tool for the analysis of sets through Venn diagrams. *BMC Bioinformatics*. 2015;16(1):169.
140. Kaji T, Yoshida S, Kawai K, Fuchigami Y, Watanabe W, Kubodera H, Kishimoto T. ASK3, a novel member of the apoptosis signal-regulating kinase family, is essential for stress-induced cell death in HeLa cells. *Biochemical and biophysical research communications*. 2010;395(2):213-218.
141. Wherry EJ. T cell exhaustion. *Nat Immunol*. 2011;12(6):492-499.
142. Kieran M, Blank V, Logeat F, Vandekerckhove J, Lottspeich F, Le Bail O, Urban MB, Kourilsky P, Baeuerle PA, Israël A. The DNA binding subunit of NF-κB is identical to factor KBF1 and homologous to the rel oncogene product. *Cell*. 1990;62(5):1007-1018.
143. Wang JQ, Jeelall YS, Humburg P, Batchelor EL, Kaya SM, Yoo HM, Goodnow CC, Horikawa K. Synergistic cooperation and crosstalk between MYD88L265P and mutations that dysregulate CD79B and surface IgM. *The Journal of Experimental Medicine*. 2017.
144. Bro R, Smilde AK. Principal component analysis. *Analytical Methods*. 2014;6(9):2812-2831.

145. Younes A, Ansell S, Fowler N, Wilson W, de Vos S, Seymour J, Advani R, Forero A, Morschhauser F, Kersten MJ. The landscape of new drugs in lymphoma. *Nature reviews Clinical oncology*. 2017;14(6):335-346.
146. Rovira J, Karube K, Valera A, Colomer D, Enjuanes A, Colomo L, Martínez-Trillo A, Giné E, Dlouhy I, Magnano L. MYD88 L265P mutations, but no other variants, identify a subpopulation of DLBCL patients of activated B-cell origin, extranodal involvement, and poor outcome. *Clinical Cancer Research*. 2016;22(11):2755-2764.
147. Lesokhin AM, Ansell SM, Armand P, Scott EC, Halwani A, Gutierrez M, Millenson MM, Cohen AD, Schuster SJ, Lebovic D, Dhodapkar M, Avigan D, Chapuy B, Ligon AH, Freeman GJ, Rodig SJ, Cattray D, Zhu L, Gross JF, Bradley Garelik MB, Shipp MA, Borrello I, Timmerman J. Nivolumab in Patients With Relapsed or Refractory Hematologic Malignancy: Preliminary Results of a Phase Ib Study. *Journal of Clinical Oncology*. 2016;34(23):2698-2704.
148. Nayak L, Iwamoto FM, LaCasce A, Mukundan S, Roemer MGM, Chapuy B, Armand P, Rodig SJ, Shipp MA. PD-1 blockade with nivolumab in relapsed/refractory primary central nervous system and testicular lymphoma. *Blood*. 2017;3071-3073.
149. Hashwah H, Schmid CA, Kasser S, Bertram K, Stelling A, Manz MG, Müller A. Inactivation of CREBBP expands the germinal center B cell compartment, down-regulates MHCII expression and promotes DLBCL growth. *Proceedings of the National Academy of Sciences*. 2017;114(36):9701-9706.
150. Kortlever RM, Sodir NM, Wilson CH, Burkhardt DL, Pellegrinet L, Swigart LB, Littlewood TD, Evan GI. Myc cooperates with Ras by programming inflammation and immune suppression. *Cell*. 2017;171(6):1301-1315. e1314.
151. Goodman A, Patel SP, Kurzrock R. PD-1-PD-L1 immune-checkpoint blockade in B-cell lymphomas. *Nature Reviews Clinical Oncology*. 2017;14(4):203-220.
152. Casey SC, Tong L, Li Y, Do R, Walz S, Fitzgerald KN, Gouw AM, Baylot V, Gütgemann I, Eilers M. MYC regulates the antitumor immune response through CD47 and PD-L1. *Science*. 2016;352(6282):227-231.
153. Hogg SJ, Vervoort SJ, Deswal S, Ott CJ, Li J, Cluse LA, Beavis PA, Darcy PK, Martin BP, Spencer A, Traunbauer AK, Sadovnik I, Bauer K, Valent P, Bradner JE, Zuber J, Shortt J, Johnstone RW. BET-Bromodomain Inhibitors Engage the Host

Immune System and Regulate Expression of the Immune Checkpoint Ligand PD-L1. Cell Reports. 2017;18(9):2162-2174.

154. Zou W, Wolchok JD, Chen L. PD-L1 (B7-H1) and PD-1 pathway blockade for cancer therapy: Mechanisms, response biomarkers, and combinations. Science translational medicine. 2016;8(328):328rv324-328rv324.
155. Consortium GO. Expansion of the Gene Ontology knowledgebase and resources. Nucleic acids research. 2017;45(D1):D331-D338.
156. Kanehisa M, Sato Y, Kawashima M, Furumichi M, Tanabe M. KEGG as a reference resource for gene and protein annotation. Nucleic acids research. 2016;44(D1):D457-D462.
157. Cardenas MG, Oswald E, Yu W, Xue F, MacKerell AD, Melnick AM. The expanding role of the BCL6 oncprotein as a cancer therapeutic target. Clinical Cancer Research. 2017;23(4):885-893.
158. Dobashi A. Molecular pathogenesis of diffuse large B-cell lymphoma. Journal of Clinical and Experimental Hematopathology. 2016;56(2):71-78.
159. Chapuy B, Roemer MG, Stewart C, Tan Y, Abo RP, Zhang L, Dunford AJ, Meredith DM, Thorner AR, Jordanova ES, Liu G, Feuerhake F, Ducar MD, Illerhaus G, Gusenleitner D, Linden EA, Sun HH, Homer H, Aono M, Pinkus GS, Ligon AH, Ligon KL, Ferry JA, Freeman GJ, van Hummelen P, Golub TR, Getz G, Rodig SJ, de Jong D, Monti S, Shipp MA. Targetable genetic features of primary testicular and primary central nervous system lymphomas. Blood. 2016;127(7):869-881.
160. Knies N, Alankus B, Weilemann A, Tzankov A, Brunner K, Ruff T, Kremer M, Keller UB, Lenz G, Ruland J. Lymphomagenic CARD11/BCL10/MALT1 signaling drives malignant B-cell proliferation via cooperative NF-kappaB and JNK activation. Proceedings of the National Academy of Sciences. 2015;112(52):E7230-7238.
161. Genovese G, Kähler AK, Handsaker RE, Lindberg J, Rose SA, Bakhour SF, Chambert K, Mick E, Neale BM, Fromer M, Purcell SM, Svantesson O, Landén M, Höglund M, Lehmann S, Gabriel SB, Moran JL, Lander ES, Sullivan PF, Sklar P, Grönberg H, Hultman CM, McCarroll SA. Clonal Hematopoiesis and Blood-Cancer Risk Inferred from Blood DNA Sequence. New England Journal of Medicine. 2014;371(26):2477-2487.

162. Kubuki Y, Yamaji T, Hidaka T, Kameda T, Shide K, Sekine M, Kamiunten A, Akizuki K, Shimoda H, Tahira Y. TET2 mutation in diffuse large B-cell lymphoma. *Journal of Clinical and Experimental Hematopathology*. 2017;56(3):145-149.
163. Batool M, Anwar MA, Choi S. Toll-like receptors targeting technology for the treatment of lymphoma. *Expert opinion on drug discovery*. 2016;11(11):1047-1059.
164. Kawai T, Adachi O, Ogawa T, Takeda K, Akira S. Unresponsiveness of MyD88-deficient mice to endotoxin. *Immunity*. 1999;11(1):115-122.
165. Galluzzi L, Vacchelli E, Eggermont A, Fridman WH, Galon J, Sautès-Fridman C, Tartour E, Zitvogel L, Kroemer G. Trial Watch: Experimental Toll-like receptor agonists for cancer therapy. *Oncoimmunology*. 2012;1(5):699-739.
166. Atefi M, Avramis E, Lassen A, Wong DJ, Robert L, Foulad D, Cerniglia M, Titz B, Chodon T, Graeber TG. Effects of MAPK and PI3K pathways on PD-L1 expression in melanoma. *Clinical cancer research*. 2014;20(13):3446-3457.
167. Annemann M, Plaza-Sirvent C, Schuster M, Katsoulis-Dimitriou K, Kliche S, Schraven B, Schmitz I. Atypical I κ B proteins in immune cell differentiation and function. *Immunology letters*. 2016;171:26-35.
168. Hantschel O, Rix U, Schmidt U, Bürckstümmer T, Kneidinger M, Schütze G, Colinge J, Bennett KL, Ellmeier W, Valent P. The Btk tyrosine kinase is a major target of the Bcr-Abl inhibitor dasatinib. *Proceedings of the National Academy of Sciences*. 2007;104(33):13283-13288.
169. Napoli M, Flores ER. The p53 family orchestrates the regulation of metabolism: physiological regulation and implications for cancer therapy. *Br J Cancer*. 2017;116(2):149-155.
170. Stenson M, Pedersen A, Hasselblom S, Nilsson-Ehle H, Karlsson BG, Pinto R, Andersson P-O. Serum nuclear magnetic resonance-based metabolomics and outcome in diffuse large B-cell lymphoma patients—a pilot study. *Leukemia & lymphoma*. 2016;57(8):1814-1822.
171. Megías-Vericat JE, Montesinos P, Herrero MJ, Moscardó F, Bosó V, Martínez-Cuadrón D, Rojas L, Rodríguez-Veiga R, Boluda B, Sendra L. Influence of cytarabine metabolic pathway polymorphisms in acute myeloid leukemia induction treatment. *Leukemia & Lymphoma*. 2017:1-15.

172. Ko M, Huang Y, Jankowska AM, Pape UJ, Tahiliani M, Bandukwala HS, An J, Lamperti ED, Koh KP, Ganetzky R, Liu XS, Aravind L, Agarwal S, Maciejewski JP, Rao A. Impaired hydroxylation of 5-methylcytosine in myeloid cancers with mutant TET2. *Nature*. 2010;468:839-843.
173. Ko M, An J, Pastor WA, Koralov SB, Rajewsky K, Rao A. TET proteins and 5-methylcytosine oxidation in hematological cancers. *Immunological reviews*. 2015;263(1):6-21.
174. Deckert M, Montesinos-Rongen M, Brunn A, Siebert R. Systems biology of primary CNS lymphoma: from genetic aberrations to modeling in mice. *Acta neuropathologica*. 2014;127(2):175-188.

RNA Sequencing Data: Annotation Cluster and Gene List Appendix

Dissertation Jens Schrezenmeier

For DAVID analyses the annotation cluster contributing databases are depicted in the first column, the name of the gene lists in the second, the count of contributing genes in the third, p-value and Benjamini-Hochberg adjusted p-values in the fourth and fifth column. The enrichment score is depicted above every annotation cluster.

For the shown individual gene lists, the first column denotes the contrast (empty vs. lesion), the second column denotes the number of reads mapped to the named genes in the empty reference group, the third column gives the log2fold change as a $\log_2(\text{empty}) - \log_2(\text{lesion})$ ratio, the fourth column denotes the Benjamini-Hochberg adjusted p-value, the fifth column shows the chromosomal location of the respective gene and the sixth column shows the mgf symbol of the analyzed gene. See also Material and Methods section. As this work has so far not been published, the data is not yet deposited on publicly accessible transcriptome data repositories. Additionally, only a representative subfraction of differentially regulated genes is shown in the individual gene analyses. For DAVID analyses all genes passing a padjust threshold $p < 0.05$ were included for the respective genotypes.

1. Table Appendix 1: The E μ -myc Fetal Liver Cell approach DAVID and Individual gene analysis

MYD88L265P vs. empty E μ -myc Fetal Liver Cell

Annotation Cluster 1	Enrichment Score: 2.87	Count	P_Value	Benjamini
KEGG_PATHWAY	Tuberculosis	48	1.70E-08	2.40E-06
KEGG_PATHWAY	Leishmaniasis	24	2.90E-07	2.70E-05
GOTERM_CC_DIRECT	MHC class II protein complex	9	5.40E-06	3.30E-04
GOTERM_BP_DIRECT	antigen processing and presentation of exogenous peptide antigen via MHC class II	9	2.70E-05	1.40E-02
KEGG_PATHWAY	Intestinal immune network for IgA production	16	3.70E-05	1.30E-03
KEGG_PATHWAY	Phagosome	39	6.50E-05	2.00E-03
KEGG_PATHWAY	Toxoplasmosis	28	1.50E-04	3.30E-03
KEGG_PATHWAY	Rheumatoid arthritis	21	8.10E-04	1.30E-02
KEGG_PATHWAY	Asthma	10	9.10E-04	1.40E-02
GOTERM_BP_DIRECT	antigen processing and presentation of peptide or polysaccharide antigen via MHC class II	6	1.20E-03	1.60E-01
KEGG_PATHWAY	Inflammatory bowel disease (IBD)	16	2.30E-03	2.90E-02
KEGG_PATHWAY	Influenza A	32	6.80E-03	6.40E-02
GOTERM_MF_DIRECT	MHC class II protein complex binding	6	1.60E-02	4.30E-01

GOTERM_BP_DIRECT	antigen processing and presentation	12	2.50E-02	6.60E-01
KEGG_PATHWAY	Graft-versus-host disease	11	7.10E-02	3.10E-01
KEGG_PATHWAY	Antigen processing and presentation	15	8.50E-02	3.50E-01
KEGG_PATHWAY	Type I diabetes mellitus	12	9.60E-02	3.70E-01
KEGG_PATHWAY	Allograft rejection	11	1.10E-01	3.70E-01
KEGG_PATHWAY	Viral myocarditis	14	1.20E-01	4.00E-01
KEGG_PATHWAY	Autoimmune thyroid disease	12	1.90E-01	5.10E-01
KEGG_PATHWAY	Herpes simplex infection	29	2.20E-01	5.30E-01
Annotation Cluster 2	Enrichment Score: 2.56	Count	P_Value	Benjamini
GOTERM_MF_DIRECT	cadherin binding involved in cell-cell adhesion	48	7.80E-04	8.30E-02
GOTERM_CC_DIRECT	cell-cell adherens junction	52	1.60E-03	4.30E-02
GOTERM_BP_DIRECT	cell-cell adhesion	31	1.70E-02	5.60E-01
Annotation Cluster 3	Enrichment Score: 2.55	Count	P_Value	Benjamini
KEGG_PATHWAY	Pertussis	21	1.90E-04	3.80E-03
KEGG_PATHWAY	Chagas disease (American trypanosomiasis)	23	2.90E-03	3.40E-02
KEGG_PATHWAY	Toll-like receptor signaling pathway	22	5.00E-03	5.30E-02
KEGG_PATHWAY	TNF signaling pathway	21	2.30E-02	1.60E-01
Annotation Cluster 4	Enrichment Score: 2.52	Count	P_Value	Benjamini
GOTERM_BP_DIRECT	release of cytochrome c from mitochondria	12	3.30E-05	1.30E-02
GOTERM_BP_DIRECT	extrinsic apoptotic signaling pathway in absence of ligand	12	3.70E-03	3.00E-01
GOTERM_MF_DIRECT	channel activity	6	8.00E-03	3.10E-01
GOTERM_BP_DIRECT	mitochondrial fusion	7	1.20E-02	4.90E-01
GOTERM_MF_DIRECT	BH domain binding	5	2.20E-02	4.80E-01

PD-L1 vs. empty E μ -myc Fetal Liver Cell

Annotation Cluster 1	Enrichment Score: 9.91	Count	P_Value	Benjamini
KEGG_PATHWAY	Herpes simplex infection	47	1.50E-14	3.90E-12
KEGG_PATHWAY	Antigen processing and presentation	29	2.50E-14	2.10E-12
KEGG_PATHWAY	Allograft rejection	24	5.40E-14	3.50E-12
KEGG_PATHWAY	Type I diabetes mellitus	25	7.40E-14	3.80E-12
KEGG_PATHWAY	Graft-versus-host disease	22	1.00E-12	3.80E-11
KEGG_PATHWAY	Cell adhesion molecules (CAMs)	37	1.10E-11	3.10E-10
KEGG_PATHWAY	Autoimmune thyroid disease	24	1.90E-11	4.40E-10
KEGG_PATHWAY	HTLV-I infection	47	6.70E-10	1.40E-08
KEGG_PATHWAY	Viral myocarditis	21	4.60E-08	7.00E-07
KEGG_PATHWAY	Phagosome	32	8.20E-08	1.10E-06
GOTERM_BP_DIRECT	antigen processing and presentation of peptide antigen via MHC class I	10	9.60E-05	9.30E-03
GOTERM_MF_DIRECT	peptide antigen binding	11	1.50E-04	1.70E-02
Annotation Cluster 2	Enrichment Score: 9.38	Count	P_Value	Benjamini
KEGG_PATHWAY	Inflammatory bowel disease (IBD)	25	2.00E-14	2.50E-12
KEGG_PATHWAY	Leishmaniasis	23	1.40E-11	3.50E-10
KEGG_PATHWAY	Tuberculosis	35	2.20E-09	4.40E-08
KEGG_PATHWAY	Asthma	12	6.00E-08	8.50E-07
KEGG_PATHWAY	Toxoplasmosis	24	3.50E-07	4.50E-06
Annotation Cluster 3	Enrichment Score: 6.23	Count	P_Value	Benjamini
GOTERM_CC_DIRECT	MHC class II protein complex	10	7.90E-10	7.40E-08
KEGG_PATHWAY	Viral myocarditis	21	4.60E-08	7.00E-07
KEGG_PATHWAY	Asthma	12	6.00E-08	8.50E-07
GOTERM_BP_DIRECT	antigen processing and presentation of exogenous peptide antigen via MHC class II	9	1.60E-07	5.00E-05
KEGG_PATHWAY	Intestinal immune network for IgA production	14	8.90E-07	1.00E-05
KEGG_PATHWAY	Staphylococcus aureus infection	15	1.30E-06	1.40E-05
GOTERM_BP_DIRECT	antigen processing and presentation of peptide or polysaccharide antigen via MHC class II	7	1.80E-06	4.80E-04
KEGG_PATHWAY	Systemic lupus erythematosus	17	2.10E-02	1.10E-01
Annotation Cluster 4	Enrichment Score: 4.31	Count	P_Value	Benjamini
GOTERM_CC_DIRECT	MHC class II protein complex	10	7.90E-10	7.40E-08

GOTERM_BP_DIRECT	antigen processing and presentation of exogenous peptide antigen via MHC class II	9	1.60E-07	5.00E-05
GOTERM_BP_DIRECT	antigen processing and presentation	14	4.40E-06	8.60E-04
GOTERM_MF_DIRECT	MHC class II protein complex binding	5	8.00E-03	2.70E-01
GOTERM_CC_DIRECT	multivesicular body	6	1.90E-02	2.40E-01
GOTERM_BP_DIRECT	chaperone mediated protein folding requiring cofactor	3	1.50E-01	9.40E-01
Annotation Cluster 5				
GOTERM_BP_DIRECT	Enrichment Score: 4	Count	P_Value	Benjamini
GOTERM_CC_DIRECT	defense response to protozoan	11	2.30E-06	5.30E-04
GOTERM_BP_DIRECT	symbiont-containing vacuole membrane	5	5.20E-04	1.90E-02
GOTERM_BP_DIRECT	adhesion of symbiont to host	5	8.60E-04	5.60E-02
Annotation Cluster 6				
GOTERM_BP_DIRECT	Enrichment Score: 3.35	Count	P_Value	Benjamini
GOTERM_MF_DIRECT	phagocytosis, engulfment	13	3.20E-06	7.10E-04
GOTERM_BP_DIRECT	immunoglobulin receptor binding	10	3.30E-05	5.00E-03
GOTERM_BP_DIRECT	B cell receptor signaling pathway	12	1.50E-04	1.30E-02
GOTERM_BP_DIRECT	phagocytosis, recognition	9	8.20E-04	5.40E-02
GOTERM_BP_DIRECT	positive regulation of B cell activation	8	1.70E-03	8.40E-02
GOTERM_BP_DIRECT	complement activation, classical pathway	9	9.10E-03	2.70E-01
GOTERM_CC_DIRECT	immunoglobulin complex, circulating	6	1.90E-02	2.40E-01
Annotation Cluster 7				
BIOCARTA	Enrichment Score: 3.16	Count	P_Value	Benjamini
BIOCARTA	NO2-dependent IL 12 Pathway in NK cells	11	4.80E-07	8.70E-05
BIOCARTA	CTL mediated immune response against target cells	10	1.50E-06	1.40E-04
BIOCARTA	T Helper Cell Surface Molecules	9	4.70E-06	2.90E-04
BIOCARTA	HIV Induced T Cell Apoptosis	8	5.80E-06	2.60E-04
BIOCARTA	IL12 and Stat4 Dependent Signaling Pathway in Th1 Development	11	1.10E-05	3.80E-04
GOTERM_CC_DIRECT	alpha-beta T cell receptor complex	5	4.20E-05	2.40E-03
BIOCARTA	T Cytotoxic Cell Surface Molecules	8	6.40E-05	1.90E-03
KEGG_PATHWAY	Primary immunodeficiency	10	1.70E-04	1.40E-03
BIOCARTA	Lck and Fyn tyrosine kinases in initiation of TCR Activation	6	1.20E-03	2.80E-02
BIOCARTA	T Cell Receptor and CD3 Complex	4	7.40E-03	1.30E-01
GOTERM_CC_DIRECT	T cell receptor complex	5	7.40E-03	1.30E-01
BIOCARTA	IL 17 Signaling Pathway	5	3.70E-02	3.90E-01
BIOCARTA	Activation of Csk by cAMP-dependent Protein Kinase	6	4.30E-02	4.10E-01
Inhibits Signaling through the T Cell Receptor				
BIOCARTA	T Cell Receptor Signaling Pathway	9	5.10E-02	4.50E-01
BIOCARTA	The Co-Stimulatory Signal During T-cell Activation	5	8.40E-02	5.90E-01
BIOCARTA	Role of Tob in T-cell activation	5	1.20E-01	6.40E-01
BIOCARTA	Stathmin and breast cancer resistance to antimicrotubule agents	4	3.50E-01	8.90E-01
Annotation Cluster 8				
GOTERM_MF_DIRECT	Enrichment Score: 2.53	Count	P_Value	Benjamini
GOTERM_BP_DIRECT	beta-2-microglobulin binding	7	3.60E-05	4.80E-03
GOTERM_BP_DIRECT	antigen processing and presentation of peptide antigen via MHC class I	10	9.60E-05	9.30E-03
GOTERM_MF_DIRECT	peptide antigen binding	11	1.50E-04	1.70E-02
GOTERM_MF_DIRECT	TAP binding	5	5.60E-04	3.60E-02
GOTERM_CC_DIRECT	MHC class I protein complex	6	1.30E-03	3.70E-02
GOTERM_CC_DIRECT	endoplasmic reticulum exit site	6	2.90E-03	6.70E-02
GOTERM_MF_DIRECT	T cell receptor binding	5	6.10E-03	2.40E-01
GOTERM_CC_DIRECT	Golgi medial cisterna	5	1.20E-02	1.80E-01
GOTERM_BP_DIRECT	antigen processing and presentation of exogenous peptide antigen via MHC class I, TAP-dependent	6	2.10E-02	4.70E-01
GOTERM_CC_DIRECT	phagocytic vesicle membrane	7	4.20E-02	3.80E-01
GOTERM_CC_DIRECT	integral component of lumenal side of endoplasmic reticulum membrane	4	4.50E-02	3.90E-01
GOTERM_MF_DIRECT	peptide binding	9	1.50E-01	8.80E-01
Annotation Cluster 9				
GOTERM_BP_DIRECT	Enrichment Score: 2.48	Count	P_Value	Benjamini
GOTERM_BP_DIRECT	microglial cell activation	9	1.90E-06	4.80E-04
GOTERM_BP_DIRECT	toll-like receptor signaling pathway	8	1.60E-05	2.40E-03
GOTERM_BP_DIRECT	MyD88-dependent toll-like receptor signaling pathway	7	1.20E-04	1.10E-02
GOTERM_BP_DIRECT	positive regulation of interleukin-6 production	11	4.10E-04	3.20E-02
GOTERM_BP_DIRECT	positive regulation of interleukin-6 biosynthetic process	5	8.60E-04	5.60E-02
GOTERM_BP_DIRECT	positive regulation of interleukin-8 production	7	1.80E-03	8.90E-02
GOTERM_BP_DIRECT	positive regulation of interferon-beta biosynthetic process	4	4.70E-03	1.90E-01
GOTERM_BP_DIRECT	positive regulation of NF-kappaB import into nucleus	5	1.70E-02	4.10E-01
GOTERM_BP_DIRECT	regulation of cytokine secretion	4	1.90E-02	4.30E-01
GOTERM_BP_DIRECT	positive regulation of chemokine production	5	2.10E-02	4.60E-01
GOTERM_BP_DIRECT	positive regulation of interleukin-8 biosynthetic process	3	6.60E-02	7.80E-01
GOTERM_BP_DIRECT	regulation of protein phosphorylation	7	1.20E-01	9.00E-01

GOTERM_BP_DIRECT	I-kappaB phosphorylation	3	1.30E-01	9.20E-01
GOTERM_BP_DIRECT	activation of NF-kappaB-inducing kinase activity	3	2.30E-01	9.80E-01

NFKBIZ vs. empty E μ -myc Fetal Liver Cell

Annotation Cluster 1	Enrichment Score: 3.89	Count	P_Value	Benjamini
GOTERM_MF_DIRECT	Kinase activity	99	1.60E-06	5.50E-04
GOTERM_BP_DIRECT	phosphorylation	89	2.50E-06	4.00E-03
GOTERM_MF_DIRECT	transferase activity	184	3.80E-06	8.90E-04
GOTERM_BP_DIRECT	protein phosphorylation	81	2.50E-05	2.40E-02
GOTERM_MF_DIRECT	protein kinase activity	76	7.00E-05	1.20E-02
GOTERM_MF_DIRECT	protein serine/threonine kinase activity	60	7.40E-04	7.20E-02
GOTERM_BP_DIRECT	protein autophosphorylation	30	1.30E-03	3.00E-01
GOTERM_MF_DIRECT	ATP binding	162	1.30E-02	5.00E-01
GOTERM_MF_DIRECT	nucleotide binding	200	2.90E-02	6.10E-01
Annotation Cluster 2	Enrichment Score: 3.17	Count	P_Value	Benjamini
GOTERM_CC_DIRECT	cell-cell adherens junction	51	3.20E-05	2.10E-03
GOTERM_MF_DIRECT	cadherin binding involved in cell-cell adhesion	44	3.90E-04	4.40E-02
GOTERM_BP_DIRECT	cell-cell adhesion	26	2.50E-02	7.50E-01
Annotation Cluster 3	Enrichment Score: 2.28	Count	P_Value	Benjamini
GOTERM_BP_DIRECT	B cell receptor signaling pathway	19	5.30E-07	1.20E-03
GOTERM_BP_DIRECT	phagocytosis, recognition	12	3.00E-04	1.60E-01
GOTERM_MF_DIRECT	immunoglobulin receptor binding	10	1.30E-03	1.10E-01
GOTERM_CC_DIRECT	immunoglobulin complex, circulating	9	2.80E-03	7.30E-02
GOTERM_BP_DIRECT	phagocytosis, engulfment	11	4.90E-03	5.20E-01
GOTERM_BP_DIRECT	complement activation, classical pathway	11	2.00E-02	7.20E-01
GOTERM_BP_DIRECT	positive regulation of B cell activation	8	2.20E-02	7.20E-01
GOTERM_BP_DIRECT	immunoglobulin mediated immune response	6	3.90E-02	7.90E-01
GOTERM_CC_DIRECT	blood microparticle	18	7.40E-02	5.30E-01
GOTERM_BP_DIRECT	humoral immune response mediated by circulating immunoglobulin	4	8.20E-02	9.10E-01
GOTERM_BP_DIRECT	defense response to bacterium	20	3.20E-01	1.00E+00
Annotation Cluster 4	Enrichment Score: 1.94	Count	P_Value	Benjamini
GOTERM_MF_DIRECT	transcription factor activity, sequence-specific DNA binding	108	1.10E-03	9.50E-02
GOTERM_BP_DIRECT	regulation of transcription, DNA-templated	239	1.80E-03	3.30E-01
GOTERM_BP_DIRECT	transcription, DNA-templated	188	3.50E-02	7.90E-01
GOTERM_MF_DIRECT	DNA binding	176	2.70E-01	9.70E-01

CD79BY196H vs. empty E μ -myc Fetal Liver Cell

Annotation Cluster 1	Enrichment Score: 4.18	Count	P_Value	Benjamini
KEGG_PATHWAY	Allograft rejection	13	3.90E-07	9.30E-05
KEGG_PATHWAY	Type I diabetes mellitus	13	1.20E-06	1.50E-04
KEGG_PATHWAY	Autoimmune thyroid disease	13	5.50E-06	4.50E-04
KEGG_PATHWAY	Cell adhesion molecules (CAMs)	19	1.40E-05	8.20E-04
GOTERM_BP_DIRECT	antigen processing and presentation of peptide antigen via MHC class I	9	1.50E-05	6.10E-03
KEGG_PATHWAY	Viral myocarditis	13	1.70E-05	8.30E-04
KEGG_PATHWAY	Antigen processing and presentation	13	2.50E-05	1.00E-03
KEGG_PATHWAY	Phagosome	19	3.60E-05	1.10E-03
KEGG_PATHWAY	Graft-versus-host disease	10	6.90E-05	1.90E-03
KEGG_PATHWAY	Herpes simplex infection	20	1.20E-04	2.90E-03
KEGG_PATHWAY	Epstein-Barr virus infection	19	5.40E-04	9.90E-03
KEGG_PATHWAY	HTLV-I infection	22	7.40E-04	1.30E-02
GOTERM_MF_DIRECT	peptide antigen binding	7	4.00E-03	3.60E-01
KEGG_PATHWAY	Endocytosis	13	2.70E-01	7.40E-01
Annotation Cluster 2	Enrichment Score: 3.94	Count	P_Value	Benjamini
GOTERM_BP_DIRECT	phagocytosis, recognition	10	2.40E-06	2.00E-03
GOTERM_MF_DIRECT	immunoglobulin receptor binding	9	6.70E-06	2.70E-03
GOTERM_BP_DIRECT	positive regulation of B cell activation	9	7.30E-06	3.60E-03
GOTERM_CC_DIRECT	immunoglobulin complex, circulating	8	2.90E-05	2.70E-03
GOTERM_BP_DIRECT	B cell receptor signaling pathway	10	5.80E-05	1.40E-02
GOTERM_BP_DIRECT	phagocytosis, engulfment	9	8.10E-05	1.70E-02
GOTERM_BP_DIRECT	complement activation, classical pathway	9	3.40E-04	5.60E-02

GOTERM_CC_DIRECT	blood microparticle	14	3.60E-04	1.80E-02
GOTERM_BP_DIRECT	defense response to bacterium	15	3.50E-03	2.70E-01
GOTERM_BP_DIRECT	humoral immune response mediated by circulating immunoglobulin	3	5.50E-02	8.70E-01

PD-L1 individual genes μ -myc Fetal Liver Cell

contrast	baseMean	log2FoldChange	pvalue	padj	chromosome_name	mgf_symbol
empty vs. PD-L1	365.9568935	2.474066855	5.40078E-05	0.001414436	10	Aim1
empty vs. PD-L1	1210.53153	2.40330942	0.003285361	0.030363551	1	Bcl2
empty vs. PD-L1	502.9894292	2.511429721	0.001608695	0.018199253	7	Bcl3
empty vs. PD-L1	473.0607948	6.71668311	1.09396E-12	1.16403E-09	16	Bcl6
empty vs. PD-L1	4137.102882	1.886148801	3.44811E-05	0.001009812	9	Birc3
empty vs. PD-L1	3816.974787	2.273702015	0.000102579	0.002325087	16	Blta
empty vs. PD-L1	3667.115728	1.244071382	0.004334637	0.037212594	5	Card11
empty vs. PD-L1	197.7812991	2.664777059	0.006005473	0.046193904	2	Card9
empty vs. PD-L1	447.8791057	7.535497077	5.65335E-17	2.70697E-13	9	Casp4
empty vs. PD-L1	5296.852965	1.320428999	0.002086034	0.022086128	3	Cd2
empty vs. PD-L1	262.6911924	3.682535416	0.000109479	0.002443883	1	Cd247
empty vs. PD-L1	231.0748294	3.464877928	2.80307E-05	0.000864529	6	Cd27
empty vs. PD-L1	2309.08624	-2.045781757	0.001228075	0.014924696	19	Cd274
empty vs. PD-L1	48.38999618	5.290034594	1.19385E-06	7.75115E-05	9	Cd276
empty vs. PD-L1	221.8845215	4.482833463	6.66524E-06	0.000301084	7	Cd33
empty vs. PD-L1	1418.2477993	4.756086541	1.19351E-09	3.00779E-07	2	Cd40
empty vs. PD-L1	46670.11495	3.60886911	5.15832E-11	2.59993E-08	4	Cd52
empty vs. PD-L1	151.6215594	3.595695767	0.000202914	0.003817696	2	Cd59a
empty vs. PD-L1	3602.442269	4.310495743	1.21007E-09	3.00993E-07	2	Cd82
empty vs. PD-L1	6972.418345	7.538735348	1.37982E-13	2.0329E-10	13	Cd83
empty vs. PD-L1	8150.936909	3.214625677	2.65688E-05	0.000829825	16	Cita
empty vs. PD-L1	1269.049198	6.224526921	8.5305E-09	1.48532E-06	1	Cr2
empty vs. PD-L1	837.2863148	4.628007834	8.47644E-08	9.66364E-06	X	Cxcr3
empty vs. PD-L1	2804.060631	5.341039694	1.4549E-09	3.46426E-07	9	Cxcr5
empty vs. PD-L1	202.6110483	2.279932123	5.65302E-05	0.001469095	1	Dstyk
empty vs. PD-L1	427.3501201	4.141565334	9.90292E-08	1.10918E-05	19	Fas
empty vs. PD-L1	71.82212575	5.232037225	7.76617E-06	0.000337291	1	Fasl
empty vs. PD-L1	1315.497336	5.034232529	4.68306E-09	8.91827E-07	5	Flt3
empty vs. PD-L1	203.5734379	2.260519743	0.001918397	0.020700316	7	Fosb
empty vs. PD-L1	12.9153942	3.787945826	0.00195905	0.021067764	X	Gata1
empty vs. PD-L1	4768.764324	2.220107305	8.48046E-05	0.001995409	11	Grap
empty vs. PD-L1	26409.29434	3.338527588	4.10205E-06	0.000202491	17	H2-DMa
empty vs. PD-L1	16887.99015	3.786533891	9.24583E-07	6.39297E-05	17	H2-DMb2
empty vs. PD-L1	324.8938871	2.48391167	0.00068244	0.009596756	17	H2-Eb2
empty vs. PD-L1	24276.94205	2.365893397	4.59607E-05	0.001253969	17	H2-K1
empty vs. PD-L1	213.9524438	4.035728785	1.73313E-06	0.00010538	17	H2-K2
empty vs. PD-L1	8.668646616	4.190042741	0.001159269	0.014352605	17	H2-M5
empty vs. PD-L1	8368.084124	2.681130437	0.000143349	0.002947017	17	H2-Ob
empty vs. PD-L1	21.11966479	4.263632245	0.000181731	0.003498178	17	H2-Q10
empty vs. PD-L1	25.91806744	4.868363239	4.0859E-06	0.000202491	17	H2-Q2
empty vs. PD-L1	80.60841252	2.311340335	0.003692529	0.03307683	17	H2-Q4
empty vs. PD-L1	111.9812534	5.897927281	1.46507E-09	3.46426E-07	17	H2-Q5
empty vs. PD-L1	1921.541398	5.652829014	4.51861E-10	1.33146E-07	17	H2-Q6
empty vs. PD-L1	380.5335846	3.344277896	7.63091E-05	0.001851335	17	H2-T10
empty vs. PD-L1	2433.522634	2.509832932	5.66555E-05	0.001470344	17	H2-T22
empty vs. PD-L1	3848.220499	2.958203588	2.20564E-05	0.000729283	2	Hck
empty vs. PD-L1	3420.22709	7.589422366	9.27278E-17	3.55203E-13	10	Icosl
empty vs. PD-L1	135.7399456	4.057582911	0.000111061	0.002467688	1	Ikzf2
empty vs. PD-L1	132.3379488	4.061759159	8.45589E-05	0.001992074	1	Il10
empty vs. PD-L1	351.559195	4.059363298	0.000235138	0.004285054	3	Il12a
empty vs. PD-L1	878.2320279	4.877873723	1.83057E-10	6.69599E-08	6	Irak2
empty vs. PD-L1	6629.746816	1.965649421	0.002093804	0.022143909	11	Irf1
empty vs. PD-L1	6596.570372	1.256359396	0.000219266	0.004077274	6	Irf5
empty vs. PD-L1	1115.720001	2.76906273	7.90029E-06	0.00034234	7	Irf7
empty vs. PD-L1	2514.916952	2.138433162	0.000490599	0.007422153	14	Irf9
empty vs. PD-L1	4833.78465	1.051586296	0.006681293	0.049792533	4	Jak1
empty vs. PD-L1	1115.019369	2.339080505	0.000123607	0.00266729	19	Jak2
empty vs. PD-L1	412.6020316	4.097082823	3.91699E-09	7.98108E-07	4	Jun
empty vs. PD-L1	615.5427854	7.794765082	2.80783E-16	8.96307E-13	2	Kynu
empty vs. PD-L1	94.99458712	4.182645554	2.52955E-05	0.000797925	6	Lag3
empty vs. PD-L1	548.2712034	3.469429404	0.000205211	0.00384957	7	Lat

empty vs. PD-L1	5277.42579	2.767954407	1.7614E-07	1.76629E-05	5	Lat2
empty vs. PD-L1	2697.598921	2.434439455	0.001647875	0.018554819	4	Lck
empty vs. PD-L1	5114.264085	3.046382823	8.79003E-11	3.91524E-08	8	Lrrc25
empty vs. PD-L1	509.9068697	6.195866495	1.2432E-11	8.8189E-09	17	Lta
empty vs. PD-L1	183.6395798	3.218929907	0.000269827	0.004728276	17	Ltb
empty vs. PD-L1	571.7033274	2.431889718	0.003438685	0.031413806	15	Mapk11
empty vs. PD-L1	2687.789315	1.327738632	0.000655014	0.009320563	18	Nfatc1
empty vs. PD-L1	489.7670991	3.021665899	9.08393E-06	0.00038071	19	Nfkb2
empty vs. PD-L1	9089.218741	1.718998951	0.001215381	0.014855263	12	Nfkbia
empty vs. PD-L1	2065.635993	2.624375435	8.76251E-06	0.000372125	16	Nfkbiz
empty vs. PD-L1	3113.44509	2.007845542	0.000635441	0.009096116	12	Pik3cg
empty vs. PD-L1	951.2609592	-1.220222534	0.000976959	0.012608955	3	Plk4
empty vs. PD-L1	424.7146623	4.874320394	2.06721E-07	1.99966E-05	10	Prdm1
empty vs. PD-L1	1805.224302	1.652551654	0.000579586	0.008512891	11	Rel
empty vs. PD-L1	302.5597071	5.380117616	8.4595E-08	9.66364E-06	8	Smad1
empty vs. PD-L1	2831.85859	2.215599009	0.000936301	0.012240939	1	Stat1
empty vs. PD-L1	403.5671637	4.520717724	5.94727E-06	0.000274477	1	Stat4
empty vs. PD-L1	3757.640731	1.092987316	0.003009522	0.028422765	3	Tet2
empty vs. PD-L1	1596.023856	2.327607194	7.78022E-05	0.001876757	5	Tlr1
empty vs. PD-L1	396.4584178	2.685598747	0.000407097	0.006433282	4	Tlr4
empty vs. PD-L1	447.3529036	1.869917745	1.1154E-05	0.000442386	5	Tlr6
empty vs. PD-L1	553.6384288	5.130182771	3.64903E-09	7.59672E-07	X	Tlr7
empty vs. PD-L1	113.6187601	2.46096308	7.79981E-05	0.001879117	9	Tlr9
empty vs. PD-L1	141.8136466	5.71262426	3.40571E-09	7.24772E-07	17	Tnf
empty vs. PD-L1	597.3957548	3.898002033	3.72731E-07	3.20131E-05	10	Tnfaip3
empty vs. PD-L1	39.57879102	2.960219027	0.000612081	0.008852446	7	Tnfrsf23
empty vs. PD-L1	1448.947139	5.609506932	1.20096E-13	1.91682E-10	2	Traf1

MYD88L265P individual genes E μ -myc Fetal Liver Cell

contrast	baseMean	log2FoldChange	pvalue	padj	chromosome_name	mgi_symbol
empty vs. MYD88L265P	2092.612201	-2.200990237	6.66615E-15	7.81392E-13	12	Batf
empty vs. MYD88L265P	6024.700569	-1.453479408	2.44342E-36	3.41785E-33	7	Bax
empty vs. MYD88L265P	502.9894292	-1.782541418	0.004924572	0.02800959	7	Bcl3
empty vs. MYD88L265P	357.6259507	2.705865567	2.1044E-08	7.5349E-07	10	Bcr
empty vs. MYD88L265P	1979.908969	4.766128002	1.09398E-14	1.25431E-12	14	Blk
empty vs. MYD88L265P	9314.319885	0.801938251	0.001254365	0.009491193	18	Brd8
empty vs. MYD88L265P	3816.974787	1.888069144	3.85048E-05	0.000534507	16	Btla
empty vs. MYD88L265P	197.7812991	-2.120768723	0.00736775	0.037954858	2	Card9
empty vs. MYD88L265P	128.8422891	-3.092408089	1.15388E-05	0.000194308	11	Ccl2
empty vs. MYD88L265P	719.5207893	-2.778752339	6.58465E-10	3.27314E-08	9	Ccr2
empty vs. MYD88L265P	1020.085969	-4.508729036	6.80295E-10	3.35858E-08	18	Cd14
empty vs. MYD88L265P	25615.30109	2.564516806	0.001785393	0.012597177	7	Cd19
empty vs. MYD88L265P	654.6162995	5.123128183	9.14335E-12	6.59264E-10	16	Cd200
empty vs. MYD88L265P	1494.56241	-1.688838739	0.000663143	0.005768688	1	Cd244
empty vs. MYD88L265P	231.0748294	2.494500956	0.000174435	0.001886591	6	Cd27
empty vs. MYD88L265P	2309.08624	-1.931013629	0.000106726	0.001251717	19	Cd274
empty vs. MYD88L265P	221.8845215	-3.800310355	3.71754E-07	9.6776E-06	7	Cd33
empty vs. MYD88L265P	1418.247993	1.725324348	0.005754299	0.031589927	2	Cd40
empty vs. MYD88L265P	7086.422787	-1.026910168	8.65173E-06	0.000150898	2	Cd44
empty vs. MYD88L265P	1868.163997	3.767118706	1.03356E-12	8.99837E-11	1	Cd55
empty vs. MYD88L265P	110006.1414	2.309901446	3.50355E-05	0.000494361	18	Cd74
empty vs. MYD88L265P	34344.80445	1.629623028	0.006427535	0.034272562	7	Cd79a
empty vs. MYD88L265P	68277.08694	1.757441186	8.9564E-05	0.001082791	11	Cd79b
empty vs. MYD88L265P	140.0644937	-2.327537285	2.55608E-05	0.000379559	16	Cd80
empty vs. MYD88L265P	6972.418345	4.613359167	5.38273E-08	1.76746E-06	13	Cd83
empty vs. MYD88L265P	1246.663694	1.729076173	0.000332174	0.003262961	1	Cd84
empty vs. MYD88L265P	876.7815432	2.743054858	3.87941E-05	0.000537634	2	Cd93
empty vs. MYD88L265P	1430.653783	-4.506493566	3.40783E-17	5.81325E-15	17	Cdkn1a
empty vs. MYD88L265P	497.2130746	1.161808657	0.003653884	0.022113004	4	Cdkn2c
empty vs. MYD88L265P	97.27422462	-4.442175275	1.99897E-15	2.58904E-13	16	Cebpd
empty vs. MYD88L265P	1269.049198	7.090025736	1.01408E-14	1.17555E-12	1	Cr2
empty vs. MYD88L265P	4350.29776	1.236160511	1.37161E-05	0.000224137	5	Cux1
empty vs. MYD88L265P	145.7914237	-1.783554493	0.005921609	0.032255244	11	Cxcl16
empty vs. MYD88L265P	1714.183397	2.087649584	2.76587E-07	7.42115E-06	1	Cxcr4
empty vs. MYD88L265P	2804.060631	6.351033075	9.68563E-19	1.91721E-16	9	Cxcr5
empty vs. MYD88L265P	174.4347352	-2.709477166	0.006373054	0.034059538	7	Dkk3

empty vs. MYD88L265P	1263.587731	-1.718643979	5.5894E-06	0.000102734	6	Etv6
empty vs. MYD88L265P	1858.393837	-1.266940778	0.000386832	0.003714653	8	Fanca
empty vs. MYD88L265P	1987.715164	-2.314602689	4.64235E-06	8.7832E-05	7	Fes
empty vs. MYD88L265P	203.5734379	2.386242189	3.86383E-05	0.000535829	7	Fosb
empty vs. MYD88L265P	1322.574306	2.132911753	3.04287E-07	8.0817E-06	3	Foxo1
empty vs. MYD88L265P	179.9387562	1.003572897	9.7969E-05	0.00116662	X	Foxo4
empty vs. MYD88L265P	87.98409227	4.53485317	0.001102079	0.008542428	19	Gfra1
empty vs. MYD88L265P	29.78108272	2.566159489	0.00915593	0.04479126	14	Gfra2
empty vs. MYD88L265P	125010.9615	2.330199981	2.53786E-05	0.000377387	17	H2-Aa
empty vs. MYD88L265P	64139.7553	2.391722296	9.98793E-06	0.000170935	17	H2-Ab1
empty vs. MYD88L265P	26409.29434	2.263888984	8.55828E-05	0.001040985	17	H2-DMa
empty vs. MYD88L265P	3351.898721	1.248801184	0.007372543	0.037969327	17	H2-DMb1
empty vs. MYD88L265P	16887.99015	2.804838158	5.49772E-06	0.000101454	17	H2-DMb2
empty vs. MYD88L265P	61199.65956	1.831786391	0.001103006	0.008546259	17	H2-Eb1
empty vs. MYD88L265P	324.8938871	4.874945325	1.22665E-16	1.92568E-14	17	H2-Eb2
empty vs. MYD88L265P	213.9524438	2.954469672	1.34219E-05	0.000220358	17	H2-K2
empty vs. MYD88L265P	28.420706	1.873493451	2.91278E-06	5.89353E-05	17	H2-Ke6
empty vs. MYD88L265P	8.668646616	4.137582513	0.000477659	0.004417027	17	H2-M5
empty vs. MYD88L265P	6583.270465	5.537952578	5.68814E-19	1.14758E-16	17	H2-Oa
empty vs. MYD88L265P	8368.084124	3.830561779	7.58303E-12	5.52455E-10	17	H2-Ob
empty vs. MYD88L265P	1921.541398	3.186535962	1.59596E-05	0.000254263	17	H2-Q6
empty vs. MYD88L265P	380.5335846	1.808100896	0.007995938	0.040378044	17	H2-T10
empty vs. MYD88L265P	3848.220499	-3.731990811	1.13355E-11	8.08985E-10	2	Hck
empty vs. MYD88L265P	3420.22709	5.258785075	1.45545E-12	1.24139E-10	10	Icosl
empty vs. MYD88L265P	1169.212152	-2.66011299	3.39101E-27	1.77875E-24	1	Idh1
empty vs. MYD88L265P	8379.526116	0.474354986	0.001161092	0.008917286	11	Ikzf1
empty vs. MYD88L265P	135.7399456	2.784898822	0.001507849	0.010981496	1	Ikzf2
empty vs. MYD88L265P	132.3379488	-4.046359264	4.40458E-08	1.48342E-06	1	Il10
empty vs. MYD88L265P	136.5240176	-3.649262741	2.06378E-06	4.37839E-05	2	Il1b
empty vs. MYD88L265P	35.25196619	-4.085564162	0.000185159	0.001979421	5	Il6
empty vs. MYD88L265P	748.9863641	4.28796995	1.10701E-09	5.26697E-08	15	Il7r
empty vs. MYD88L265P	1652.359206	2.243845493	0.009328459	0.045425818	11	Il9r
empty vs. MYD88L265P	197.9919172	2.042519404	0.00115928	0.00890663	8	Inpp4b
empty vs. MYD88L265P	746.5286622	-3.000309571	0.000259231	0.002641664	10	Irak3
empty vs. MYD88L265P	10793.35391	1.637368593	0.001392751	0.010330666	8	Ir8f
empty vs. MYD88L265P	4.918731202	3.207273072	0.005926157	0.032271638	6	Klra4
empty vs. MYD88L265P	2162.622326	-1.613133094	3.73282E-05	0.000521105	8	Lamp1
empty vs. MYD88L265P	548.2712034	2.598386767	0.000690123	0.005944236	7	Lat
empty vs. MYD88L265P	2697.598921	3.339452607	6.85167E-08	2.19819E-06	4	Lck
empty vs. MYD88L265P	5114.264085	-6.273439265	8.80144E-78	1.84672E-73	8	Lrrc25
empty vs. MYD88L265P	509.9068697	2.034770785	0.005826306	0.03184359	17	Lta
empty vs. MYD88L265P	183.6395798	2.147559371	0.002674399	0.017279157	17	Ltb
empty vs. MYD88L265P	26.2240394	4.719252782	9.70151E-06	0.000166713	2	Ltk
empty vs. MYD88L265P	11278.5063	-1.511845199	3.63882E-07	9.48443E-06	4	Lyn
empty vs. MYD88L265P	723.0196837	-0.577065294	0.007374178	0.037969327	11	Map2k4
empty vs. MYD88L265P	2751.672914	0.569122562	0.006636877	0.035085653	1	Mdm4
empty vs. MYD88L265P	3471.682112	-2.15098473	1.10015E-24	4.7109E-22	9	Myd88
empty vs. MYD88L265P	761.5254929	2.297548885	5.51281E-09	2.26804E-07	9	Neil1
empty vs. MYD88L265P	9089.218741	-1.299445799	0.001713637	0.012192446	12	Nfkbia
empty vs. MYD88L265P	878.1908977	1.526879226	0.000723432	0.006172852	17	Nfkbie
empty vs. MYD88L265P	139.8311176	-8.177374274	9.65929E-25	4.22232E-22	2	Noxa1
empty vs. MYD88L265P	3113.44509	-1.18162634	0.010263538	0.048710596	12	Pik3cg
empty vs. MYD88L265P	6924.489603	-1.402051171	4.26175E-07	1.09315E-05	17	Pim1
empty vs. MYD88L265P	362.4462935	1.880961046	0.000515483	0.004690311	2	Plcg1
empty vs. MYD88L265P	7296.88872	-0.588274755	0.001012448	0.008004215	8	Plcg2
empty vs. MYD88L265P	190.8470375	2.297254307	7.76373E-05	0.000957101	13	Plk2
empty vs. MYD88L265P	424.7146623	-2.527278592	0.000483449	0.004460738	10	Prdm1
empty vs. MYD88L265P	198.1313949	2.720894979	7.36551E-10	3.61928E-08	11	Prkca
empty vs. MYD88L265P	3231.342362	-0.758490056	0.003193155	0.019878078	14	Prkcd
empty vs. MYD88L265P	3398.484206	-0.359801585	0.006549476	0.034737388	19	Pten
empty vs. MYD88L265P	6715.842511	-2.496397921	3.89031E-45	7.4206E-42	7	Pycard
empty vs. MYD88L265P	128.9028537	4.953454526	1.00048E-05	0.000171085	2	Rag1
empty vs. MYD88L265P	3897.66194	0.989474759	0.000531377	0.004785128	19	Rela
empty vs. MYD88L265P	53.41542568	2.651179801	3.39054E-05	0.000480785	14	Rgcc
empty vs. MYD88L265P	3251.719435	1.569880244	0.000251431	0.002577194	3	S1pr1
empty vs. MYD88L265P	209.4167307	-2.06074359	5.10688E-05	0.000671902	9	S1pr2
empty vs. MYD88L265P	25.45713923	-3.139828621	0.00937298	0.045587358	2	Siglec1
empty vs. MYD88L265P	5052.250247	1.094589011	0.000166662	0.001819412	1	Slamf6
empty vs. MYD88L265P	1745.197209	1.101165519	0.007366263	0.037954858	10	Stat2
empty vs. MYD88L265P	32.0615535	2.563328143	0.000738679	0.006274882	13	Tert

empty vs. MYD88L265P	3757.640731	-0.908889433	0.001376312	0.010240347	3	Tet2
empty vs. MYD88L265P	128.8303426	2.908189952	0.006224743	0.033437675	1	Tgfb2
empty vs. MYD88L265P	1195.126379	-1.295261563	1.96517E-05	0.000304079	6	Tigar
empty vs. MYD88L265P	1596.023856	-1.256957315	0.006352065	0.033973751	5	Tlr1
empty vs. MYD88L265P	806.4393302	-3.645227074	1.84484E-18	3.48725E-16	3	Tlr2
empty vs. MYD88L265P	110.9717202	-5.879677048	5.98979E-18	1.11219E-15	X	Tlr8
empty vs. MYD88L265P	8883.693065	0.726362912	0.000395859	0.00378919	18	Tnfaip8
empty vs. MYD88L265P	1056.938729	2.836979444	1.75858E-05	0.000277016	7	Tnrsf26
empty vs. MYD88L265P	2.399808204	-3.031983361	0.005378449	0.030035142	11	Tnfsf13
empty vs. MYD88L265P	1114.332131	1.821242225	7.78422E-05	0.000959063	1	Traf5
empty vs. MYD88L265P	1026.108425	0.70595956	7.38224E-06	0.000131489	1	Trak2
empty vs. MYD88L265P	25.22863429	-4.394719564	2.07556E-06	4.39892E-05	4	Trp73
empty vs. MYD88L265P	266.4954336	2.963161068	4.82029E-05	0.000641747	1	Zap70

NFKBIZ individual genes E μ -myc Fetal Liver Cell

contrast	baseMean	log2FoldChange	pvalue	padj	chromosome_nam	mgi_symbol
empty vs. NFKBIZ	365.9568935	1.191563647	0.010228019	0.048729403	10	Aim1
empty vs. NFKBIZ	2092.612201	-0.847198654	0.001933595	0.013469236	12	Batf
empty vs. NFKBIZ	6024.700569	-0.796871919	9.32565E-13	1.01912E-10	7	Bax
empty vs. NFKBIZ	1210.53153	4.858548897	3.02826E-14	4.60428E-12	1	Bcl2
empty vs. NFKBIZ	473.0607948	1.898384544	0.009802578	0.047273617	16	Bcl6
empty vs. NFKBIZ	4137.102882	1.378574059	5.44639E-05	0.000715567	9	Birc3
empty vs. NFKBIZ	1979.908969	3.644248377	1.04176E-09	5.41045E-08	14	Blk
empty vs. NFKBIZ	4852.14082	0.573912218	0.007100703	0.037170281	17	Brd2
empty vs. NFKBIZ	1132.606186	1.415196247	0.0004559	0.004279951	15	Card6
empty vs. NFKBIZ	447.8791057	2.545092897	0.000133935	0.001539849	9	Casp4
empty vs. NFKBIZ	13.93661901	4.285571078	0.000374328	0.003644617	9	Ccr4
empty vs. NFKBIZ	25615.30109	5.529605953	4.34721E-12	4.05392E-10	7	Cd19
empty vs. NFKBIZ	5296.852965	2.547130533	2.29203E-15	4.58013E-13	3	Cd2
empty vs. NFKBIZ	231.0748294	2.539377731	8.10783E-05	0.001008408	6	Cd27
empty vs. NFKBIZ	18122.22292	2.748583497	7.198E-13	8.03343E-11	7	Cd37
empty vs. NFKBIZ	46670.11495	-1.174137071	0.004706651	0.027048743	4	Cd52
empty vs. NFKBIZ	151.6215594	-3.036485257	3.17179E-05	0.000452724	2	Cd59a
empty vs. NFKBIZ	10.67214217	-2.287760247	0.000869358	0.007172969	2	Cd59b
empty vs. NFKBIZ	34344.80445	3.637521342	3.49277E-10	2.00233E-08	7	Cd79a
empty vs. NFKBIZ	68277.08694	2.003776261	3.93836E-06	7.63719E-05	11	Cd79b
empty vs. NFKBIZ	6972.418345	5.422378601	5.06894E-11	3.49857E-09	13	Cd83
empty vs. NFKBIZ	97.27422462	-3.375414326	5.36685E-10	2.95557E-08	16	Cebpd
empty vs. NFKBIZ	1269.049198	7.362509105	1.58339E-16	4.20541E-14	1	Cr2
empty vs. NFKBIZ	4350.29776	1.259334924	4.58839E-06	8.7442E-05	5	Cux1
empty vs. NFKBIZ	9.869759833	2.18979139	0.00648495	0.034711027	1	Cxcr2
empty vs. NFKBIZ	12080.74255	-0.810967141	0.003802877	0.022935315	9	Dnmt1
empty vs. NFKBIZ	348.6619114	-0.889566578	0.007041755	0.036928294	12	E2f6
empty vs. NFKBIZ	1987.715164	-1.800751086	0.000233492	0.00246972	7	Fes
empty vs. NFKBIZ	24.39043098	-2.804123205	0.003789323	0.022873293	5	Flt1
empty vs. NFKBIZ	203.5734379	2.32055002	3.5477E-05	0.000496583	7	Fosb
empty vs. NFKBIZ	1322.574306	1.917479214	1.93501E-06	4.1813E-05	3	Foxo1
empty vs. NFKBIZ	87.98409227	4.767554094	0.00057662	0.005139611	19	Gfra1
empty vs. NFKBIZ	79.41010628	2.92719021	0.007281802	0.039885679	17	H2-M2
empty vs. NFKBIZ	80.60841252	2.192629088	0.000385526	0.00374149	17	H2-Q4
empty vs. NFKBIZ	3848.220499	-2.179711964	4.27311E-05	0.000585238	2	Hck
empty vs. NFKBIZ	3420.22709	4.233033185	4.35327E-09	1.96431E-07	10	Icosl
empty vs. NFKBIZ	2551.491236	-1.198065488	0.001991936	0.01377317	7	Idh2
empty vs. NFKBIZ	8379.526116	0.464761825	0.000986097	0.007960861	11	Ikzf1
empty vs. NFKBIZ	135.7399456	2.483327432	0.003616615	0.022001685	1	Ikzf2
empty vs. NFKBIZ	3021.378292	1.136948687	0.000921596	0.007540915	11	Ikzf3
empty vs. NFKBIZ	132.3379488	-2.858919875	6.95532E-05	0.000879501	1	Il10
empty vs. NFKBIZ	351.559195	7.867620486	3.5562E-17	1.16588E-14	3	Il12a
empty vs. NFKBIZ	3.51635791	4.407150559	0.001543626	0.011313869	1	Il24
empty vs. NFKBIZ	748.9863641	6.099413707	6.1264E-19	2.92146E-16	15	Il7r
empty vs. NFKBIZ	1652.359206	3.398529711	5.22517E-05	0.000691264	11	Il9r
empty vs. NFKBIZ	285.8472221	1.449398011	0.009826081	0.04734118	1	Inpp1
empty vs. NFKBIZ	878.2320279	2.092482068	0.00037694	0.003668349	6	Irak2
empty vs. NFKBIZ	2836.426418	-0.690009829	0.007209268	0.037581173	15	Irak4
empty vs. NFKBIZ	4877.814732	0.77461733	0.002480116	0.016384693	8	Irf2
empty vs. NFKBIZ	1565.81275	1.011138586	0.000433247	0.004111438	13	Irf4
empty vs. NFKBIZ	9.351259382	4.371580197	0.001072902	0.008498163	1	Irs1

empty vs. NFKBIZ	92.80925286	5.590767278	2.18742E-13	2.71948E-11	8	Irs2
empty vs. NFKBIZ	4833.78465	1.404246802	1.24431E-06	2.82861E-05	4	Jak1
empty vs. NFKBIZ	99.74695216	3.813926567	0.000522602	0.004753028	5	Kit
empty vs. NFKBIZ	265.9751297	4.539778823	6.62226E-10	3.5997E-08	4	Klf4
empty vs. NFKBIZ	2697.598921	2.166702119	0.000304219	0.003091102	4	Lck
empty vs. NFKBIZ	5114.264085	-5.868201283	8.09423E-73	1.69833E-68	8	Lrrc25
empty vs. NFKBIZ	509.9068697	5.235130148	3.5236E-13	4.27353E-11	17	Lta
empty vs. NFKBIZ	26.2240394	4.968251449	1.81621E-06	3.96131E-05	2	Ltk
empty vs. NFKBIZ	32.87173588	-3.149308491	2.76484E-06	5.66668E-05	4	Map3k6
empty vs. NFKBIZ	562.817193	-1.034444975	0.000259546	0.002699946	12	Map4k5
empty vs. NFKBIZ	16.65069363	3.49160082	0.003704297	0.022438676	11	Meis1
empty vs. NFKBIZ	1557.229589	0.791295496	0.002284932	0.015307291	10	Mum1
empty vs. NFKBIZ	3471.682112	-0.559457231	0.005809048	0.031923897	9	Myd88
empty vs. NFKBIZ	489.7670991	1.360028008	0.008866319	0.043834379	19	Nfkb2
empty vs. NFKBIZ	2065.635993	-1.422483483	0.001384652	0.010353802	16	Nfkbiz
empty vs. NFKBIZ	3720.927086	1.59114198	1.62628E-05	0.000260279	4	Pax5
empty vs. NFKBIZ	56.88821139	2.234264653	0.007396653	0.03827289	4	Pik3r3
empty vs. NFKBIZ	964.3751096	0.690405388	0.007785951	0.039757376	7	Polg
empty vs. NFKBIZ	647.06738	0.951665549	6.52951E-05	0.000833347	11	Polg2
empty vs. NFKBIZ	424.7146623	-2.748629817	9.26229E-05	0.001132526	10	Prdm1
empty vs. NFKBIZ	740.6301016	1.543435431	1.05935E-07	3.24487E-06	17	Prkce
empty vs. NFKBIZ	6715.842511	-2.124927125	2.11963E-35	8.89481E-32	7	Pycard
empty vs. NFKBIZ	1805.224302	1.254939874	0.000505557	0.004634165	11	Rel
empty vs. NFKBIZ	746.6417586	0.742489132	0.000764495	0.006494182	12	Sos2
empty vs. NFKBIZ	3520.451305	0.365812378	0.001992259	0.01377317	X	Stag2
empty vs. NFKBIZ	806.4393302	-1.336238138	0.000910662	0.007466787	3	Tlr2
empty vs. NFKBIZ	41.07698441	4.670212398	1.45038E-06	3.23743E-05	8	Tlr3
empty vs. NFKBIZ	110.9717202	-1.812506686	0.006744837	0.035800703	X	Tlr8
empty vs. NFKBIZ	141.8136466	2.298869693	0.001058882	0.008425211	17	Tnf
empty vs. NFKBIZ	597.3957548	1.774885052	0.002585223	0.016898177	10	Tnfaip3
empty vs. NFKBIZ	7749.165514	-1.094262417	1.41881E-06	3.17033E-05	11	Tnfrsf13b
empty vs. NFKBIZ	1160.826627	-1.215840868	0.001163893	0.009024388	4	Tnfrsf1b
empty vs. NFKBIZ	1448.947139	2.508598518	1.60983E-05	0.000258041	2	Traf1
empty vs. NFKBIZ	3661.32144	0.95988687	0.002257279	0.015146217	2	Traf2
empty vs. NFKBIZ	1114.332131	1.608148903	0.000311362	0.003147728	1	Traf5
empty vs. NFKBIZ	1026.108425	0.640119841	2.49772E-05	0.00037317	1	Trak2

2. Table Appendix 2: The manifest transduced Eμ-myc lymphoma approach

DAVID and Individual gene analysis

CD79BY196H vs. empty manifest transduced Eμ-myc lymphomas

Annotation Cluster 1	Enrichment Score: 7.61	Count	P_Value	Benjamini
GOTERM_BP_DIRECT	immune system process	30	2.70E-15	3.70E-12
GOTERM_BP_DIRECT	response to virus	14	2.30E-11	1.60E-08
GOTERM_BP_DIRECT	defense response to virus	15	1.50E-08	6.80E-06
GOTERM_BP_DIRECT	innate immune response	22	1.80E-08	5.90E-06
GOTERM_MF_DIRECT	double-stranded RNA binding	8	2.60E-05	2.00E-03
GOTERM_MF_DIRECT	RNA binding	11	5.10E-01	9.90E-01
Annotation Cluster 2	Enrichment Score: 4.36	Count	P_Value	Benjamini
KEGG_PATHWAY	Cell adhesion molecules (CAMs)	15	2.80E-08	5.00E-06
GOTERM_MF_DIRECT	peptide antigen binding	9	7.30E-08	2.80E-05
KEGG_PATHWAY	Herpes simplex infection	16	9.90E-08	8.80E-06
GOTERM_MF_DIRECT	beta-2-microglobulin binding	6	3.40E-07	6.40E-05
KEGG_PATHWAY	Graft-versus-host disease	9	3.80E-07	2.20E-05
KEGG_PATHWAY	Allograft rejection	9	6.90E-07	3.00E-05
KEGG_PATHWAY	Viral myocarditis	10	9.70E-07	3.40E-05
KEGG_PATHWAY	Type I diabetes mellitus	9	1.50E-06	4.50E-05
GOTERM_MF_DIRECT	TAP binding	5	1.60E-06	2.00E-04
	antigen processing and presentation of peptide antigen via MHC class I	7	4.10E-06	9.10E-04
GOTERM_BP_DIRECT	Autoimmune thyroid disease	9	4.40E-06	1.10E-04
KEGG_PATHWAY	Antigen processing and presentation	9	1.30E-05	2.90E-04
GOTERM_MF_DIRECT	T cell receptor binding	5	2.10E-05	2.00E-03

GOTERM_CC_DIRECT	MHC class I protein complex	5	3.80E-05	3.00E-03
GOTERM_CC_DIRECT	Golgi medial cisterna	5	4.90E-05	2.90E-03
GOTERM_CC_DIRECT	endoplasmic reticulum exit site	5	7.90E-05	3.70E-03
KEGG_PATHWAY	Viral carcinogenesis	12	2.60E-04	4.60E-03
GOTERM_BP_DIRECT	antigen processing and presentation	6	4.80E-04	8.60E-02
KEGG_PATHWAY	Epstein-Barr virus infection	11	6.00E-04	8.20E-03
GOTERM_MF_DIRECT	receptor binding	15	6.70E-04	3.20E-02
KEGG_PATHWAY	Phagosome	9	2.30E-03	2.90E-02
KEGG_PATHWAY	Endocytosis	10	1.20E-02	1.20E-01
KEGG_PATHWAY	HTLV-I infection	10	1.20E-02	1.20E-01
GOTERM_CC_DIRECT	integral component of luminal side of endoplasmic reticulum membrane	3	1.50E-02	2.90E-01
GOTERM_CC_DIRECT	phagocytic vesicle membrane	4	2.10E-02	3.60E-01
GOTERM_MF_DIRECT	peptide binding	5	2.90E-02	4.80E-01
	antigen processing and presentation of exogenous peptide antigen via MHC class I, TAP-dependent	3	5.00E-02	8.80E-01
Annotation Cluster 3	Enrichment Score: 2.79	Count	P_Value	Benjamini
GOTERM_MF_DIRECT	double-stranded RNA binding	8	2.60E-05	2.00E-03
GOTERM_MF_DIRECT	2'-5'-oligoadenylate synthetase activity	4	2.90E-04	1.60E-02
KEGG_PATHWAY	Measles	9	4.70E-04	7.50E-03
KEGG_PATHWAY	Influenza A	10	4.70E-04	6.90E-03
GOTERM_BP_DIRECT	purine nucleotide biosynthetic process	4	1.70E-03	2.00E-01
KEGG_PATHWAY	Hepatitis C	6	3.60E-02	2.80E-01
GOTERM_MF_DIRECT	nucleotidyltransferase activity	3	2.90E-01	9.60E-01
Annotation Cluster 4	Enrichment Score: 1.71	Count	P_Value	Benjamini
KEGG_PATHWAY	Intestinal immune network for IgA production	6	2.30E-04	4.50E-03
KEGG_PATHWAY	Rheumatoid arthritis	4	9.80E-02	4.70E-01
KEGG_PATHWAY	Systemic lupus erythematosus	4	3.20E-01	7.50E-01

CARD11L244P vs. empty manifest transduced E μ -myc lymphomas

Annotation Cluster 1	Enrichment Score: 1.96	Count	P_Value	Benjamini
KEGG_PATHWAY	Focal adhesion	6	2.20E-03	2.60E-01
KEGG_PATHWAY	Leukocyte transendothelial migration	4	1.70E-02	5.30E-01
GOTERM_CC_DIRECT	cell-cell junction	4	3.40E-02	7.10E-01
Annotation Cluster 2	Enrichment Score: 1.85	Count	P_Value	Benjamini
KEGG_PATHWAY	Hematopoietic cell lineage	4	6.30E-03	3.40E-01
KEGG_PATHWAY	PI3K-Akt signaling pathway	6	2.00E-02	4.10E-01
GOTERM_CC_DIRECT	cell surface	7	2.30E-02	6.70E-01

I κ B α Δ N vs. empty manifest transduced E μ -myc lymphomas

Annotation Cluster 1	Enrichment Score: 2.6	Count	P_Value	Benjamini
GOTERM_BP_DIRECT	inflammatory response	7	1.50E-03	1.70E-01
GOTERM_BP_DIRECT	immune system process	7	2.50E-03	2.30E-01
GOTERM_BP_DIRECT	innate immune response	7	3.10E-03	2.50E-01
GOTERM_BP_DIRECT	response to virus	4	3.40E-03	2.50E-01
Annotation Cluster 2	Enrichment Score: 2.43	Count	P_Value	Benjamini
GOTERM_BP_DIRECT	cellular response to cytokine stimulus	5	5.80E-06	4.30E-03
GOTERM_MF_DIRECT	protein phosphatase binding	4	5.10E-03	6.30E-01
GOTERM_BP_DIRECT	phosphorylation	6	6.90E-02	8.70E-01
GOTERM_BP_DIRECT	cytokine-mediated signaling pathway	3	9.70E-02	9.30E-01
Annotation Cluster 3	Enrichment Score: 1.78	Count	P_Value	Benjamini
GOTERM_BP_DIRECT	cellular response to cytokine stimulus	5	5.80E-06	4.30E-03
KEGG_PATHWAY	Chemokine signaling pathway	4	4.30E-02	5.20E-01
KEGG_PATHWAY	Measles	3	1.00E-01	6.90E-01
KEGG_PATHWAY	Epstein-Barr virus infection	3	2.10E-01	8.70E-01
KEGG_PATHWAY	Viral carcinogenesis	3	2.40E-01	8.80E-01
Annotation Cluster 4	Enrichment Score: 1.76	Count	P_Value	Benjamini
KEGG_PATHWAY	T cell receptor signaling pathway	4	8.10E-03	3.80E-01
KEGG_PATHWAY	Pathways in cancer	6	2.00E-02	4.40E-01

KEGG_PATHWAY	Chronic myeloid leukemia	3	3.40E-02	4.90E-01
--------------	--------------------------	---	----------	----------

MYD88L265P vs. empty manifest transduced Eμ-myc lymphomas

Annotation Cluster 1	Enrichment Score: 1.93	Count	P_Value	Benjamini
GOTERM_BP_DIRECT	immune system process	13	1.20E-03	5.50E-01
GOTERM_BP_DIRECT	adaptive immune response	7	4.60E-03	6.40E-01
GOTERM_BP_DIRECT	innate immune response	7	2.80E-01	9.90E-01
Annotation Cluster 2	Enrichment Score: 1.93	Count	P_Value	Benjamini
GOTERM_MF_DIRECT	ATP binding	31	2.00E-03	5.70E-01
GOTERM_BP_DIRECT	phosphorylation	16	3.60E-03	7.90E-01
GOTERM_MF_DIRECT	nucleotide binding	36	4.30E-03	5.90E-01
GOTERM_MF_DIRECT	kinase activity	17	4.80E-03	4.90E-01
GOTERM_MF_DIRECT	protein kinase activity	13	2.00E-02	6.50E-01
GOTERM_MF_DIRECT	protein serine/threonine kinase activity	11	2.60E-02	6.70E-01
GOTERM_BP_DIRECT	protein phosphorylation	13	2.80E-02	8.30E-01
GOTERM_MF_DIRECT	transferase activity	22	1.80E-01	9.80E-01

PD-L1 vs. empty manifest transduced Eμ-myc lymphomas

Annotation Cluster 1	Enrichment Score: 9.64	Count	P_Value	Benjamini
GOTERM_BP_DIRECT	cell cycle	75	1.20E-12	4.00E-09
GOTERM_BP_DIRECT	mitotic nuclear division	43	9.80E-11	1.60E-07
GOTERM_BP_DIRECT	cell division	45	1.00E-07	6.60E-05
Annotation Cluster 2	Enrichment Score: 6.17	Count	P_Value	Benjamini
GOTERM_BP_DIRECT	transcription, DNA-templated	148	1.30E-08	1.50E-05
GOTERM_BP_DIRECT	regulation of transcription, DNA-templated	161	2.50E-06	1.40E-03
GOTERM_MF_DIRECT	DNA binding	134	9.10E-06	1.20E-03
Annotation Cluster 3	Enrichment Score: 3.77	Count	P_Value	Benjamini
GOTERM_CC_DIRECT	cell-cell adherens junction	34	2.70E-05	1.60E-03
GOTERM_MF_DIRECT	cadherin binding involved in cell-cell adhesion	32	2.80E-05	3.30E-03
GOTERM_BP_DIRECT	cell-cell adhesion	19	6.20E-03	4.80E-01
Annotation Cluster 4	Enrichment Score: 3.24	Count	P_Value	Benjamini
GOTERM_CC_DIRECT	nuclear pore	14	9.40E-06	1.20E-03
GOTERM_MF_DIRECT	structural constituent of nuclear pore	7	1.20E-04	1.10E-02
KEGG_PATHWAY	RNA transport	21	1.60E-04	2.10E-02
GOTERM_BP_DIRECT	RNA export from nucleus	6	5.90E-04	1.10E-01
GOTERM_BP_DIRECT	protein import into nucleus	11	1.00E-03	1.50E-01
GOTERM_MF_DIRECT	nucleocytoplasmic transporter activity	6	1.20E-03	7.40E-02
GOTERM_BP_DIRECT	mRNA transport	12	4.10E-03	4.00E-01
GOTERM_CC_DIRECT	nuclear inclusion body	4	2.20E-02	2.60E-01
Annotation Cluster 5	Enrichment Score: 2.65	Count	P_Value	Benjamini
GOTERM_CC_DIRECT	chromosome, centromeric region	19	1.50E-04	6.90E-03
GOTERM_CC_DIRECT	kinetochore	16	6.70E-04	2.20E-02
GOTERM_CC_DIRECT	condensed chromosome kinetochore	8	1.10E-01	6.30E-01
Annotation Cluster 6	Enrichment Score: 2.41	Count	P_Value	Benjamini
GOTERM_CC_DIRECT	MCM complex	6	2.80E-05	1.50E-03
GOTERM_BP_DIRECT	DNA replication initiation	7	9.20E-04	1.50E-01
GOTERM_BP_DIRECT	DNA unwinding involved in DNA replication	5	1.00E-03	1.50E-01
KEGG_PATHWAY	DNA replication	8	1.10E-03	9.30E-02
GOTERM_MF_DIRECT	ATP-dependent DNA helicase activity	6	4.00E-03	1.70E-01
KEGG_PATHWAY	Cell cycle	14	6.00E-03	2.00E-01
GOTERM_MF_DIRECT	DNA helicase activity	5	1.10E-02	3.00E-01
GOTERM_CC_DIRECT	nuclear chromosome, telomeric region	11	8.70E-02	5.60E-01
BIOCARTA	CDK Regulation of DNA Replication	3	2.80E-01	1.00E+00
Annotation Cluster 7	Enrichment Score: 2.13	Count	P_Value	Benjamini
GOTERM_CC_DIRECT	kinesin complex	10	7.70E-04	2.40E-02
GOTERM_BP_DIRECT	microtubule-based movement	10	1.50E-02	6.50E-01
GOTERM_MF_DIRECT	microtubule motor activity	9	3.60E-02	5.40E-01

NFKBIZ vs. empty manifest transduced E μ -myc lymphomas

none

I κ B α Δ Individual genes manifest transduced E μ -myc lymphomas

contrast	baseMean	log2FoldChange	pvalue	padj	chromosome_name	mgi_symbol
empty vs. I κ BdeltaN	615.063648	0.623018789	0.000146108	0.038255264	3	Bcar3
empty vs. I κ BdeltaN	258.5262982	0.767153105	2.6706E-08	0.000172721	7	Bcl3
empty vs. I κ BdeltaN	6975.255844	0.359997988	0.000116958	0.037806571	9	Cbl
empty vs. I κ BdeltaN	3013.612529	0.284408697	0.000157547	0.038255264	16	Cblb
empty vs. I κ BdeltaN	3151.616113	0.372104374	0.000139257	0.038255264	13	Cd180
empty vs. I κ BdeltaN	1528.212168	0.672573582	5.19973E-05	0.030221079	18	Csf1r
empty vs. I κ BdeltaN	32.73187781	0.788665706	5.60731E-05	0.030221079	5	Cxcl2
empty vs. I κ BdeltaN	220.9719646	0.653735356	0.00029474	0.04706739	12	Fos
empty vs. I κ BdeltaN	2220.312952	0.503068185	6.91493E-05	0.033127657	8	Jak3
empty vs. I κ BdeltaN	13016.56199	-2.091471234	5.39401E-33	6.97715E-29	12	Nfkbia
empty vs. I κ BdeltaN	1591.811617	0.393718999	1.92065E-05	0.015527238	2	Notch1
empty vs. I κ BdeltaN	6971.344352	0.520331869	1.48976E-06	0.003211676	3	Notch2
empty vs. I κ BdeltaN	1607.085367	0.533956006	5.94886E-06	0.007694853	17	Pim1
empty vs. I κ BdeltaN	5829.366766	0.604804846	8.14789E-05	0.034283089	3	S1pr1
empty vs. I κ BdeltaN	31.5428406	-0.621435187	3.69229E-05	0.026533201	X	Smarca1
empty vs. I κ BdeltaN	1691.050467	0.748743306	5.40746E-05	0.030221079	13	Tgfb1
empty vs. I κ BdeltaN	93.00810547	0.724918356	0.000111513	0.036985297	X	Tlr8

CD79BY196H individual genes manifest transduced E μ -myc lymphomas

contrast	baseMean	log2FoldChange	pvalue	padj	chromosome_name	mgi_symbol
empty vs. CD79BY196H	1056.786541	0.704143364	0.000175321	0.016356709	10	Aim1
empty vs. CD79BY196H	28.21695982	0.892886322	0.000488592	0.033607798	1	Batf3
empty vs. CD79BY196H	597.2714424	1.079747807	2.05852E-06	0.000891216	19	Casp7
empty vs. CD79BY196H	242.197084	0.858474067	0.000616404	0.038047863	1	Cd28
empty vs. CD79BY196H	41928.88429	-0.387291579	0.000546371	0.035677283	11	Cd79b
empty vs. CD79BY196H	1001.010559	-0.894231181	0.000521715	0.034749515	8	Enpp6
empty vs. CD79BY196H	12965.14668	0.363952316	0.000175568	0.016356709	6	Foxp1
empty vs. CD79BY196H	32412.53865	0.706369791	0.000148813	0.01483421	17	H2-Aa
empty vs. CD79BY196H	28208.68357	0.457257424	6.54977E-06	0.002008596	17	H2-D1
empty vs. CD79BY196H	26979.79218	0.523861113	0.000457887	0.032718884	17	H2-K1
empty vs. CD79BY196H	801.4446074	0.684568027	0.00059612	0.037499499	17	H2-Oa
empty vs. CD79BY196H	1939.86105	0.819788133	4.805E-13	3.53648E-09	17	H2-Q4
empty vs. CD79BY196H	399.4400996	1.514790242	1.49619E-12	7.3413E-09	17	H2-Q5
empty vs. CD79BY196H	1529.512739	1.638529647	2.29469E-15	3.37779E-11	17	H2-Q6
empty vs. CD79BY196H	760.3135062	1.125253377	7.24928E-06	0.002092343	17	H2-Q7
empty vs. CD79BY196H	366.4604958	0.77741784	2.03357E-06	0.000891216	17	H2-T10
empty vs. CD79BY196H	1298.259112	0.554620412	1.49839E-05	0.003190849	17	H2-T22
empty vs. CD79BY196H	82.60570531	0.917176897	2.05647E-06	0.000891216	11	Havcr2
empty vs. CD79BY196H	142.954873	0.939523436	9.529E-05	0.011133761	1	Icos
empty vs. CD79BY196H	81.18232758	0.987936147	0.000149148	0.01483421	12	Ighv1-33
empty vs. CD79BY196H	47.09193326	1.010489971	0.000135038	0.014198267	12	Ighv1-54
empty vs. CD79BY196H	121.6518223	0.864104749	0.00049701	0.033993214	1	Ikzf2
empty vs. CD79BY196H	3981.194949	0.61612582	4.94355E-06	0.001732596	9	Il10ra
empty vs. CD79BY196H	2656.716432	0.851631199	9.57796E-07	0.00054226	3	Il6ra
empty vs. CD79BY196H	285.8190191	0.683617354	0.000212467	0.018616132	6	Irak2
empty vs. CD79BY196H	1013.919997	1.086621232	1.5968E-05	0.003310543	7	Irf7
empty vs. CD79BY196H	82.27464499	0.841453551	0.000163218	0.015703039	5	Kit
empty vs. CD79BY196H	582.963061	1.059923727	1.05567E-05	0.002643677	15	Ly6a
empty vs. CD79BY196H	195.6426098	-0.879713942	1.63049E-06	0.000799858	4	Pik3r3
empty vs. CD79BY196H	6277.181025	-0.453765251	0.00050214	0.033993214	1	Pycr2
empty vs. CD79BY196H	127.4650141	0.999978961	1.01525E-05	0.002643677	17	Runx2
empty vs. CD79BY196H	6500.044081	0.567301672	6.87727E-06	0.002065989	17	Tap1
empty vs. CD79BY196H	1692.573544	0.898970209	5.04332E-07	0.000337444	13	Tgfb1
empty vs. CD79BY196H	198.7538371	1.382465336	4.49407E-11	1.65382E-07	11	Trim7

CARD11L244P individual genes manifest transduced E μ -myc lymphomas

contrast	baseMean	log2FoldChange	pvalue	padj	chromosome_name	mgi_symbol
empty vs. CARD11L244P	12160.03005	-0.657108495	5.89328E-10	3.67476E-06	5	Card11
empty vs. CARD11L244P	112.6165292	-0.543417631	2.57659E-09	5.35545E-06	8	Cbln1
empty vs. CARD11L244P	1692.162065	0.673178043	4.82353E-08	7.51928E-05	18	Csf1r
empty vs. CARD11L244P	128.7431484	-0.550183293	1.77507E-09	5.35545E-06	Y	Kdm5d
empty vs. CARD11L244P	478.9438913	-0.448779025	0.000266152	0.044676873	2	Ltk
empty vs. CARD11L244P	482.3031055	-0.485884173	0.000121547	0.029150276	X	Map3k15
empty vs. CARD11L244P	199.0887683	-0.46551526	0.000282588	0.045571844	4	Pik3r3
empty vs. CARD11L244P	230.8205738	-0.500593376	9.48789E-05	0.024650713	7	Prkg

MYD88L265P individual genes manifest transduced E μ -myc lymphomas

contrast	baseMean	log2FoldChange	pvalue	padj	chromosome_name	mgi_symbol
empty vs. MYD88L265P	10092.27908	0.905428196	7.10993E-08	3.75527E-05	3	Bank1
empty vs. MYD88L265P	885.9864344	-0.879658067	0.000153146	0.009653227	12	Batf
empty vs. MYD88L265P	81.53711791	-2.329651896	2.11893E-08	1.41111E-05	8	Bcar1
empty vs. MYD88L265P	1331.847123	-0.958702577	0.00205248	0.04898609	3	Bcar3
empty vs. MYD88L265P	628.7145656	-1.086354762	8.54421E-05	0.006352996	7	Bcl3
empty vs. MYD88L265P	656.2976522	-1.627566999	9.16928E-07	0.000254882	1	Bmpr2
empty vs. MYD88L265P	3217.426152	0.649444396	0.001361461	0.038689237	5	Brca2
empty vs. MYD88L265P	60.66766101	-1.807548752	7.53124E-06	0.001164448	19	Cabp4
empty vs. MYD88L265P	438.4979407	-1.374001941	4.57797E-06	0.000844828	9	Casp4
empty vs. MYD88L265P	33.12130547	-1.326963388	0.001456661	0.040102819	7	Cblc
empty vs. MYD88L265P	701.3412877	-0.696417936	8.96845E-07	0.000254882	16	Cbr1
empty vs. MYD88L265P	1268.831587	-1.072524424	0.000210355	0.011757807	1	Cd244
empty vs. MYD88L265P	2293.729946	-1.541626545	9.26762E-06	0.00133917	5	Cd36
empty vs. MYD88L265P	2539.731054	0.914362707	0.000328401	0.016019504	4	Cdkn2c
empty vs. MYD88L265P	335.419716	-1.231638438	6.59927E-05	0.005428224	16	Cebpd
empty vs. MYD88L265P	6872.640552	0.384765254	0.001454889	0.040102819	1	Cenpf
empty vs. MYD88L265P	4054.20377	0.982478858	8.89849E-06	0.001304362	5	Cit
empty vs. MYD88L265P	822.6923263	1.070155012	0.001150153	0.034542942	1	Cr2
empty vs. MYD88L265P	848.4388827	-1.608195672	2.96232E-06	0.000630192	1	Ctla4
empty vs. MYD88L265P	10828.56382	0.89947687	5.73823E-05	0.004965673	5	Cux1
empty vs. MYD88L265P	36.10220577	-1.711090317	3.51304E-05	0.003563767	X	Dach2
empty vs. MYD88L265P	1441.824085	0.619279608	0.001213017	0.035530991	10	E2f7
empty vs. MYD88L265P	4159.899037	0.869795151	0.000791436	0.028079654	7	E2f8
empty vs. MYD88L265P	203.3882137	-1.635721284	7.52275E-05	0.005939482	11	Etv4
empty vs. MYD88L265P	8798.559012	1.113987751	4.95774E-07	0.00016875	1	Fcgr2b
empty vs. MYD88L265P	904.7027655	-1.13897044	9.63567E-06	0.001379342	3	Gbp2
empty vs. MYD88L265P	3524.26068	-0.948338544	2.54212E-07	9.69703E-05	11	Grap
empty vs. MYD88L265P	535.4500501	-1.80873107	9.93154E-06	0.001408531	10	Gstt1
empty vs. MYD88L265P	1689.815783	-0.65761946	0.001100208	0.033502755	10	Gstt2
empty vs. MYD88L265P	3700.512543	0.865475307	0.001772724	0.045210337	17	H2-Dma
empty vs. MYD88L265P	78.81136079	1.875105673	8.1519E-06	0.001224143	12	Ighv1-33
empty vs. MYD88L265P	320.7385265	-1.392519734	1.31427E-06	0.000341197	3	Il12a
empty vs. MYD88L265P	1148.493912	-1.013632744	3.07421E-06	0.000636362	8	Irs2
empty vs. MYD88L265P	88.98206501	-1.850581357	6.58089E-06	0.001072335	11	Itga3
empty vs. MYD88L265P	552.5541748	-1.01119257	3.62426E-05	0.003605019	4	Jun
empty vs. MYD88L265P	2301.499212	-0.789165234	0.000422008	0.018589849	8	Jund
empty vs. MYD88L265P	241.7873187	-1.650697147	4.38958E-06	0.000830064	17	Map4k3
empty vs. MYD88L265P	289.7226092	-0.799924802	0.000899718	0.029828965	1	Mreg
empty vs. MYD88L265P	1557.229589	1.253436071	3.07075E-06	6.18928E-05	10	Mum1
empty vs. MYD88L265P	3733.00971	-1.060430423	8.12262E-09	6.22071E-06	9	Myd88
empty vs. MYD88L265P	3045.119727	-1.286026163	0.000211222	0.011757807	9	Neil1
empty vs. MYD88L265P	2240.920119	-0.749546564	0.001108145	0.033677506	19	Nfkbia
empty vs. MYD88L265P	4627.758348	-0.733826662	6.39243E-05	0.005321354	12	Nfkbid
empty vs. MYD88L265P	1112.610306	-0.726450225	0.000759687	0.02737911	7	Nfkbie
empty vs. MYD88L265P	1300.885964	-0.725424647	0.000904938	0.029937212	17	Nlrbp10
empty vs. MYD88L265P	1584.358591	-1.242242064	5.5352E-05	0.004817197	16	Noxa1
empty vs. MYD88L265P	225.0066494	1.131231761	3.64173E-06	0.000715133	7	
empty vs. MYD88L265P	19.24169132	-1.669833712	6.89042E-05	0.005496902	2	

empty vs. MYD88L265P	532.810359	-2.452848618	8.77808E-11	1.32101E-07	4	Pcsk9
empty vs. MYD88L265P	14319.61502	-0.988167855	0.000155732	0.009736126	4	Pik3cd
empty vs. MYD88L265P	2917.132895	-0.894265651	2.22604E-05	0.002525649	17	Pim1
empty vs. MYD88L265P	4262.168875	-1.707740693	4.35144E-06	0.000830064	X	Pim2
empty vs. MYD88L265P	1480.698213	-0.791454232	7.60232E-06	0.001164448	2	Plcg1
empty vs. MYD88L265P	5274.453345	-0.452382481	0.000883987	0.029571881	10	Polr2e
empty vs. MYD88L265P	649.7269027	-1.793663615	8.94157E-06	0.001304362	10	Prdm1
empty vs. MYD88L265P	11029.13961	0.787457936	8.33886E-05	0.006252742	3	Prkacb
empty vs. MYD88L265P	70.72996871	-1.3952633	0.000297231	0.015017815	4	Prkc
empty vs. MYD88L265P	352.2338859	-1.751730377	1.28344E-07	5.78192E-05	7	Pvr
empty vs. MYD88L265P	505.447921	-1.458385973	0.000394114	0.017795097	2	Rag2
empty vs. MYD88L265P	837.8549425	-1.709041359	3.15621E-05	0.003365794	6	Ret
empty vs. MYD88L265P	423.793188	-1.328475025	3.51398E-05	0.003563767	14	Rgcc
empty vs. MYD88L265P	6170.922176	-0.925091896	0.00013737	0.008803776	1	Slamf6
empty vs. MYD88L265P	295.1148717	-1.393564991	0.000387256	0.017653587	1	Stau2
empty vs. MYD88L265P	1486.591463	-0.646358254	0.000658154	0.025076985	2	Tank
empty vs. MYD88L265P	2001.636607	-1.16188801	1.46564E-05	0.001810417	10	Tnfaip3
empty vs. MYD88L265P	44.3867416	-1.467652874	0.000423572	0.018589849	4	Trp73
empty vs. MYD88L265P	122.1822592	-1.894473961	6.45091E-06	0.001062459	1	Wnt10a
empty vs. MYD88L265P	278.0733697	-3.006853609	2.21763E-13	8.49186E-10	15	Wnt10b
empty vs. MYD88L265P	475.695549	-1.178956174	0.000655751	0.025047733	5	Yes1

PD-L1 individual genes manifest transduced E μ -myc lymphomas

contrast	baseMean	log2FoldChange	pvalue	padj	chromosome_name	mgi_symbol
empty vs. PD-L1	1266.561668	-0.729068356	0.001042233	0.027869165	1	Aim2
empty vs. PD-L1	2340.679885	-0.411134193	0.001234763	0.030092759	1	Atg16l1
empty vs. PD-L1	6024.99461	0.445189532	0.00240516	0.041193394	4	Bach2
empty vs. PD-L1	11.05712745	-1.013126304	0.00143081	0.032218673	8	Bcar1
empty vs. PD-L1	1334.308073	-0.499479506	0.000622445	0.021438755	1	Bcl2
empty vs. PD-L1	97.46932728	-0.919050943	0.000211767	0.013301962	14	Bmp1
empty vs. PD-L1	2858.906149	0.576029689	2.07984E-07	0.00015678	11	Brca1
empty vs. PD-L1	2439.453161	0.931461861	3.46664E-11	2.74384E-07	5	Brca2
empty vs. PD-L1	7799.573203	0.346352531	0.001916667	0.037136897	17	Brd4
empty vs. PD-L1	61.68120662	-1.244936255	1.07374E-05	0.002333267	11	Ccl8
empty vs. PD-L1	6947.830927	-0.620666383	0.000873163	0.025425332	4	Ccnl2
empty vs. PD-L1	505.4487148	-0.869764216	0.002483994	0.04192071	1	Cd247
empty vs. PD-L1	377.02332	-0.94774117	0.000842079	0.025185694	6	Cd27
empty vs. PD-L1	7779.58205	-3.13035133	5.16102E-28	8.16989E-24	19	Cd274
empty vs. PD-L1	127.1943858	-0.630722961	0.000911798	0.025753288	2	Cd302
empty vs. PD-L1	2182.029612	0.571640949	0.002396923	0.041153241	4	Cdkn2c
empty vs. PD-L1	823.5459626	-0.711524788	6.16656E-05	0.006178271	7	Cln3
empty vs. PD-L1	7015.309686	0.326596765	0.002459677	0.041599028	6	Cul1
empty vs. PD-L1	9123.29034	0.775416171	4.49777E-05	0.00535336	5	Cux1
empty vs. PD-L1	3251.5059	0.420960332	0.001253918	0.030232887	12	Dnmt3a
empty vs. PD-L1	3701.787976	0.415991654	0.002385603	0.041055103	15	Drosha
empty vs. PD-L1	1220.259616	0.566965694	4.70648E-05	0.005559967	10	E2f7
empty vs. PD-L1	3686.330743	0.54042579	0.000858048	0.025388596	7	E2f8
empty vs. PD-L1	348.8786936	-0.581918499	0.00123832	0.030092759	7	Flt3l
empty vs. PD-L1	3699.389796	0.728460481	9.80055E-05	0.00815162	13	Gfod1
empty vs. PD-L1	18.01185255	-0.997507177	0.000271967	0.015085463	10	Gli1
empty vs. PD-L1	312.7260793	-0.691227178	0.000217234	0.013432865	17	H2-K2
empty vs. PD-L1	104.9960094	-0.945117382	0.001099647	0.028597804	17	H2-M2
empty vs. PD-L1	1472.389741	-0.771669876	0.002160862	0.039499359	17	H2-Q7
empty vs. PD-L1	17.68990067	-1.051384959	0.001232284	0.030092759	3	Hey1
empty vs. PD-L1	1747.72435	-0.525113343	0.001908601	0.037111844	9	Icam1
empty vs. PD-L1	1901.937535	-0.490190493	0.001147581	0.029165426	16	Ifngr2
empty vs. PD-L1	737.3110808	-0.785808193	0.000353241	0.01731458	1	Ikbike
empty vs. PD-L1	8678.556047	0.378297061	0.002503798	0.042030875	11	Ikzf3
empty vs. PD-L1	323.7205047	-0.868985467	7.85595E-05	0.007272495	1	Inpp1
empty vs. PD-L1	4264.938637	0.801793313	1.46553E-05	0.002578377	3	Jade1
empty vs. PD-L1	512.3644525	0.789305976	0.002156156	0.039458899	12	Klf11
empty vs. PD-L1	49.75828759	-1.056320423	0.000210328	0.013290353	6	Klre1
empty vs. PD-L1	1008.807963	-1.018621671	0.000303352	0.016083811	7	Lat
empty vs. PD-L1	154.0407375	-0.884127744	0.001734073	0.035283266	17	Lta

empty vs. PD-L1	55.28006536	-1.047926147	0.001239576	0.030092759	X	Maoa
empty vs. PD-L1	10332.29922	0.622072735	0.00088376	0.025529055	8	Nfatc3
empty vs. PD-L1	3065.659761	-0.37276366	0.003043878	0.046846808	12	Nfkbia
empty vs. PD-L1	940.5291178	-0.612394098	0.00197333	0.037635921	7	Nfkbid
empty vs. PD-L1	582.7959921	-0.808091856	5.18443E-05	0.005759413	16	Nfkbiz
empty vs. PD-L1	5756.462228	0.646733107	0.000127511	0.009657877	3	Notch2
empty vs. PD-L1	60.36818094	-0.904444286	0.000101836	0.008238544	17	Notch4
empty vs. PD-L1	15270.19875	0.523625652	1.43727E-05	0.002578377	1	Nucks1
empty vs. PD-L1	5557.108629	0.582134871	0.000794613	0.024664151	3	Pik3ca
empty vs. PD-L1	224.8785955	-1.233651487	1.45347E-05	0.002578377	4	Pik3r3
empty vs. PD-L1	1268.207713	-0.717862211	0.000828138	0.025113845	2	Plcg1
empty vs. PD-L1	308.9852375	-0.676873483	0.001821391	0.036131098	4	Plk3
empty vs. PD-L1	3784.090586	0.693896615	0.000578111	0.020993788	3	Plk4
empty vs. PD-L1	6133.872807	0.520512236	0.000529453	0.020306356	X	Pola1
empty vs. PD-L1	7055.276299	0.502182196	2.7766E-05	0.004051215	5	Pole
empty vs. PD-L1	3250.263194	-0.559162687	0.000899499	0.025753288	19	Poir2g
empty vs. PD-L1	8881.855366	0.619214192	0.001632483	0.033981145	3	Prkacb
empty vs. PD-L1	1687.204363	0.457459157	0.001331568	0.031073603	11	Prkca
empty vs. PD-L1	2954.469232	0.699709498	0.000210731	0.013290353	3	Prkci
empty vs. PD-L1	41.48236501	-1.061136509	0.000212596	0.013301962	4	Prkcz
empty vs. PD-L1	7743.468293	0.552567822	0.002991807	0.046477244	19	Pten
empty vs. PD-L1	2840.019508	0.493447675	0.001634007	0.033981145	1	Ptpn4
empty vs. PD-L1	318.9993459	-0.987075698	0.00055599	0.020806915	14	Rgcc
empty vs. PD-L1	4926.817354	0.681575799	0.002309515	0.040397376	3	S1pr1
empty vs. PD-L1	6261.228508	-0.459870185	0.00020897	0.013290353	18	Sec11c
empty vs. PD-L1	4726.662169	-0.590033299	0.001854374	0.036601921	1	Slamf6
empty vs. PD-L1	749.954664	0.636751258	0.000131744	0.009745376	11	Slfn3
empty vs. PD-L1	10.69432909	-1.491004152	2.82164E-06	0.00099259	X	Smarca1
empty vs. PD-L1	12422.20177	0.504385522	0.000168927	0.011576563	9	Smarcc1
empty vs. PD-L1	61.34932316	-0.820916211	0.000903262	0.025753288	1	Snora41
empty vs. PD-L1	1724.157236	0.814919886	9.93849E-05	0.00815162	12	Syne3
empty vs. PD-L1	44.30921811	-0.910046597	0.001778928	0.035792283	14	Tlr11
empty vs. PD-L1	145.5575392	-0.851335274	0.001107027	0.028728251	17	Tnf
empty vs. PD-L1	43.30910158	-0.87536428	0.000841405	0.025185694	17	Tnfsf9
empty vs. PD-L1	791.0054193	-0.893434985	0.000678486	0.02223691	2	Traf1
empty vs. PD-L1	7409.112571	0.292485203	0.001871589	0.036804047	9	Trak1
empty vs. PD-L1	4196.644753	0.492393499	0.000353292	0.01731458	11	Trim37
empty vs. PD-L1	41.23503278	-0.968516981	0.002898707	0.045740016	16	Vpreb1

3. Table Appendix 3: T-cell activation and evasion signatures

contrast	baseMean	log2FoldChange	pvalue	padj	chr	mgj_symbol
empty vs. MYD88L265P	848.4388827	-1.608195672	2.96232E-06	0.000630192	1	Ctla4
empty vs. MYD88L265P	23.30158153	-1.171713246	0.002605402	0.055860856	1	Il10
empty vs. MYD88L265P	320.7385265	-1.392519734	1.31427E-06	0.000341197	3	Il12a
empty vs. MYD88L265P	649.7269027	-1.793663615	8.94157E-06	0.001304362	10	Prdm1
empty vs. MYD88L265P	1268.831587	-1.072524424	0.000210355	0.011757807	1	Cd244
empty vs. MYD88L265P	927.6897968	-1.404911276	3.83318E-05	0.003732195	6	Cd69
empty vs. MYD88L265P	885.9864344	-0.879658067	0.000153146	0.009653227	12	Batf
empty vs. MYD88L265P	91.87976268	-0.867613714	0.007710197	0.105038212	17	Ebi3
empty vs. MYD88L265P	1794.448624	-0.739811705	0.010976072	0.127848284	10	Vsir
empty vs. MYD88L265P	5318.3161	0.442912107	0.049484808	0.269198472	16	Btla
empty vs. MYD88L265P	243.1860435	0.452767032	0.224878828	0.543478798	16	Cd96
empty vs. MYD88L265P	131.2775578	0.264207754	0.404887209	0.701023511	11	Havcr2
empty vs. MYD88L265P	136.7179504	0.440082658	0.112654367	0.403920018	6	Lag3
empty vs. MYD88L265P	6923.849283	0.271448142	0.163479998	0.476140546	7	Spn
empty vs. MYD88L265P	8377.950153	-0.201139186	0.223744592	0.543078603	2	Cd44
empty vs. MYD88L265P	5430.608897	0.290616801	0.213402526	0.532972319	7	Tgfb1
empty vs. MYD88L265P	106.7759493	0.225344069	0.548373458	0.795041504	16	Tigit

empty vs. MYD88L265P	95.250837	0.190726618	0.544025791	0.793289091	9	Eomes
empty vs. MYD88L265P	58.41910232	0.116871816	0.695805431	0.874599244	3	Cd160
empty vs. MYD88L265P	61.45121018	0.006861842	0.983860148	0.993227419	11	Tbx21
empty vs. MYD88L265P	146.9973839	-0.133510323	0.722530469	0.888344774	1	Pcdcd1

Components of the T-Cell evasion signature. Underlined with blue bars are significantly upregulated genes for p<0.05 also found in our pre-designed signature.

contrast	baseMean	log2FoldChange	pvalue	padj	chr	mgi_symbol
empty vs. MYD88L265P	352.2338859	-1.751730377	1.28344E-07	5.78192E-05	7	Pvr
empty vs. MYD88L265P	54.45103523	-1.09711964	0.000467158	0.020043303	17	Tnfsf9
empty vs. MYD88L265P	910.7721288	-0.473925355	0.008816287	0.114041513	16	Cd86
empty vs. MYD88L265P	793.5732853	0.740451001	0.02700652	0.199835201	9	Lamb2
empty vs. MYD88L265P	6493.480321	-0.763881459	0.031602508	0.218323452	15	Il7r
empty vs. MYD88L265P	288.0116963	-0.773487792	0.036722258	0.233810499	16	Cd80
empty vs. MYD88L265P	402.9664098	0.691860141	0.037450433	0.236694102	1	Cd28
empty vs. MYD88L265P	1061.597693	0.551745526	0.060638484	0.298170038	10	Icosl
empty vs. MYD88L265P	1061.597693	0.551745526	0.060638484	0.298170038	10	Icosl
empty vs. MYD88L265P	4916.122431	-0.341590453	0.109331636	0.399100398	1	Cd48
empty vs. MYD88L265P	4766.164502	0.236236184	0.116722527	0.410938551	3	Cd2
empty vs. MYD88L265P	683.3089579	-0.411372073	0.167589019	0.480524336	2	Cd40
empty vs. MYD88L265P	283.3132865	0.421033589	0.217378514	0.536338063	6	Cd27
empty vs. MYD88L265P	18687.37871	0.224776535	0.368678282	0.670938221	1	Sell
empty vs. MYD88L265P	173.2680354	0.3238848	0.383376905	0.684183936	4	Tnfsf8
empty vs. MYD88L265P	12.15357528	0.357434759	0.391240043	0.690076432	10	Ifng
empty vs. MYD88L265P	58.07912713	0.277179756	0.404095159	0.700251787	17	Tnfsf14
empty vs. MYD88L265P	128.1327325	-0.218040522	0.410793513	0.705206821	17	Tnf
empty vs. MYD88L265P	243.016475	-0.161093449	0.506388518	0.769250089	4	Tnfrsf4
empty vs. MYD88L265P	29.97435498	-0.189421197	0.631519755	0.84257906	1	Tnfsf18
empty vs. MYD88L265P	154.3352635	-0.159209347	0.642102394	0.846975747	4	Tnfrsf9
empty vs. MYD88L265P	34.31407631	0.125227931	0.757159421	0.903929139	4	Tnfrsf8
empty vs. MYD88L265P	9.171039626	-0.254337763	0.544096611	1	1	Tnfrsf4

T-cell activation signature. Note that only Pvr and Tnfsf9 could be found with p<0.05. A total of 646 genes passed this threshold.

Eidesstattliche Versicherung

„Ich, Jens Florian Schrezenmeier, versichere an Eides statt durch meine eigenhändige Unterschrift, dass ich die vorgelegte Dissertation mit dem Thema:

„Functional genomic investigation of the human aggressive lymphoma derived genetic lesions MYD88L265P, NFKBIZ, CARD11L244P, CD79BY196H and PD-L1 in a murine Eμ-myc lymphoma model“

selbstständig und ohne nicht offengelegte Hilfe Dritter verfasst und keine anderen als die angegebenen Quellen und Hilfsmittel genutzt habe.

Alle Stellen, die wörtlich oder dem Sinne nach auf Publikationen oder Vorträgen anderer Autoren beruhen, sind als solche in korrekter Zitierung (siehe „Uniform Requirements for Manuscripts (URM)“ des ICMJE -www.icmje.org) kenntlich gemacht. Die Abschnitte zu Methodik (insbesondere praktische Arbeiten, Laborbestimmungen, statistische Aufarbeitung) und Resultaten (insbesondere Abbildungen, Graphiken und Tabellen) entsprechen den URM (s.o) und werden von mir verantwortet.

Meine Anteile an etwaigen Publikationen zu dieser Dissertation entsprechen denen, die in der untenstehenden gemeinsamen Erklärung mit dem/der Betreuer/in, angegeben sind. Sämtliche Publikationen, die aus dieser Dissertation hervorgegangen sind und bei denen ich Autor bin, entsprechen den URM (s.o) und werden von mir verantwortet.

Die Bedeutung dieser eidesstattlichen Versicherung und die strafrechtlichen Folgen einer unwahren eidesstattlichen Versicherung (§156,161 des Strafgesetzbuches) sind mir bekannt und bewusst.“

Datum

Unterschrift

Curriculum Vitae

Mein Lebenslauf wird aus datenschutzrechtlichen Gründen in der elektronischen Version meiner Arbeit nicht veröffentlicht.

Unterschrift

Publications not associated with this dissertation

Publications

Riesner, K., Shi, Y., Jacobi, A., Kräter, M., Kalupa, M., McGearey, A., Mertlitz, S., Cordes, S., Schrezenmeier, J., Mengwasser, J., Westphal, S., Perez-Hernandez, D., Schmitt, C., Dittmar, G., Guck, J., & Penack, O. (2017). Initiation of acute graft-versus-host disease by angiogenesis. *Blood*, 129(14), 2021-2032

Conference Contributions

Reimann, M., Masswig, S., Schleich, K., Herrmann, A., Lohneis, P., Schrezenmeier, J., Dörken, B., & Schmitt, C. (2015). Modeling the CNS Tropism of Diffuse Large B-Cell Lymphomas *in Vivo*. *Blood*, 126(23), 576. Accessed June 25, 2017. Retrieved from <http://www.bloodjournal.org/content/126/23/576>.

Eva Schrezenmeier, Klemens Budde, Jan Lisec, Jens Schrezenmeier, Petra Glander, Carsten Jaeger, Friederike Hoffmann, Fabian Halleck, Oliver Staeck, Lukas Lehner, Dmytro Khadzhynov, Michael Duerr; TO016 CLINICAL PHARMACOKINETICS OF SOFOSBUVIR AND DACLATASVIR IN KIDNEY TRANSPLANT RECIPIENTS. *Nephrol Dial Transplant* 2017; 32 (suppl_3): iii84-iii85. doi: 10.1093/ndt/gfx130

Danksagung

Prof. C.A. Schmitt gilt der Dank mich in sein Labor aufgenommen zu haben und mir eine umfassende und herausfordernde wissenschaftliche Arbeit und die Ausbildung in der Molekularbiologie ermöglicht zu haben. Prof. K. Rajewsky möchte ich für seine präzisen Eingaben in wichtigen Momenten unseres Projektes danken.

Dr. Maurice Reimann gilt mein großer Dank als mein wissenschaftlicher Partner der letzten Jahre, der mit mir im immerwährenden Diskurs, ständigem Austausch und harter Arbeit geforscht hat.

Sven Masswig bin ich dankbar für seine Fähigkeit mir die Arbeit im Labor als solides Handwerk beizubringen, das mit Ruhe und Können ausgeführt werden will.

Andrea Herrmann, Marika Drescher und Nadine Burbach möchte ich dafür danken, das Labor und unsere Experimente am Laufen zu halten und dem Labor einen familiären Charakter zu geben.

Dimitri Belenki hat mit hervorragenden Diskussionen und sehr guten Ratschlägen zur praktischen Immunologie und Molekularbiologie viele Wege abgekürzt.

Dr. Jan Lisec danke ich für seine immer offene Tür. Er ist ein großartiger Statistiker von dem ich viel, was Abstraktion und theoretische Modellierung biologischer Prozesse anbetrifft, gelernt habe. Seine Zähigkeit, stringent große Experimente mit mir durchzuführen, ist unübertroffen.

Dr. Liam Childs und Dr. Dorothee Childs gilt mein Dank dafür, ihre großartigen Fähigkeiten der mathematischen Modellierung und statistischen Analyse in unsere Forschung eingebracht zu haben und damit wesentlich zum Erfolg unserer Forschung beigetragen zu haben.

Dr. Philipp Lohneis danke ich für die Einbringung seiner pathologischen Kunstfertigkeit und Präzision und die viele Zeit, die er für uns geopfert hat.

Den Mitgliedern der AG Penack gilt mein großer Dank für viele hilfreiche Diskussionen zur murinen Stammzelltransplantation, gute wissenschaftliche Zusammenarbeit und einige Kubikmeter Kaffee.

Meinem Papa und meiner Mama, Dr. Gerlinde Schmidtke-Schrezenmeier und Prof. Dr. Hubert Schrezenmeier, und meiner Schwester, meinem Schwager und meiner Nichte, Dr. Eva Schrezenmeier, Dr. Fabian Halleck und Anna Halleck, danke ich für ihre Liebe, ihren Rat und ihre Ruhe. Ihr Zutrauen und ihre Nestwärme haben mich immer getragen und gestützt. Dasselbe gilt auch für die Dackel, Dr. Fienchen und Sissi, und den Beagle, Heidi.